MODELING IRRADIATIVE DAMAGE TO DNA

by

MARIA C. LIND

(Under the Direction of Henry F. Schaefer III)

ABSTRACT

Hydrogen-abstracted and deprotonated structures of the two DNA base pairs, guanine-cytosine and adenine-thymine (G-C and A-T), have been studied using Density Functional Theory (DFT). Such structures are of interest as products created along the radiation track which results in damage to living cells. DFT is well-suited to provide reliable predictions both for optimized geometries for systems of this size, as well as electronic properties and relative energies. For the various deprotonated G-C base pair structures, the most stable pair results from the loss of a proton analogous to the glycosidic bond (which connects base to the sugar-phosphate backbone in double-stranded DNA) and corresponds to the hydrogen-abstracted radical with the greatest adiabatic electron affinity, 3.65 eV. The most stable A-T radical results from loss of a hydrogen atom from thymine's methyl group. The next two most stable structures, lying only about 1 kcal mol^{-1} apart, result from a loss of hydrogen at the sites analogous to the two glycosidic bonds. In general, hydrogen-abstracted radicals of the A-T base pair exhibited fewer geometric perturbations than the G-C structures, despite having only two hydrogen bonds connecting the pair. The energetic interleaving of the H-abstracted individual bases adenine and thymine are found to be the same as those for the hydrogen bonded pair, suggesting that predictions made for smaller fragments may be extrapolated to larger systems.

Additionally, the electronic ground states ($\tilde{X}\ ^1\Sigma^+$) of HNSi, HSiN, and the transition state connecting the two isomers were systematically studied using highly correlated *ab initio* methods in conjunction with large correlation consistent type basis sets. The HNSi isomer has been confirmed to be the global minimum on the ground state HSiN-HNSi surface and is predicted to lie 65.4 kcal/mol below the HSiN isomer at the aug-cc-pCVQZ CCSD(T) level of theory. The barrier height for the isomerization reaction (HNSi→ HSiN) is determined to be 79.6 kcal/mol.

INDEX WORDS: DNA, Density Functional Theory, DFT, molecular modeling, computational chemistry, base pair, HNSi, HSiN.

MODELING IRRADIATIVE DAMAGE TO DNA

by

MARIA C. LIND

B.S. Chemistry, University of North Carolina at Chapel Hill, 2002

A Dissertation Submitted to the Graduate Faculty of The University of Georgia in Partial Fulfillment of the Requirements for the Degree

DOCTOR OF PHILOSOPHY

ATHENS, GEORGIA

2008

© 2008

Maria C. Lind

All Rights Reserved

MODELING IRRADIATIVE DAMAGE TO DNA

by

MARIA C. LIND

Major Professor: Henry F. Schaefer III

Committee: Geoffrey D. Smith
Nigel G. Adams

Electronic Version Approved:

Maureen Grasso
Dean of the Graduate School
The University of Georgia
May 2008

DEDICATION

This work is dedicated in loving memory of Evelyn B. Lind 1906-2006, a smart lady and a great grandmother.

ACKNOWLEDGEMENTS

I would first like to thank Dr. Henry F. Schaefer, an excellent graduate advisor. I could not imagine a better graduate school experience than that I've had here at the University of Georgia Chemistry Department and the Center for Computational Chemistry in the Schaefer Group. My informal mentor in my first years here, Partha Bera, was an invaluable guide in my first research project. Holly, Veronika, Martin, and Frank have all been supportive and fun office mates as well as our fishes, Peter and Quincy. Especially, thank you Drs. Nigel Adams and Geoffrey Smith for your time, attention, and helpful suggestions as members of my committee. Thanks to our administrative support here at CCC Linda, Karen, and Amy for having been so helpful in all my administrative needs.

I would also like to thank Dr. Lee G. Pedersen for giving me a start in the field of Computational Chemistry by taking me on as an undergraduate researcher. The rest of the Chemistry department and faculty of the University of North Carolina at Chapel Hill provided me with a rigorous background in Chemistry. I am especially grateful to Drs. Brookhart and Pielak for their interesting courses. My early research mentors, Dr. Gary Pielak, Sorina Morar, and Chetan Patel were also wonderful teachers and role models.

TABLE OF CONTENTS

Page

ACKNOWLEDGEMENTS v

LIST OF TABLES ix

LIST OF FIGURES xi

CHAPTER

1 INTRODUCTION AND LITERATURE REVIEW 1

1.1 COMPUTATIONAL CHEMISTRY 2

1.2 DENSITY FUNCTIONAL THEORY 2

1.3 IRRADIATIVE DAMAGE TO DNA 4

1.4 COUPLED-CLUSTER THEORY 5

1.5 OVERVIEW OF CHAPTERS 6

1.6 REFERENCES 7

2 THE DEPROTONATED GUANINE-CYTOSINE BASE PAIR 9

2.1 ABSTRACT 10

2.2 INTRODUCTION 11

2.3 RESULTS AND DISCUSSION 13

2.4 CONCLUSIONS 19

2.5 METHODS 20

2.6 ACKNOWLEDGEMENTS 22

2.7 REFERENCES 22

3 HYDROGEN-ABSTRACTED ADENINE-THYMINE RADICALS WITH INTERESTING TRANSFERABLE PROPERTIES 46

3.1 ABSTRACT 47

3.2 INTRODUCTION 48

3.3 METHODS 50

3.4 RESULTS 51

3.5 DISCUSSION 54

3.6 CONCLUDING REMARKS 56

3.7 ACKNOWLEDGEMENTS 57

3.8 REFERENCES 57

4 CHARACTERIZATION OF THE HSiN – HNSi SYSTEM IN ITS ELECTRONIC GROUND STATE 71

4.1 ABSTRACT 72

4.2 INTRODUCTION 73

4.3 ELECTRONIC STRUCTURE CONSIDERATIONS 77

4.4 THEORETICAL PROCEDURES 78

4.5 RESULTS AND DISCUSSION 79

4.6 CONCLUDING REMARKS 92

4.7 ACKNOWLEDGEMENTS 93

4.8 REFERENCES 93

5 CONCLUDING REMARKS..111

LIST OF TABLES

Page

Table 2.1: Total energies (hartree), relative energies (kcal mol^{-1}), vertical detachment energy (VDE) and relaxation energies E_{R1} (kcal mol^{-1}) of the deprotonated G-C base pair structures. 27

Table 2.2: A second set of relaxation energies E_{R2} (kcal mol^{-1}), and vertical electron affinity VEA (eV) for the deprotonated G-C base pair structures. 28

Table 2.3: A third set of relaxation energies E_{R3} (kcal mol^{-1}) for the deprotonated G-C base pair structures. 29

Table 2.4: Dihedral angles of the deprotonated G-C base pair structures, in degrees. 30

Table 2.5: Hydrogen bond distances of the deprotonated G-C structures, in Angstroms. 31

Table 2.6: Adiabatic electron affinities of the G-C base pair H-abstracted radicals, in eV; deprotonated G-C dissociation energies (to the respective base plus deprotonated base).....32

Table 2.7: Gas phase acidities (G-C → Anion + H^+), in eV for the G-C base pair. 33

Table 3.1: Relative energies (ΔE), Relaxation Energies (RE), and Dissociation Energies (DE) of Hydrogen-Abstracted A-T radicals (ZPVE Corrected Energies in Parentheses).....64

Table 3.2: Selected Interatomic Distances (Å) for Hydrogen Abstracted A-T Radicals.....65

Table 3.3: X-H Bond Dissociation Energies (eV) for Adenine and Thymine, Compared with the Hydrogen-Bonded A-T Base Pair. 66

Table 4.1: Theoretical predictions of the total energy (in hartree), dipole moment (in debye), harmonic vibrational frequencies (in cm^{-1}), and zero point vibrational energies (ZPVE in kcal mol^{-1}) for the linear ground state ($\tilde{X}\ ^1\Sigma^+$) of HNSi. 97

Table 4.2: Theoretical predictions of the total energy (in hartree), dipole moment (in debye), harmonic vibrational frequencies (in cm^{-1}), and zero point vibrational energies (ZPVE in kcal mol^{-1}) for the linear ground state ($\tilde{X}\ ^1\Sigma^+$) of HSiN. 98

Table 4.3: Theoretical predictions of the total energy (in hartree), dipole moment (in debye), harmonic vibrational frequencies (in cm^{-1}), and zero point vibrational energy (ZPVE in kcal mol^{-1}) for the transition state ($\tilde{X}\ ^1A'$) of the HSiN ←→ HNSi isomerization reaction. 99

Table 4.4. Theoretical predictions of harmonic vibrational frequencies (in cm^{-1}) for the linear ($\tilde{X}\ ^1\Sigma^+$) states of the HNSi and DNSi molecules at the CCSD, CCSD(T), and ICMRCI levels of theory. 100

Table 4.5. Theoretical predictions of harmonic vibrational frequencies (in cm^{-1}) for the linear ($\tilde{X}\ ^1\Sigma^+$) states of the HSiN and DSiN molecules at the CCSD, CCSD(T), and ICMRCI levels of theory. 101

Table 4.6. Relative energies in kcal mol^{-1} (zero-point vibrational energy corrected values in parentheses) for the HSiN - HNSi system with respect to the global minimum $\tilde{X}\ ^1\Sigma^+$ state of HNSi. 102

Table 4.7. Total SCF, CASSCF, CCSD, and CCSD(T) energies in hartrees for the ground states of H(^{2}S) and SiN ($X\ ^1\Sigma^+$), and the dissociation energies of HNSi and HSiN to H + SiN in kcal mol^{-1}. 103

LIST OF FIGURES

Page

Figure 2.1: The standard IUPAC G-C base pair numbering scheme. 34

Figure 2.2.: The (closed-shell neutral) G-C base pair optimized geometry. 35

Figure 2.3: G-C(N1)$^-$ optimized anion. 36

Figure 2.4: G(N2a)-C$^-$ optimized anion. 37

Figure 2.5: G(N9)-C$^-$ optimized anion. 38

Figure 2.6: G-C(N4b)$^-$ optimized anion. 39

Figure 2.7: G(N1)-C$^-$ optimized anion. 40

Figure 2.8: G-C(N4a)$^-$ optimized anion. 41

Figure 2.9: G(N2b)-C$^-$ optimized anion. 42

Figure 2.10: G-C(C6)$^-$ optimized anion. 43

Figure 2.11: G-C(C5)$^-$ optimized anion. 44

Figure 2.12: G(C8)-C$^-$ optimized anion. 45

Figure 3.1: IUPAC numbering scheme for the A-T base pair. 67

Figure 3.2: Optimized geometry of the closed-shell neutral ground state A-T base pair 68

Figure 3.3: Optimized geometries of neutral doublet radicals derived from A-T by abstraction of one hydrogen atom from adenine. 69

Figure 3.4: Optimized geometries of neutral doublet radicals derived from A-T by abstraction of one hydrogen atom from thymine 70

Figure: 4.1 The 7σ (a), 2π (b), and 3π (c) molecular orbitals of HNSi at the cc-pVTZ CASSCF level of theory.....104

Figure: 4.2. The 7σ (a), 2π (b), and 3π (c) molecular orbitals of HSiN at the cc-pVTZ CASSCF level of theory. 105

Figure 4.3. Potential energy surfaces for the HSiN - HNSi system at six levels of theory with the cc-pVTZ basis 106

Figure 4.4. Predicted geometries for the $\tilde{X}\ ^1\Sigma^+$ ground state of the HNSi molecule at six levels of theory with six basis sets. Bond lengths are in Å.....107

Figure 4.5. Predicted geometries for the $\tilde{X}\ ^1\Sigma^+$ ground state of the HSiN molecule at six levels of theory with six basis sets. Bond lengths are in Å.....108

Figure 4.6. Predicted geometries of the transition state for the isomerization reaction (HNSi←→HSiN) at six levels of theory with six basis sets. Bond lengths are in Å and bond angles are in degrees.....109

Figure 4.7. Model potential energy surface for the HSiN - HNSi system at the CCSD(T) level of theory. Energetic values reported are from the aug-cc-pVQZ ICMRCI (in roman), aug-cc-pV5Z CCSD(T) (in italic), and the aug-cc-pCVQZ CCSD(T) (in bold) levels of theory.....110

CHAPTER 1

INTRODUCTION AND BACKGROUND MATERIAL

1.1 COMPUTATIONAL CHEMISTRY

The late nineteenth and early twentieth centuries led to many interesting discoveries for physics and chemistry regarding characteristics of the particles making up the macroscopic world. Classical mechanics had for the past 200+ years successfully and accurately predicted the behavior of objects in the macroscopic world, from projectiles and machinery to planetary motion. The concept that matter could exhibit both wavelike and particle-like properties was surprising to many. In 1926 Schrodinger proposed his eponymous equation to predict discrete energetics of a system where Newton's equation of motion had failed. The seemingly simple differential equation $\hat{H}\Psi=E\Psi$ can be quite a challenge to solve. With the advent of computers, researchers worldwide have developed elegant methods to compute energies and other properties of molecules using quantum mechanics. The various methods each have their benefits and drawbacks for different systems. Ultimately, computational methods can help us to understand chemical processes, predict structures and electronic properties, and glean many other sorts of chemical information.

1.2 DENSITY FUNCTIONAL THEORY

Density Functional Theory is a popular method for computing structures and energies of molecules. It differs from other *ab initio* and semiempirical Molecular Orbital (MO) methods in what is optimized; for MO theory it is the many-electron wavefunction, whereas for DFT it is the electron density. For an n-electron molecule, the electronic wavefunction depends on 3n spatial plus n spin coordinates.[1] Hohenberg and Kohn proved in 1964 that molecular properties are uniquely determined by the ground-

state electron probability density, a function of only three variables, regardless of the system size.[2] DFT attempts to calculate the electronic energy and other properties from the electron density. To date, the exact functional forms for the electron correlation and exchange are not known, so we must rely on some approximations. In contrast, in MO theory, it is possible to systematically improve the computations to work towards the exact solution of the Schrödinger equation.

Originally, the Local Density Approximation, or LDA was used, with the assumption that the energy density relied only on the electron density.[3,4] Later, the correlation functional was improved by adding an additional dependence on the gradient of the density, in so-called generalized gradient approximation (GGA) functionals. An early popular functional was developed by Becke, called "B," uses known exchange energies of six noble gas atoms.[5]

DFT, although an inexact theory, is favored by scaling- N^3, N being the number of basis functions used to represent the Kohn Sham orbitals. Hartree-Fock theory scales as N^4, and the current 'gold standard' of electronic structure calculations, coupled cluster with singles, doubles and partial triples corrections, CCSD(T), scales as N^7. Practically speaking, although CCSD(T) can yield very high accuracy for most molecular properties, the computational cost is too high for larger molecules and DFT is the only tractable method to obtain results for many systems.

Since the exact functional form of electronic behavior is not known, the accuracy of DFT in making predictions of a system cannot be guaranteed. Typically, when a new functional is introduced, its performance is assessed by benchmarking the results for various properties for a standard test set of molecules with known experimental data.[6-9]

For systems of the size of a DNA base pair (~30 atoms) DFT is the obvious choice for large studies; other methods like coupled cluster simply will require more computational capacity than is reasonable. Fortunately, in 2002 Rienstra-Kiracofe *et. al.* studied the performance of DFT for predicting atomic and molecular electron affinities.[10] They found that DFT can predict electron affinities within 0.2 kcal/mol of experiment, and B3LYP with a DZP++ basis set is an excellent choice for such calculations.

1.3 IRRADIATIVE DAMAGE TO DNA

The interaction of high-energy radiation (UV rays from the sun, x-rays, etc.) with DNA is a topic of great interest.[11-14] Excitement over the development of x-ray apparatus for medical purposes around 1900 was quickly dissipated with the obvious correlation of exposure to x-rays with the appearance of cancers and defects. Although today methods have been improved by reducing the amount of radiation patients are exposed to, the exact nature of the interaction of radiation with DNA is not thoroughly understood.

One factor complicating our understanding of the effects of radiation on DNA is the plethora of other molecules surrounding DNA. In addition to direct damage from radiation impinging on DNA, we can expect some amount of indirect damage, for example from a reactive hydroxyl radical produced by the radiolysis of water molecules present in the cell, or damage by free electrons produced by radiation impinging on other molecules. It has been shown that such free electrons (in the 0-20 eV range) are the most abundant so-called 'secondary species,' or radiation by-products, produced.[15]

In 2000, Sanche and coworkers showed in a clever experiment that electrons in the 0-20 eV range, or low-energy electrons (LEEs) can indeed cause strand breaks in

DNA[12] although the ionization threshold is ~7.5 eV. Subsequent studies have shown that LEEs interacting with individual bases result in deprotonation primarily at nitrogen sites.[16-18] Since we know that DFT yields reliable results for the electronic properties for systems of that size, such experiments can be enhanced with information gleaned from computational studies, for example which protons exactly are most susceptible to dissociative electron attachment or other processes.

1.4 COUPLED-CLUSTER THEORY

Coupled-cluster theory was developed by Cizek and Paldus to describe electronic correlation in the 1960s.[1,19] Coupled-cluster theory describes the full configuration interaction (CI) wave function as:

$\Psi = e^{T}\Psi_{HF}$,

where they defined the 'cluster operator' T as:

$T = T_1 + T_2 + T_3 + \ldots + T_n$,

n being the number of electrons. The T operators generate all possible determinants having from 0 to *n* excitations from the reference system. Typically the series is truncated at some level, depending on the system, but often at double or triple excitations, in order to make the computations more tractable. Where CCSD scales as N^6, CCSDT scales as N^8. Often the effects of including higher order excitations is estimated, for example with a method like the widely-used CCSD(T) developed by Raghavachari and coworkers, which scales as N^7.[20]

1.5 OVERVIEW OF CHAPTERS

The interaction of radiation with living cells is known to create free (ballistic) electrons as the radiation impinges on molecules like water *in vivo*. Such electrons can thermalize, or alternately, cause damage to other molecules. In the gas phase, the process of dissociative electron attachment can result in fragments of a DNA nucleobase pair being lost, with the most likely product being the singly deprotonated species. Therefore, this work seeks to further examine through computational predictions the geometries, relative energetics, and electronic properties of the various deprotonated derivatives of the guanine-cytosine (G-C) base pair, as well as the for the various hydrogen-abstracted adenine-thymine (A-T) base pairs.

Chapter 2 addresses relative energetics, electronic properties, and geometric perturbations for the various deprotonated G-C base pairs. Different properties are discussed as such damage can result from a number of processes, including straightforward deprotonation, dissociative electron attachment, or electron attachment to the hydrogen-abstracted open-shell structure. The most stable deprotonated structure is a substantial 12 kcal mol^{-1} lower in energy than any of the other nine structures. A number of interesting geometric changes are discussed for the various deprotonated structures, including dihedral torsional twists between the two bases, rotation in the plane of the two molecules, and changes in the hydrogen bonds.

In chapter 3, abstraction of the nine possible unique hydrogens from the A-T base pair is studied systematically. The relative energetic results are compared with results of H abstraction from the individual bases, adenine and thymine, and found to have interesting similarities in relative energies. Unexpectedly, the H-abstracted A-T base

pairs considered exhibit less geometric distortion than was seen for the G-C pair although A-T is bound by only two hydrogen bonds, one less than G-C.

The isomers HNSi, HSiN, and the transition state connecting the two are discussed in chapter 4. This system is isovalent to the well-known HCN-HNC system with ten valence electrons. However, the HSiN system exhibits the opposite trend in relative stability of the isomers. High accuracy studies to predict relative energies of the two isomers, the barrier to isomerization between them, as well as harmonic vibrational frequencies are presented.

1.6 REFERENCES

[1] C. J. Cramer, *Essentials of Computational Chemistry: Theories and Models*. (John Wiley & Sons Ltd, West Sussex, England, 2002).

[2] P. Hohenberg and W. Kohn, Physical Review B **136** (3B), B864 (1964).

[3] D. M. Ceperley and B. J. Alder, Physical Review Letters **45** (7), 566 (1980).

[4] S. H. Vosko, L. Wilk, and M. Nusair, Canadian Journal of Physics **58** (8), 1200 (1980).

[5] A. D. Becke, Physical Review A **38** (6), 3098 (1988).

[6] Y. Zhao and D. G. Truhlar, Journal of Chemical Theory and Computation **1** (3), 415 (2005).

[7] J. Antony and S. Grimme, Physical Chemistry Chemical Physics **8** (45), 5287 (2006).

[8] G. T. de Jong and F. M. Bickelhaupt, Journal of Chemical Theory and Computation **2** (2), 322 (2006).

[9] M. Kabelac, H. Valdes, E. C. Sherer, C. J. Cramer, and P. Hobza, Physical Chemistry Chemical Physics **9**, 5000 (2007).

[10] J. C. Rienstra-Kiracofe, G. S. Tschumper, H. F. Schaefer, S. Nandi, and G. B. Ellison, Chemical Reviews **102** (1), 231 (2002).

[11] B. D. Michael and P. O'Neill, Science **287** (5458), 1603 (2000).

[12] B. Boudaiffa, P. Cloutier, D. Hunting, M. A. Huels, and L. Sanche, Science **287** (5458), 1658 (2000).

[13] S. Steenken, Chemical Reviews **89** (3), 503 (1989).

[14] I. S. Hong, H. Ding, and M. M. Greenberg, Journal of the American Chemical Society **128** (2), 485 (2006).

[15] J. A. La Verne and S. M. Pimblott, Radiation Research **141** (2), 208 (1995).

[16] H. Abdoul-Carime, J. Langer, M. A. Huels, and E. Illenberger, European Physical Journal D: Atomic, Molecular and Optical Physics **35** (2), 399 (2005).

[17] S. Ptasinska, S. Denifl, V. Grill, T. D. Maerk, E. Illenberger, and P. Scheier, Physical Review Letters **95** (9), 093201 (2005).

[18] S. Ptasinska, S. Denifl, S. Gohlke, P. Scheier, E. Illenberger, and T. D. Maerk, Angewandte Chemie, International Edition **45** (12), 1893 (2006).

[19] J. Cizek, Journal of Chemical Physics **45** (11), 4256 (1966).

[20] K. Raghavachari, G. W. Trucks, J. A. Pople, and M. Headgordon, Chemical Physics Letters **157** (6), 479 (1989).

CHAPTER 2

THE DEPROTONATED GUANINE-CYTOSINE BASE PAIR[†]

[†] Maria C. Lind, Partha P. Bera, Nancy A. Richardson, Steven E. Wheeler, and Henry F. Schaefer III. PNAS 2006 103: 7554-7559. Reprinted here with permission of publisher.

2.1 ABSTRACT

Awareness of the harmful effects of radiation has increased interest in finding the mechanisms of DNA damage. Radical and anion formation among the DNA base pairs are thought to be important steps in such damage [Collins, G. P. (2003) Sci. Am. 289 (3), 26-27]. Energetic properties and optimized geometries of 10 radicals and their respective anions derived through hydrogen abstraction from the Watson-Crick guanine-cytosine (G-C) base pair have been studied using reliable theoretical methods. The most favorable deprotonated structure (dissociation energy 42 kcal mol^{-1}, vertical detachment energy 3.79 eV) ejects the proton analogous to the cytosine glycosidic bond in DNA. This structure is a surprisingly large 12 kcal mol^{-1} lower in energy than any of the other nine deprotonated G-C structures. This system retains the qualitative G-C structure but with the H ••• O2 distance dramatically reduced from 1.88 to 1.58 angstrom, an extremely short hydrogen bond. The most interesting deprotonated G-C structure is a "reverse wobble" incorporating two N-H ••• N hydrogen bonds. Three different types of relaxation energies (4.3-54 kcal mol^{-1}) are defined and reported to evaluate the energy released via different mechanisms for the preparation of the deprotonated species. Relative energies, adiabatic electron affinities (ranging from 1.93 to 3.65 eV), and pairing energies are determined to discern which radical will most alter the G-C properties. The most stable deprotonated base pair corresponds to the radical with the largest adiabatic electron affinity, 3.65 eV. This value is an enormous increase over the electron affinity (0.60 eV) of the closed-shell G-C base pair.

2.2 INTRODUCTION

Lesions in DNA caused by both high- and low-energy electrons are thought to result in cancer cell formation. Consequently, the mechanisms of primary and secondary damage to purine–pyrimidine base pairs have been under intense investigation in recent years.[1-15] Radical and anion formation in DNA are thought to be steps in pathways arising from radiation damage, which can lead to mutations.[15] This mutation can happen in several different ways, including direct radiation damage, secondary ballistic electron damage, or chemical damage by oxidative species.[15] Additionally, electronic properties of DNA have been under scrutiny with the hopes of using DNA strands in molecular electronic devices.[16-18]

Illenberger and coworkers[3,4] have noted, based on electron/nucleobase collision experiments, that dehydrogenation of bases is the predominant dissociative channel for DNA. High-energy photons, for example in the form of UV radiation from the sun, release electrons, which, in turn, may induce alterations such as single- and double-strand breaks in DNA or deletions of entire segments of the strand.[19] This process can occur through a number of pathways, one of which is dissociative electron attachment (DEA), whereby electrons formed as secondary products of radiation bind to nucleobases and cause bonds to break.

Abdoul-Carime *et al.*[3] have shown that DEA yields bases that are dehydrogenated predominantly at nitrogen sites. Furthermore, their work notes that the N–H bond that is cleaved in the isolated base pairs is at the same site as the glycosidic N–C bond between the base pair and the sugar phosphate backbone in the double-helical form of DNA and that the N–C bond should be even more easily cleaved.

The works of Sanche[20] and of Folkard *et al.*[21] have shown that indirect damage to DNA can be caused in a number of ways, including oxidative damage through hydrogen peroxide, hydroxyl radicals, and hydrated electrons produced from ionization of water molecules surrounding DNA *in vivo*. Of these, low-energy electrons with energies <20 eV (1 eV = 1.602 x 10^{-19} J) have been shown to be the most abundant secondary species.[22] It has recently been demonstrated that even very low energy electrons (0–5 eV) can induce strand breaks in DNA.[2,5,20,23,24]

Prior theoretical research has explored the structures and energetics of both the closed shell[14,25,26], H-abstracted,[1] and deprotonated[8] A-T and guanine–cytosine (G-C) base pairs, as well as the closed shell[13,27] and H-abstracted[7,11-13] individual bases. Bera and Schaefer[1] investigated the structures and energetics of the open shell H-abstracted G-C radicals. Richardson *et al.*[14,25] predicted the adiabatic electron affinities (AEAs) of the G-C and A-T base pairs to be 0.60 and 0.36 eV, respectively, by using density functional theory with a double-ζ plus polarization and diffuse functions basis set (DZP++). Kumar *et al.*[8] have reported structures, dissociation energies, and electron affinities (EAs) of three different base pairs by using a self-consistent-charge density functional tight binding method, yielding EAs ranging from 0.42 to 1.57 eV.

Luo *et al.*[12] found the AEA of guanine with a hydrogen abstracted from the N9 site to be the highest, at 2.99 eV. Luo *et al.*[11] found similar results for cytosine, with a hydrogen removed from the N1 site yielding the highest AEA of 2.98 eV. In this work, we employ the same reliable methods to compute AEAs for radicals of the G-C base pair obtained by H-abstraction.

Understanding the energetics and structural changes involved in possible reaction pathways will further elucidate the underlying cause and mechanism of DNA strand breaking. The possibility of using DNA as a molecular wire in microscale electronic devices is also a topic of current interest.[16,17] Although we are growing accustomed to ever-shrinking electronic devices, there exist size restrictions below which currently used materials fail to function effectively. Mindful of this present limitation, many researchers are looking for different materials with desirable properties in the microscale to nanoscale size range. Knowledge of the electronic characteristics of DNA and its components can be useful in tailoring its charge transport properties.[16,28]

2.3 RESULTS AND DISCUSSION

Fig. 1 illustrates the International Union of Pure and Applied Chemistry (IUPAC) atom-numbering scheme used. The formalism used to denote the individual H-abstracted radicals is as follows: the hydrogen is removed from G-C at the site mentioned in parentheses, from the base preceding the parentheses. For example, the H-abstracted radical G(N9)$^{\cdot}$-C is generated by homolytic cleavage of the N9–H bond of guanine. As an indication of the effect of anion formation on the overall base pair geometry, two dihedral angles were considered: the G(C6-C2)-C(C2-C4) angle and the G(C6-N1)-C(N3-C4) angle. Because the G-C base pair is planar in neutral DNA, a significant change in the dihedral angle on anion formation could lead to formation of a strand break or lesion in DNA.

The stabilizing effects of an added electron on the G-C radicals are noted as we consider the energetic and geometric changes manifest in the closed-shell deprotonated

G-C anions. The closed-shell anions were generated by homolytic bond cleavage to dehydrogenate the G-C base pair with subsequent anion formation by addition of a single electron. Geometric parameters, relative energies with respect to the lowest-energy anion of the series, and relaxation energies are given in Tables 1–5. AEAs, dissociation energies, and gas-phase acidities (GPAs) of the anions are reported in Table 6. EAs are predicted for all of the base pair radicals to be much greater than that for G-C itself.

Energies and Geometries.

Absolute and relative energies of all of the anions are presented in Table 1. Analogous to the results of Bera and Schaefer[1] for the neutral radicals, the lowest-energy deprotonated G-C species (shown in Fig. 2) is G-C(N1)$^-$, in which a proton has been abstracted from a sugar-binding site on the cytosine moiety. These findings are consistent with experiments showing that the nitrogen sites are more likely to hold the excess charge.[3] In all structures in which the proton removed was not involved in one of the three H-bonds, the H-bonds lengthen if the hydrogen-donating base is the site of dehydrogenation, whereas the other H-bond(s) shorten. It is interesting to note that there does not appear to be any energetic trend in the proton being removed from the guanine rather than the cytosine moiety. The relative ordering, extent of relaxation, and resultant geometric changes for each can be rationalized as follows: The lowest-energy anion was found to be G-C(N1)$^-$; shown in Fig. 2, this anion is resonance-stabilized by the carbonyl group on one side and C=C double bond on the other side. This conclusion is supported by the fact that, when compared with the geometries of both neutral G-C (Fig. 3) and the G-C(N1) radical,[1] both of the N–C bonds adjacent to N1 have shortened significantly.

The corresponding hydrogen-abstracted neutral radical is the fourth-most energetically favorable radical. The rather large change in relative stability between the radical and the anion should be reflected in the EA of the neutral radical, which we discuss in the next section. Despite being the lowest-energy H-abstracted anion, this structure deviates from planarity, with the two dihedral angles (defined above) predicted to be 8.0° and 5.3°. This deprotonated base pair also has the highest dissociation energy, 41.6 kcal·mol^{-1}. Possibly the most dramatic change in geometry due to anion formation is for the second-lowest-energy structure, G(N2a)$^{-}$-C, shown in Fig. 4. This structure lies ≈11.5 kcal·mol^{-1} higher in energy than G-C(N1)$^{-}$. One of the three hydrogens involved in G-C H-bonding is removed (from the N2 site on guanine) leaving two H-bonds in the optimized radical. Anion formation causes the next nearest H-bond to break, and the two structures rotate away from each other and form a new, second H-bond. The length of the remaining original H-bond is 1.761 Å. Although the corresponding dehydrogenated neutral radical structure displayed significant dihedral angles, 30.6° and 39.4°, on anion formation the structure returns to planarity. The N9 position on guanine is used for the base-sugar-binding site in the Watson-Crick structure. The anion generated at this position, G(N9)$^{-}$-C, is shown in Fig. 5. This structure is ≈11.7 kcal·mol^{-1} higher in energy than the most stable structure and only 0.2 kcal·mol^{-1} above the second-lowest structure. Again, the H-bonds adjacent to the site of dehydrogenation shorten considerably. As shown in Fig. 6, removal of a hydrogen from the N4 site on cytosine results in the next-lowest-energy structure. The other hydrogen on N4 is involved in H-bonding in the G-C base pair, and the distance between the hydrogen and the O6 position on guanine lengthens by ≈0.4 Å upon anion formation. The other two H-bonds both decrease in length. The fifth-lowest-

energy structure is G(N1)$^-$-C, shown in Fig. 7. This structure involves removal of the middle of the three hydrogens involved in H-bonding. Significant structural changes occur: the base pairs "slide" relative to each other in the plane (forming a "reverse wobble" structure) in such a way that they can still form two H-bonds and avoid the repulsion of the two nitrogen lone pairs. The two resulting H-bonds in this deprotonated structure are of N$^-$···H-N and N-H···N character. This result may be surprising because neutral N–H···N H-bonds are considered to be weaker than neutral O–H···O H-bonds. The two dihedral angles between the bases are 7° and 16°.The next-highest-energy structure (shown in Fig. 8) is almost 20 kcal·mol^{-1} above the lowest-energy anion. Like the fourth-lowest structure, it involves removal of a hydrogen from the N4 site on cytosine. However, this structure exhibits the largest deviation from planarity upon anion formation, with the two dihedral angles predicted to be 45° and 32°, respectively. The four remaining anions are >25 kcal·mol^{-1} above the lowest-energy anion and display relatively little dihedral distortion.

Relaxation Energies.

Three distinct relaxation energies (E_{R1}, E_{R2}, and E_{R3}) have been computed (shown in Tables 1–3) corresponding to different potential pathways from G-C to the deprotonated anions: relaxation energy E_{R1} corresponds to the energy lowering after deprotonation of neutral G-C; E_{R2} is the energy released through relaxation after electron attachment to hydrogen abstracted G-C; and E_{R3} gives the relaxation energy after hydrogen atom abstraction from the G-C radical anion.

Remarkably, the nonconventional structure G(N2a)$^{\cdot}$-C exhibits the largest relaxation energies of the 10 structures considered, presumably due to the stability afforded by the confounding C–H···N H-bond. Given the extensive rearrangement that occurs upon electron attachment in this structure, the magnitude of the relaxation energies is not too surprising. The relaxation energies for the global minimum anion structure, G-C(N1)$^{-}$, are more modest: E_{R1} = 10.1 kcal·mol^{-1}, E_{R2} = 4.3 kcal·mol^{-1}, and E_{R3} = 15.7 kcal·mol^{-1}, corresponding to the relatively minor changes in geometry after anion formation for this species. Overall, the size of the predicted relaxation energies for all structures considered is an indication of the magnitude of the driving force behind the observed geometrical relaxations upon anion formation.

EAs and GPA.

The theoretical AEAs of the H-abstracted G-C radicals range from 1.93 to 3.65 eV and are listed in Table 6. The three radicals having the highest EAs (3.65, 3.64, and 3.53 eV) all result from H-abstraction from a nitrogen site on cytosine. The general trend shows that the EAs of the radicals generated on the nitrogen sites are higher than those generated on carbon centers, a finding readily attributed to the greater electronegativity of nitrogen. All of the radicals display significantly larger AEAs than the closed-shell G-C base pair.

The radical with the highest AEA, 3.65 eV at the B3LYP/DZP++ level, results from the removal of hydrogen from the N1 site on cytosine [G-C(N1)$^{\cdot}$]. The N1 of cytosine in double-stranded DNA would be linked to the sugar–phosphate backbone. The corresponding anion is the lowest energy of the 10 studied here. That the radical with the

lowest AEA results from H-abstraction from cytosine is not surprising, because cytosine has been shown to have a higher AEA than guanine and to function as something of a sink for negative charge.[29,30]

The G-C(N4a)$^{\cdot}$ radical has the second-highest AEA (3.64 eV). Electron addition to the radical results in the sixth-lowest-energy anion of the 10 considered, suggesting that the large AEA arises (Fig. 8) primarily through destabilization of the radical rather than through stabilization of the anion. With an AEA of 3.53 eV, the radical G-C(N4b)$^{\cdot}$ comes in a close third. Like the structure previously discussed, the hydrogen was also lost from the N4 site on cytosine. The next-two-highest-predicted EAs are 3.25 and 3.03 eV, exhibited by the G(N2a)$^{\cdot}$-C and G(N1)$^{\cdot}$-C radicals, respectively. The extra electron in both the anions is resonance delocalized by the C2=N3 double bond.

These EAs are in very good agreement with the results obtained for the single bases by Abdoul-Carime *et al.* in their 2004 study,[3] in which EAs of the N-dehydrogenated radicals were predicted to be between 3.5 and 4.0 eV. The present work further supports the DEA mechanism for the generation of the proton-abstracted base pair anions as proposed by Abdoul-Carime *et al.*[3] The moderate EAs of the G-C base pair[25] make the electron capture successful. The large energy lowering of the anions and subsequently high EAs of the base pair attests to the plausibility of the DEA process.

GPAs also have been computed and are shown in Table 6. They range from 14.66 to 16.94 eV and are very similar to GPAs predicted for isolated adenine.[7] However, we do not find any correlation between relative acidity and deprotonation site (e.g., carbon vs. nitrogen).

Dissociation Energies.

The predicted dissociation energies of the deprotonated G-C structures are given in Table 6. The first seven anions in Table 6 are more difficult (higher dissociation energies) to dissociate into their component base and deprotonated base. The neutral radicals corresponding to these deprotonated structures have the highest EAs, reported in Table 6. It is interesting that, despite losing one H-bond, the dissociation energy of the G-C(N4a)$^-$ anion (30 kcal·mol^{-1}) is greater than the dissociation energy of the neutral G-C (27.2 kcal·mol^{-1}).[25,31]

The very low dissociation energies of some of the anions generated indicate that DEA could greatly alter structural and energetic characteristics of the base pairs and consequently of the DNA strand. Even very-low-energy secondary electrons (0–3 eV) would be able to split the base pairing.

2.4 CONCLUSIONS

In view of the complexity of biological systems, it is highly desirable (although difficult) to be able to discern the main chemical and physical events that are responsible for damage to genetic material. This complexity is enhanced because of exposure of the systems under study to UV or x-ray radiation or to an electron beam, because such conditions can cause many chemical changes, including cleavage of bonds and production of radicals and free electrons. Low-energy free electrons also can be produced by various other mechanisms in chemical and biochemical systems, and, therefore, a study of effects of their attachment to molecules poses an interesting problem. Formation

of radicals, anions, or cations of the bases can induce strong effects on the structure of DNA, and the elucidation and exploration of these myriad effects represent an important avenue of research.

The B3LYP density functional with the DZP++ basis set has been used to study the EAs and geometrical perturbations of the 10 H-abstracted neutral doublet G-C base pair radicals upon electron attachment. The energetically most favored of these anions is created by removing a proton from the N1 site on cytosine. This result is concordant with previous experimental work showing dehydrogenation of the nucleic acid bases to be most likely to occur at nitrogen sites that are also the sites of the glycosidic bond in DNA.[3] The EAs of the various H-deleted radicals ranged from 1.93 to 3.65 eV. DEA could cause significant damage to DNA, with torsional angles indicative of deviation from planarity between guanine and cytosine ranging from <1° up to ~45°. Changes in H-bond distances by as much as 0.5 Å also occur. These significant geometrical perturbations indicate that H-abstraction by means of irradiative damage to DNA at G-C base pair sites, possibly caused by high- or low-energy electrons, could have major detrimental effects on the overall DNA structure. This effect in turn may result in mutagenesis in living cells by alteration or termination of a DNA sequence upon an attempt to replicate. The large AEAs also suggest that radical creation could potentially alter the function of microscale electronic devices made by using DNA.

2.5 METHODS

Geometry optimizations and absolute energy analyses were performed by using the Q-CHEM 2.1 suite of programs.[32] A fine grid was used for geometry optimizations,

consisting of 75 radial shells and 590 angular points. Becke's three-parameter hybrid density functional (B3),[33] was used with the correlation functional of Lee, Yang, and Parr (LYP).[34] All computations used the DZP++ basis set, which contains 6 basis functions per H atom and 19 functions per C, N, or O atom, constructed by augmenting the double-ζ Huzinaga–Dunning[35-37] set of contracted Gaussian functions with one set of *d*-type polarization functions and even-tempered diffuse functions for each C, N, and O, and one set of *p*-type polarization functions as well as one even-tempered *s* diffuse function for each H.[38] Molecular structure figures were generated by using a code written by S.E.W..[39]

The physical properties of special interest in this study rely on energetic differences as described by the following:

AEA of Dehydrogenated G-C.

AEA = *E*(optimized neutral radical) – *E*(optimized deprotonated G-C).

Vertical Detachment Energy (VDE) of Deprotonated G-C.

VDE = *E*(neutral radical at optimized deprotonated G-C geometry) – *E*(optimized deprotonated G-C).

Vertical EA (VEA) of Dehydrogenated G-C.

VEA = *E*(optimized neutral radical) – *E*(deprotonated G-C at optimized neutral radical geometry).

Anion Relaxation Energies (E_R).

E_{R1} = E(deprotonated G-C at optimized G-C geometry) – E(optimized deprotonated G-C);

E_{R2} = E(deprotonated G-C at optimized neutral radical geometry) – E(optimized deprotonated G-C);

E_{R3} = E(deprotonated G-C at optimized G-C radical anion geometry) – E(optimized deprotonated G-C).

Dissociation Energy (D_e) of Deprotonated G-C.

$D_e = E[(G\text{-}H^+)^- - C] - E[(G\text{-}H^+)^-] - E(C)$ and

$D_e = E[G - (C\text{-}H^+)^-] - E(G) - E[(C\text{-}H^+)^-]$.

GPA of G-C.

GPA = E(optimized G-C) – E(optimized deprotonated G-C).

2.6 ACKNOWLEDGEMENTS

This work was supported by National Science Foundation Grant CHE 0451445.

2.7 REFERENCES

[1] P. P. Bera and H. F. Schaefer, Proceedings of the National Academy of Sciences of the United States of America **102** (19), 6698 (2005).

[2] J. Berdys, I. Anusiewicz, P. Skurski, and J. Simons, Journal Of The American Chemical Society **126** (20), 6441 (2004).

[3] H. Abdoul-Carime, S. Gohlke, and E. Illenberger, Physical Review Letters **92** (16), 168103 (2004).

[4] S. Ptasinska, S. Denifl, P. Scheier, E. Illenberger, and T. D. Mark, Angewandte Chemie-International Edition **44** (42), 6941 (2005).

[5] B. Boudaiffa, P. Cloutier, D. Hunting, M. A. Huels, and L. Sanche, M S-Medecine Sciences **16** (11), 1281 (2000).

[6] G. P. Collins, Scientific American **289** (3), 26 (2003).

[7] F. A. Evangelista, A. Paul, and H. F. Schaefer, Journal Of Physical Chemistry A **108** (16), 3565 (2004).

[8] A. Kumar, M. Knapp-Mohammady, P. C. Mishra, and S. Suhai, Journal Of Computational Chemistry **25** (8), 1047 (2004).

[9] X. F. Li, M. D. Sevilla, and L. Sanche, Journal of Physical Chemistry B **108** (49), 19013 (2004).

[10] B. Liu, P. Hvelplund, S. B. Nielsen, and S. Tomita, Journal of Chemical Physics **121** (9), 4175 (2004).

[11] Q. Luo, J. Li, Q. S. Li, S. Kim, S. E. Wheeler, Y. M. Xie, and H. F. Schaefer, Physical Chemistry Chemical Physics **7** (5), 861 (2005).

[12] Q. Luo, Q. S. Li, Y. M. Xie, and H. F. Schaefer, Collection Of Czechoslovak Chemical Communications **70** (6), 826 (2005).

[13] L. T. M. Profeta, J. D. Larkin, and H. F. Schaefer, Molecular Physics **101** (22), 3277 (2003).

[14] N. A. Richardson, S. S. Wesolowski, and H. F. Schaefer, Journal Of Physical Chemistry B **107** (3), 848 (2003).

[15] S. Steenken, Chemical Reviews **89** (3), 503 (1989).

[16] B. Giese, Annual Review of Biochemistry **71**, 51 (2002).

[17] E. Braun and K. Keren, Advances In Physics **53** (4), 441 (2004).

[18] M. Bixon and J. Jortner, Journal Of Physical Chemistry A **105** (45), 10322 (2001).

[19] H. Abdoul-Carime, P. Cloutier, and L. Sanche, Radiation Research **155** (4), 625 (2001).

[20] L. Sanche, Physica Scripta **68** (5), C108 (2003).

[21] M. Folkard, K. M. Prise, B. Brocklehurst, and B. D. Michael, Journal Of Physics B-Atomic Molecular And Optical Physics **32** (11), 2753 (1999).

[22] J. A. Laverne and S. M. Pimblott, Radiation Research **141** (2), 208 (1995).

[23] B. Boudaiffa, P. Cloutier, D. Hunting, M. A. Huels, and L. Sanche, Science **287** (5458), 1658 (2000).

[24] X. F. Li, M. D. Sevilla, and L. Sanche, Journal of the American Chemical Society **125** (45), 13668 (2003).

[25] N. A. Richardson, S. S. Wesolowski, and H. F. Schaefer, Journal of the American Chemical Society **124** (34), 10163 (2002).

[26] X. F. Li, Z. L. Cai, and M. D. Sevilla, Journal of Physical Chemistry A **106** (40), 9345 (2002).

[27] J. R. Wiley, J. M. Robinson, S. Ehdaie, E. C. M. Chen, E. S. D. Chen, and W. E. Wentworth, Biochemical And Biophysical Research Communications **180** (2), 841 (1991).

[28] C. Nese, Z. Yuan, M. N. Schuchmann, and C. Vonsonntag, International Journal Of Radiation Biology **62** (5), 527 (1992).

[29] M. D. Sevilla, B. Besler, and A. O. Colson, Journal Of Physical Chemistry **99** (3), 1060 (1995).

[30] S. S. Wesolowski, M. L. Leininger, P. N. Pentchev, and H. F. Schaefer, Journal Of The American Chemical Society **123** (17), 4023 (2001).

[31] J. Sponer, J. Leszczynski, and P. Hobza, Biopolymers **61** (1), 3 (2001).

[32] J. Kong, C. A. White, A. I. Krylov, D. Sherrill, R. D. Adamson, T. R. Furlani, M. S. Lee, A. M. Lee, S. R. Gwaltney, T. R. Adams, C. Ochsenfeld, A. T. B. Gilbert, G. S. Kedziora, V. A. Rassolov, D. R. Maurice, N. Nair, Y. H. Shao, N. A. Besley, P. E. Maslen, J. P. Dombroski, H. Daschel, W. M. Zhang, P. P. Korambath, J. Baker, E. F. C. Byrd, T. Van Voorhis, M. Oumi, S. Hirata, C. P. Hsu, N. Ishikawa, J. Florian, A. Warshel, B. G. Johnson, P. M. W. Gill, M. Head-Gordon, and J. A. Pople, Journal of Computational Chemistry **21** (16), 1532 (2000).

[33] A. D. Becke, Journal of Chemical Physics **98** (7), 5648 (1993).

[34] C. T. Lee, W. T. Yang, and R. G. Parr, Physical Review B **37** (2), 785 (1988).

[35] T. H. Dunning, Journal of Chemical Physics **53** (7), 2823 (1970).

[36] T. H. Dunning, Journal of Chemical Physics **55** (8), 3958 (1971).

[37] S. Huzinaga, Journal of Chemical Physics **42** (4), 1293 (1965).

[38] T. J. Lee and H. F. Schaefer, Journal of Chemical Physics **83** (4), 1784 (1985).

[39] S. E. Wheeler, HFSmol (2005).

TABLES

Table 2.1. Total energies (hartree), relative energies (kcal mol^{-1}), vertical detachment energy (VDE) and relaxation energies E_{R1} (kcal mol^{-1}) of the deprotonated G-C base pair structures.

E_{R1}= E(deprotonated G-C at optimized G-C geometry) – E(optimized deprotonated G-C).

VDE= E(neutral radical at optimized deprotonated G-C geometry) – E(optimized deprotonated G-C)

H-abstracted radical	Deprotonated G-C energy at its optimized geometry (hartree)	VDE (eV)	Relative Energy (kcal mol^{-1})	Deprotonated G-C energy at the optimized neutral closed shell G-C geometry (hartree)	Relaxation Energy E_{R1} (kcal mol^{-1})
G-C(N1)•	-937.179 94	3.79	0.0	-937.163 81	10.1
G(N2a)•-C	-937.161 56	3.57	11.5	-937.109 80	32.5
G(N9)•-C	-937.161 23	3.15	11.7	-937.145 84	9.7
G-C(N4b)•	-937.160 28	3.74	12.3	-937.138 69	13.6
G(N1)•-C	-937.159 51	3.47	12.8	-937.124 02	22.3
G-C(N4a)•	-937.148 25	3.77	19.9	-937.121 52	16.8
G(N2b)•-C	-937.136 95	2.70	27.0	-937.113 72	14.6
G-C(C6)•	-937.136 39	3.53	27.3	-937.122 91	8.5
G-C(C5)•	-937.122 48	3.23	36.1	-937.109 38	8.2
G(C8)•-C	-937.096 27	2.53	52.5	-937.082 67	8.5

Table 2.2. A second set of relaxation energies E_{R2} (kcal mol^{-1}), and vertical electron affinity VEA (eV) for the deprotonated G-C base pair structures.
E_{R2} = E(deprotonated G-C at optimized neutral radical geometry) – E(optimized deprotonated G-C).
VEA = E(optimized neutral radical) – E(deprotonated G-C at optimized neutral radical geometry)

H-abstracted radical	Deprotonated G-C energy at optimized neutral radical geometry (hartree)	VEA (eV)	Relaxation Energy E_{R2} (kcal mol^{-1})
G-C(N1)•	-937.173 10	3.47	4.3
G(N2a)•-C	-937.128 10	2.34	21.0
G(N9)•-C	-937.143 75	2.10	11.0
G-C(N4b)•	-937.144 17	3.10	10.1
G(N1)•-C	-937.145 64	2.65	8.7
G-C(N4a)•	-937.141 24	3.45	4.4
G(N2b)•-C	-937.126 85	2.11	6.3
G-C(C6)•	-937.111 94	2.24	15.3
G-C(C5)•	-937.101 94	2.12	12.9
G(C8)•-C	-937.077 01	1.41	12.1

Table 2.3. A third set of relaxation energies E_{R3} (kcal mol^{-1}) for the deprotonated G-C base pair structures.
E_{R3} = E(deprotonated G-C at the optimized G-C radical anion geometry) – E(optimized deprotonated G-C).

H-abstracted radical	Deprotonated G-C energy at optimized G-C radical anion geometry (hartree)	Relaxation Energy E_{R3} (kcal mol^{-1})
G-C(N1)•	-937.154 92	15.7
G(N2a)•-C	-937.076 69	53.3
G(N9)•-C	-937.111 48	31.2
G-C(N4b)•	-937.123 93	22.8
G(N1)•-C	-937.095 98	39.9
G-C(N4a)•	-937.110 66	23.6
G(N2b)•-C	-937.077 36	37.4
G-C(C6)•	-937.128 27	5.1
G-C(C5)•	-937.100 79	13.6
G(C8)•-C	-937.048 16	30.2

Table 2.4. Dihedral angles of the deprotonated G-C base pair structures, in degrees. Angles for the neutral radicals are given in parentheses.

Deprotonated G-C Structure	G(C6C2)C(C2C4) Dihedral	G(C6N1)C(N3C4) Dihedral
G-C(N1)$^-$	8.0 (0.0)	5.3 (0.0)
G(N2a)$^-$-C	0.1 (30.6)	0.0(39.4)
G(N9)$^-$-C	6.7 (0.0)	10.9 (0.0)
G-C(N4b)$^-$	0.0 (0.2)	0.0 (0.3)
G(N1)$^-$-C	7.2 (0.0)	16.0 (0.0)
G-C(N4a)$^-$	45.3 (31.7)	32.2 (15.9)
G(N2b)$^-$-C	0.0 (0.0)	0.0 (0.0)
G-C(C6)$^-$	6.2 (0.1)	4.3 (0.2)
G-C(C5)$^-$	0.0 (0.0)	0.0 (0.1)
G(C8)$^-$-C	5.8 (0.0)	9.4(0.0)

Table 2.5. Hydrogen bond distances of the deprotonated G-C structures, in Angstroms. H-bond lengths for neutral radicals are given in parentheses. A dash (-) indicates that the H-bond has been removed upon radical or anion formation.

H-abstracted anion	G(O6)-C(H4a)	C(N3)-G(H1)	C(O2)-G(H2a)
G-C Neutral	1.724	1.886	1.884
G-C(N1)$^-$	1.905 (1.730)	1.803 (1.839)	1.576 (1.811)
G(N2a)$^-$-C	- (1.819)	- (1.932)	- (-)
G(N9)$^-$-C	1.525 (1.790)	1.978 (1.854)	2.219 (1.616)
G-C(N4b)$^-$	2.255 (1.878)	1.902 (1.944)	1.647 (1.920)
G(N1)$^-$-C	- (-)	- (-)	- (-)
G-C(N4a)$^-$	- (-)	1.846 (1.909)	1.792 (1.751)
G(N2b)$^-$-C	1.528 (1.777)	1.956 (1.916)	2.152 (2.035)
G-C(C6)$^-$	1.919 (1.714)	1.801 (1.901)	1.653 (1.917)
G-C(C5)$^-$	1.935 (1.717)	1.817 (1.909)	1.646 (1.885)
G(C8)$^-$-C	1.528 (1.733)	1.956 (1.881)	2.152 (1.871)

Table 2.6. Adiabatic electron affinities of the G-C base pair H-abstracted radicals, in eV; deprotonated G-C dissociation energies (to the respective base plus deprotonated base).

H-abstracted G-C radical	Optimized neutral radical energy (hartree)	AEA (eV)	Deprotonated G-C structure	Dissociation Energy (kcal mol^{-1})
G-C(N1)$^{\bullet}$	-937.045 65	3.65	**G-C(N1)$^{-}$**	41.6
G(N2a)$^{\bullet}$-C	-937.042 05	3.25	**G(N2a)$^{-}$-C**	22.8
G(N9)$^{\bullet}$-C	-937.066 41	2.58	**G(N9)$^{-}$-C**	23.7
G-C(N4b)$^{\bullet}$	-937.030 39	3.53	**G-C(N4b)$^{-}$**	32.4
G(N1)$^{\bullet}$-C	-937.045 65	3.03	**G(N1)$^{-}$-C**	22.1
G-C(N4a)$^{\bullet}$	-937.014 47	3.64	**G-C(N4a)$^{-}$**	30.8
G(N2b)$^{\bullet}$-C	-937.049 33	2.38	**G(N2b)$^{-}$-C**	12.8
G-C(C6)$^{\bullet}$	-937.029 46	2.91	**G-C(C6)$^{-}$**	37.1
G-C(C5)$^{\bullet}$	-937.023 86	2.68	**G-C(C5)$^{-}$**	36.9
G(C8)$^{\bullet}$-C	-937.025 21	1.93	**G(C8)$^{-}$-C**	23.7

Table 2.7. Gas phase acidities (G-C → Anion + H^+), in eV for the G-C base pair.

Resulting Anion	Gas Phase Acidity (eV)
G-C(N1)$^-$	14.66
G(N2a)$^-$-C	15.16
G(N9)$^-$-C	15.17
G-C(N4b)$^-$	15.20
G(N1)$^-$-C	15.22
G-C(N4a)$^-$	15.52
G(N2b)$^-$-C	15.83
G-C(C6)$^-$	15.85
G-C(C5)$^-$	16.22
G(C8)$^-$-C	16.94

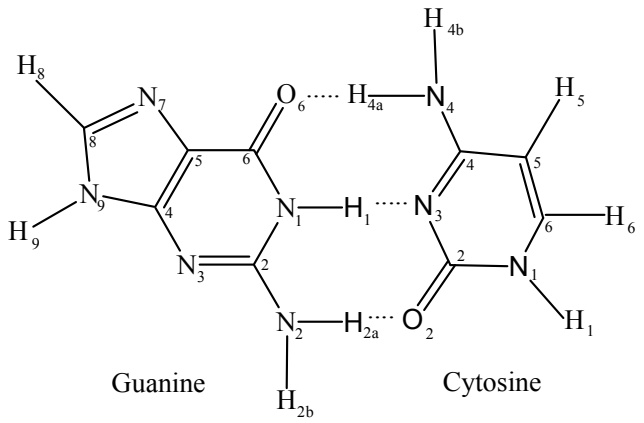

Figure 2.1. The standard IUPAC G-C base pair numbering scheme.

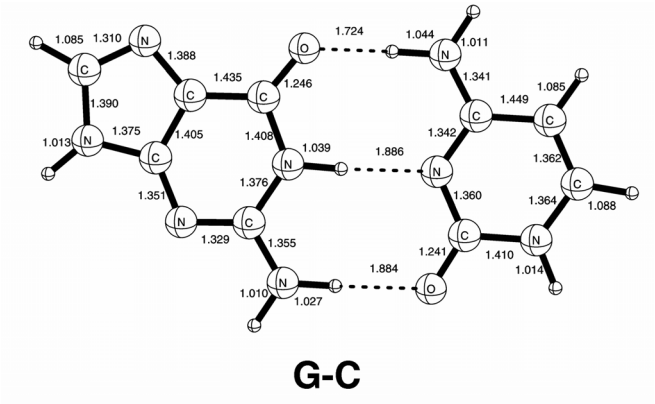

Figure 2.2. The (closed-shell neutral) G-C base pair optimized geometry. All bond lengths are given in Angstroms.

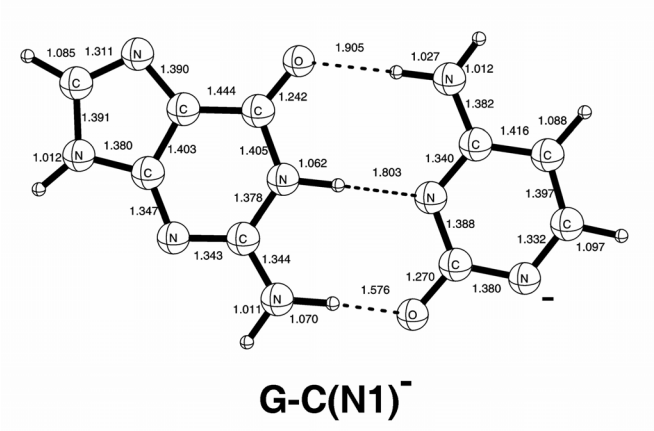

Figure 2.3. G-C(N1)¯ optimized anion. All bond lengths are given in Angstroms.

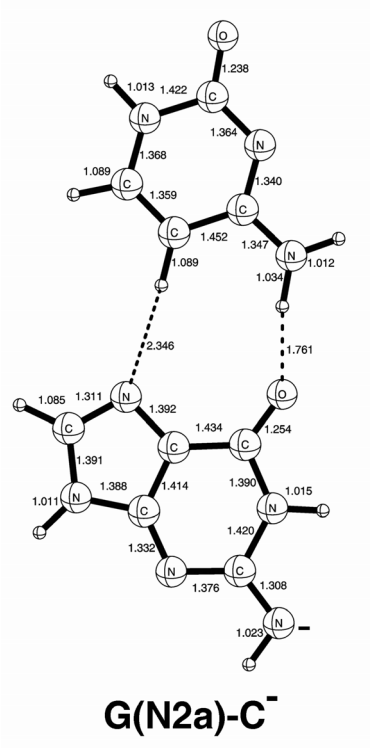

Figure 2.4. G(N2a)-C^{-} optimized anion. All bond lengths are given in Angstroms.

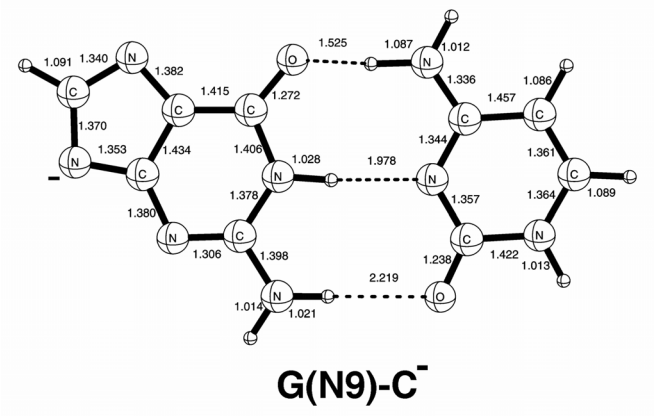

Figure 2.5. G(N9)-C^{-} optimized anion. All bond lengths are given in Angstroms.

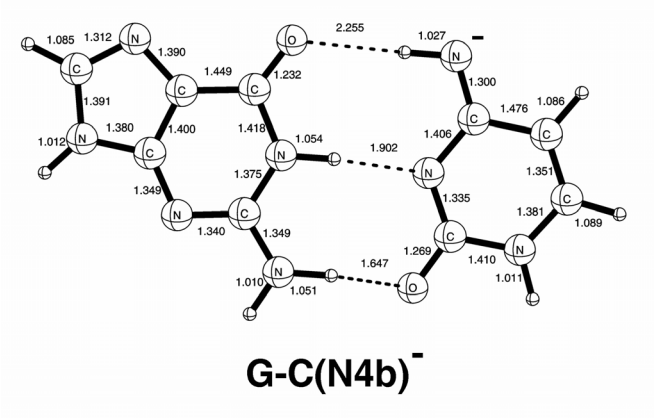

Figure 2.6. G-C(N4b)$^{-}$ optimized anion. All bond lengths are given in Angstroms.

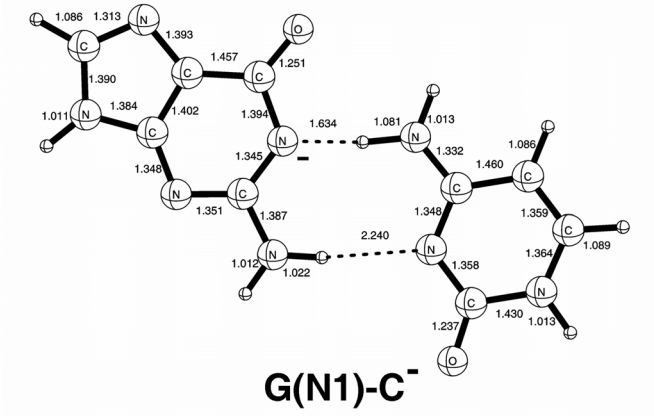

Figure 2.7. G(N1)-C^{-} optimized anion. All bond lengths are given in Angstroms.

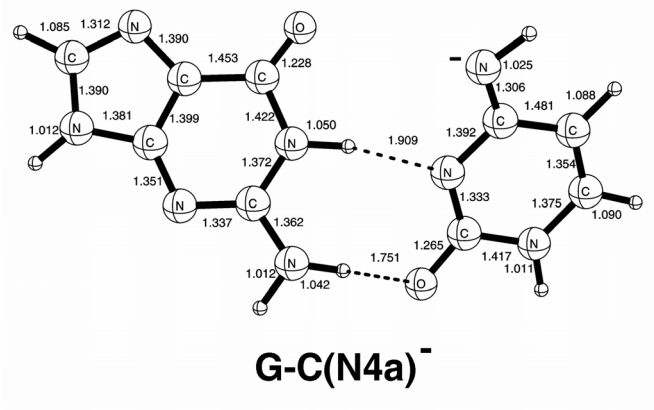

Figure 2.8. G-C(N4a)¯ optimized anion. All bond lengths are given in Angstroms.

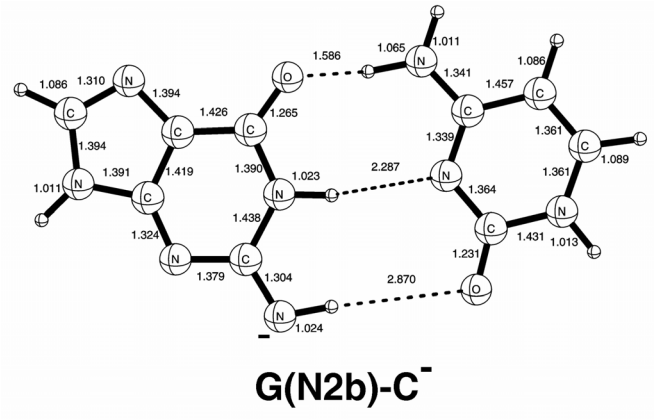

Figure 2.9 G(N2b)-C^{-} optimized anion. All bond lengths are given in Angstroms.

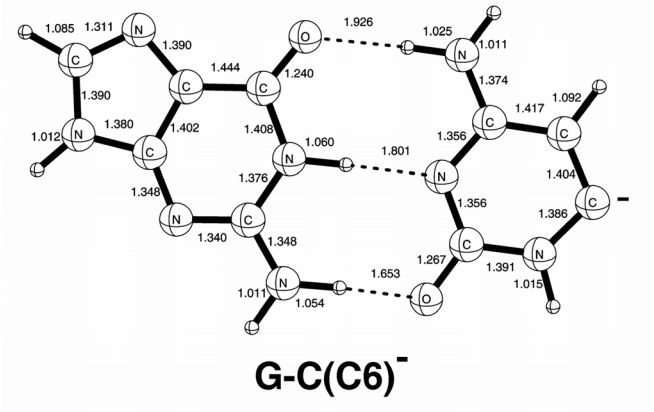

Figure 2.10. G-C(C6)¯ optimized anion. All bond lengths are given in Angstroms

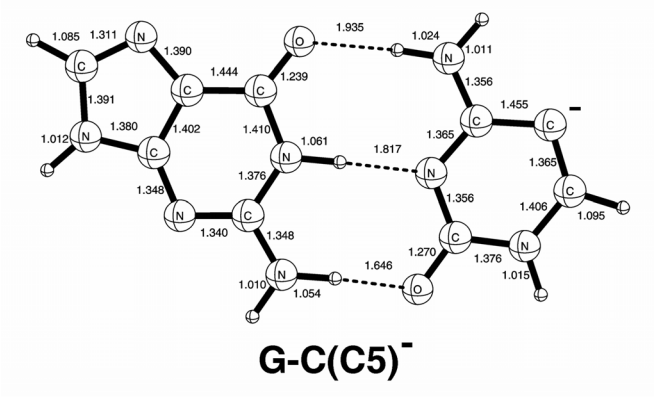

Figure 2.11. G-C(C5)¯ optimized anion. All bond lengths are given in Angstroms.

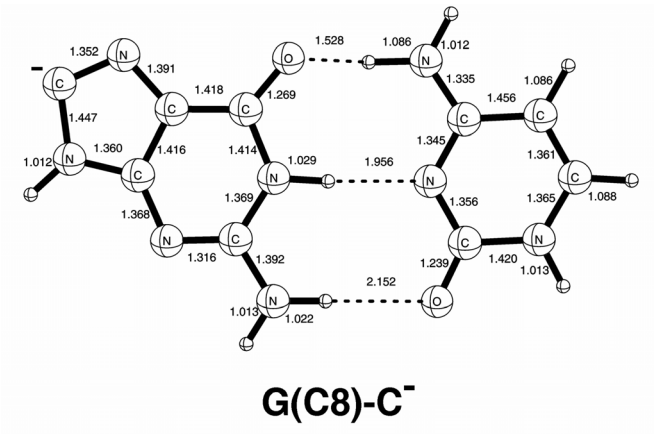

Figure 2.12. G(C8)-C^{-} optimized anion. All bond lengths are given in Angstroms.

CHAPTER 3

HYDROGEN-ABSTRACTED ADENINE-THYMINE RADICALS WITH INTERESTING TRANSFERABLE PROPERTIES[†]

[†] Maria C. Lind, Nancy A. Richardson, Steven E. Wheeler, and Henry F. Schaefer III, JOURNAL OF PHYSICAL CHEMISTRY B 111 (19): 5525-5530 MAY 17 2007. Reprinted here with permission of publisher.

3.1 ABSTRACT

The formation of radicals on DNA bases through various pathways can lead to harmful structural alterations. Such processes are of interest for preventing alteration of healthy DNA and, conversely, to develop more refined methods for inhibiting the replication of unwanted mutagenic DNA. In the present work, we explore theoretically the energetic and structural properties of the nine possible neutral radicals formed via hydrogen abstraction from the adenine-thymine base pair. The lowest energy radical is formed by loss of a hydrogen atom from the methyl group of thymine. The next lowest energy radicals, lying 8 and 9 kcal mol^{-1} higher than the global minimum, are those in which hydrogens are removed from the two nitrogens that would join the base pair to 2-deoxyribose in double-stranded DNA. The other six radicals lie between 16 and 32 kcal mol^{-1} higher in energy. Unlike the guanine-cytosine base pair, adenine-thymine (A-T) exhibits only minor structural changes upon hydrogen abstraction, with all A-T derived radicals maintaining planarity. Moreover, the energetic ordering for the radicals of the two isolated bases (adenine and thymine) is preserved upon formation of the base pair, though with a wider spread of energies. Even more significantly, the energetic interleaving of the $(A\text{-}H)^{\bullet}$ -T and A-$(T\text{-}H)^{\bullet}$ radicals is correctly predicted from the X-H bond dissociation energies of the isolated adenine and thymine. This suggests that the addition of the hydrogen-bonded complement base only marginally affects the bond energies.

3.2 INTRODUCTION

The quest to understand the role and effects of radical creation in DNA continues to be a vital aspect of exploring genetic damage and repair,[1,2] analyzing its interaction with enzymes and drugs,[3] and studying charge transport in this biologically central molecule.[4-7] Incident radiation (UV, X-ray, etc.) yields low-energy electrons as the most abundant secondary species in living cells.[8] Such electrons can then damage DNA in a number of ways, potentially leading to single- and double-strand breaks and subsequent loss of genetic information.[9-11]

One particular mode of damage by low-energy electrons arises through dissociative electron attachment.[9,12,13] In gas-phase experiments on the individual bases, anionic dehydrogenated species have been identified as the primary dissociative products.[14-16] Furthermore, nitrogen sites have been shown experimentally and theoretically to be the most likely candidates for hydrogen loss, rather than those of carbon.[17-20] We endeavor in the present research to predict energies of the neutral radicals formed by homolytic cleavage of bonds to hydrogen in the adenine-thymine (A-T) base pair.

Of particular interest are structural and energetic changes that occur upon radical formation within the subunits of DNA.[21-25] Initial steps toward such an understanding have been made by examining the effects of radical creation for the individual bases,[26] the H-added or H-abstracted individual bases,[27-31] the A-T and G-C base pairs,[32,33] and for the H-abstracted guanine-cytosine base pair.[34,35] Additionally the A-T and G-C base

pairs were found to have positive adiabatic electron affinities (0.36 and 0.60 eV, respectively).[32,33]

In the move to realistic models of the nucleic acid base radicals in DNA, an important element to include is the complementary base. Comparison of the energetic ordering for radicals of the base with its hydrogen-bonded complement will show in what ways and to what extent results (such as the energy ordering of the radicals) are similar in the two model systems. These results will indicate which aspects of the chemistry in these model systems can be extended to larger, more biologically relevant DNA models.

Figure 1 provides the IUPAC numbering scheme for the Watson-Crick adenine-thymine base pair. For reference, the optimized structure of the unaltered, gas-phase A-T base pair is shown in Figure 2. The hydrogen-abstracted radicals are specified by A for the parent adenine and T for the parent thymine, followed by the atom from which the hydrogen is removed in parentheses. Thus A(N9)$^{\bullet}$-T designates the radical created by homolytic cleavage of the N9-H bond on adenine. For the N6 site on adenine, removal of each hydrogen leads to a unique minimum, and the letters "a" and "b" are used to distinguish the two (see Figure 3). Note, however, that upon removal of any of the three methyl hydrogens from thymine the system relaxes to a single minimum, denoted by A-T(C7)$^{\bullet}$.

3.3 METHODS

Energies, optimized structures, and harmonic vibrational frequencies were computed using the generalized gradient approximation (GGA) exchange-correlation functional B3LYP. This is a pairing of Becke's three-parameter HF/DFT hybrid functional, B3,[36] with the correlation functional of Lee, Yang, and Parr, LYP.[37] All computations were performed using double-ζ quality basis sets with polarization and diffuse functions. The DZP++ basis sets were constructed by augmenting the Huzinaga-Dunning[38,39] sets of contracted double-ζ basis functions with one set of five d-type polarization functions for each C, N, and O. In addition, even tempered s and p type basis functions were added to each C, N, and O. The even tempered functions were designed following the prescription:[40]

$$\alpha_{\text{diffuse}} = \frac{1}{2}\left(\frac{\alpha_1}{\alpha_2} + \frac{\alpha_2}{\alpha_3}\right)\alpha_1$$

where α_1, α_2, and α_3 are three smallest Gaussian orbital exponents of s and p type primitive functions for a given atom ($\alpha_1 \leq \alpha_2 \leq \alpha_3$). The final DZP++ set contains 19 functions per C, N, and O atom (10s6p1d/5s3p1d). All structures were optimized via analytic gradient methods using tight convergence criteria. Harmonic vibrational frequencies were computed and used to derive zero-point vibrational energies (ZPVE) without the application of any empirical scaling factor. Numerical integration was performed using a fine grid of 75 radial shells with 302 angular points per shell. All computations were carried out using the QCHEM 3.0 suite of programs.[41]

Energetic properties of particular importance were evaluated as follows:

Relaxation Energy

RE = E(radical at optimized A-T geometry) – E(optimized radical)

Dissociation Energy

$DE = E[(A\text{-}H)^{\bullet}\text{-}T] - E(A\text{-}H)^{\bullet} - E(T)$

or

$DE = E[A\text{-}(T\text{–}H)^{\bullet}] - E(A) - E(T\text{–}H)^{\bullet}$

Bond Dissociation Energy

$BDE = E[(A\text{–}H)^{\bullet}\text{-}T] + E(H^{\bullet}) - E(A\text{-}T)$

or

$BDE = E[A\text{-}(T\text{–}H)^{\bullet}] + E(H^{\bullet}) - E(A\text{-}T)$

3.4 RESULTS

ENERGETICS

Table 1 shows relative energies for the nine A-T derived radicals, listed in energetic order. The energetically lowest lying radical (the global minimum) is $A\text{-}T(C7)^{\bullet}$, derived from loss of a methyl hydrogen on thymine. This radical has a dissociation energy, corresponding to separation of adenine from the thymine radical, of 12.5 kcal mol^{-1}. This radical is 3.7 eV higher in energy than neutral A-T.

The next two higher lying radicals arise from cleavage of N-H bonds. These nitrogen atoms are the sites of the glycosidic bonds in DNA, which attach the deoxyribose to the nucleic acid base. The amino radical formed on thymine, $A\text{-}T(N1)^{\bullet}$,

lies 8.0 kcal mol^{-1} higher than the global minimum [A-T(C7)$^{\bullet}$], while the analogous adenine radical, A(N9)$^{\bullet}$-T, lies 9.1 kcal mol^{-1} above the global minimum.

Considerably higher in energy (16.7 and 20.6 kcal mol^{-1} above the global minimum) are the amino derived radicals A(N6b)$^{\bullet}$-T and A(N6a)$^{\bullet}$-T. The removal of the hydrogen from A(N6a) disrupts one of the hydrogen bonds connecting adenine and thymine. In the isolated adenine radicals,[27] A(C2)$^{\bullet}$ is about 9 kcal mol^{-1} higher than A(N6a)$^{\bullet}$; however, the analogous species hydrogen bound to thymine are essentially isoenergetic. These two radicals, along with A(N6b)$^{\bullet}$-T, display the lowest dissociation energies, 5.9 kcal mol^{-1} for A(N6a)$^{\bullet}$-T, 8.8 kcal mol^{-1} for A(N6b)$^{\bullet}$-T, and 10.7 kcal mol^{-1} for A(C2)$^{\bullet}$-T.

Three other A-T derived radicals are higher lying still. Two result from breaking C-H bonds, A-T(C6)$^{\bullet}$ and A(C8)$^{\bullet}$-T. The highest lying of all is A-T(N3)$^{\bullet}$, indicating the steep energetic cost of removal of a hydrogen bond connecting adenine and thymine. To partially compensate for this there is a weak interaction between atom C2 on adenine and O2 on thymine, with a concomitant shortening of the H-O2 interatomic distance from 2.84 to 2.09 Å (Figure 4).

Previous analysis[27,42] of the neutral radicals derived from adenine predicted the energetic ordering to be A(N9)$^{\bullet}$ < A(N6b)$^{\bullet}$ < A(N6a)$^{\bullet}$ < A(*C*2)$^{\bullet}$ < A(C8)$^{\bullet}$. Similarly, the order for the isolated thymine radicals was found to be T(C7)$^{\bullet}$ < T(N1)$^{\bullet}$ < T(C6)$^{\bullet}$ < T(N3)$^{\bullet}$.[43] These two orderings may be compared with the presently predicted ordering for the hydrogen abstracted A-T radicals. One sees that the energetic orderings of the two

sets of radicals derived from the A-T base pair follows the same trends as the corresponding radicals derived from the individual bases.

One may propose an even more challenging test of the transferability of the properties of the $(A\text{-}H)^{\bullet}$ and $(T\text{-}H)^{\bullet}$ radicals to the $(AT\text{-}H)^{\bullet}$ family of radicals. Namely, is the energetic interleaving seen in Table 1 related to the X-H bond dissociation energies of the isolated adenine and thymine structures? Table 3 shows that this is indeed the case. The energetic ordering of the $(AT\text{-}H)^{\bullet}$ radicals perfectly follows the pattern of energies required for hydrogen atom removal from the isolated base. Thus the pairing of thymine- or adenine-derived radicals does not significantly alter the radical energetics, suggesting in this case an unexpected robustness of a single nucleic acid base as a model for paired bases. This is particularly remarkable when considering radicals in which a hydrogen involved in hydrogen bonding is removed.

Comparing radicals derived from isolated adenine and thymine bases with the analogous A-T radicals, relative energies change by less than 3 kcal mol^{-1} upon inclusion of the H-bonded complement for cases where the hydrogen removed is not involved in H-bonding. For example, $A(C8)^{\bullet}$ is 17.5 kcal mol^{-1} higher in energy than $A(N9)^{\bullet}$ and $A(C8)^{\bullet}$-T is 18.6 kcal mol^{-1} above $A(N9)^{\bullet}$-T. The largest change in relative energies occurs for $A(N6a)^{\bullet}$-T, where a hydrogen atom involved in H-bonding is removed: the paired structure lies 11.5 kcal mol^{-1} above the $A(N9)^{\bullet}$-T, whereas the isolated radical lies only 3.7 kcal mol^{-1} above $A(N9)^{\bullet}$.

GEOMETRIES

For comparison, the optimized structure of the closed-shell A-T base pair is shown in Figure 2. Fully optimized geometries of the A-T radicals formed via hydrogen abstraction from adenine are reported in Figure 3, while Figure 4 shows the fully optimized geometries of the A-T derived radicals arising from abstraction from thymine. Hydrogen bond lengths for all nine radicals are given in Table 2. All structures considered retain their planarity upon radical formation.

In both A(N6a)$^{\bullet}$-T (Figure 3) and A-T(N3)$^{\bullet}$ (Figure 4) there appears to be a weak interaction between C2 on adenine and O2 on thymine, indicated by the marked decrease in the corresponding interatomic distance relative to the unaltered A-T base pair (Table 2). However, these two radicals exhibit drastically different behavior, since the formation of this putative C-H···O interaction is accompanied by a weakening of the N6-H···O4 interaction in A(N6a)$^{\bullet}$-T, while this interaction is significantly strengthened in the case of A-T(N3)$^{\bullet}$. Indeed, the shortening of the N6-H···O4 distance to 1.65 Å affords sufficient energetic advantage to compensate for the presumably weak C2-H···O2 interaction. This yields a dissociation energy in the case of A-T(N3)$^{\bullet}$ comparable to A-T and the other radicals in which two conventional hydrogen bonds are maintained. This is not the case with A(N6a)$^{\bullet}$-T, for which the dissociation energy is a mere 5.9 kcal mol^{-1}.

3.5 DISCUSSION

How can the present theoretical results for DNA radicals be related to existing and future experiments? The experimental study of DNA bases and base pairs is a very

rapidly expanding field.[44-61] The role of DNA radicals in biochemistry is undisputed and well-described in the recent (2006) paper by Hong, Ding, and Greenberg:[22] "DNA radicals are an important family of reactive intermediates that give rise to modified intact polymers and also lead to single- and double-strand breaks."

As demonstrated in the present research, there are a number of low-lying AT radicals. In fact, the present system is unusual in that one radical isomer, A-T(C7)$^{\bullet}$, is favored over the others. This may greatly simplify the interpretation of future AT radical experiments. A more complicated case is that of the guanine radicals. Theoretical studies predict that there are four different energetically favorable (G-H)$^{\bullet}$ radicals, lying within a 5 kcal mol^{-1} range.[62] The energetically congested nature of these radical isomers has very recently been confirmed by experiment.[63] One of these four guanyl radical isomers is observed following one-electron oxidation of guanosine, while a different isomer is observed in EPR/ENDOR spectra following X-irradiation of the analogous nucleotide in the solid state at 10 K.

The three experimental papers most closely related to the present theoretical study are from the research groups of Illenberger and Märk[31,51] and Fischer.[55] In all three of these papers thymine radicals are observed in the laboratory. In the Illenberger-Märk experiments, free electron attachment to thymine is examined

$$T + e^- \rightarrow T^- \rightarrow (T-H)^{\bullet} + H^-$$

in an electron energy range 0-15 eV. The Fischer experiment is completely different,

utilizing two-color photofragment Doppler spectroscopy and one-color slice imaging to study thymine radicals $(T\text{-}H)^{\bullet}$.

Although different radical isomers have been observed in the above experiments,[20,31,51,55] the identification of the various isomers remains a challenge. Ptasinska and co-workers[31] observe three separate peaks and a broad shoulder in a mass spectrum of the DEA products of thymine. The four observed features are identified with H atom loss from N1 (5.5 eV), N3 (6.8 eV), and C6 (8.5 eV) and from the methyl group C7 (~10 eV). These are the four $(T\text{-}H)^{\bullet}$ radicals predicted in the present research for $(T\text{-}H)^{\bullet}$. The energetic ordering in our theoretical study is C7 < N1 < C6 < N3, with the C7 radical lying lowest in energy.

The experimental photodissociation paper by Schneider and co-workers[55] suggests an ordering of the thymine radicals consistent with the present research. Further, Schneider et al. note that their earlier experiments on 9-methyladenine demonstrate contributions from methyl C-H dissociation. It is certainly clear that the reliable interpretation of the thymine experiments requires parallel theoretical approaches. For the adenine-thymine system, theoretical predictions will be essential to the understanding of future experiments.

3.6 CONCLUDING REMARKS

The most likely site for hydrogen atom removal from the A-T base pair is the methyl group of thymine. Also relatively easily formed in the A-T base pair are radicals formed from N-H bond cleavage of amino nitrogens, which are not coincidentally the

sites of the glycosidic bonds in DNA. The localized energetic ordering remains the same for isolated adenine radicals as for adenine radicals hydrogen bonded to thymine and for isolated thymine radicals as for thymine radicals hydrogen bonded to adenine. While the overall intrabase ordering is maintained, certain relative energetic spacings change due to hydrogen bond disruption, though most of these changes are less than 3 kcal mol^{-1}. That the energetic ordering of radicals derived from the individual bases is unperturbed by pairing of these radicals with the complementary bases suggests that conclusions drawn based on individual bases may be extended to larger model DNA systems.

Except for hydrogen bond length changes for some of the radicals, the A-T base pair geometry is resilient to formation of radicals through hydrogen abstraction. This is in contrast to the G-C base pair, in which hydrogen abstraction invokes significant changes on base pair geometry, in some cases spurring large deviations from planarity.[34]

3.7 ACKNOWLEDGEMENTS

This research was supported by National Science Foundation under Grant CHE-0451445. Figures 2-4 were generated using *HFSMOL*.[64]

3.8 REFERENCES

1 P. Swiderek, Angewandte Chemie-International Edition **45** (25), 4056 (2006).

2 B. Boudaiffa, P. Cloutier, D. Hunting, M. A. Huels, and L. Sanche, Science **287** (5458), 1658 (2000).

3 F. Q. Ban, M. J. Lundqvist, R. J. Boyd, and L. A. Eriksson, Journal of the American Chemical Society **124** (11), 2753 (2002).

[4] M. Bixon and J. Jortner, Chemical Physics **319** (1-3), 273 (2005).

[5] K. Senthilkumar, F. C. Grozema, C. F. Guerra, F. M. Bickelhaupt, F. D. Lewis, Y. A. Berlin, M. A. Ratner, and L. D. A. Siebbeles, Journal of the American Chemical Society **127** (42), 14894 (2005).

[6] Y. A. Berlin, A. L. Burin, and M. A. Ratner, Journal of the American Chemical Society **123** (2), 260 (2001).

[7] M. Volobuyev and L. Adamowicz, Journal of Physical Chemistry B **109** (2), 1048 (2005).

[8] L. Sanche, European Physical Journal D **35** (2), 367 (2005).

[9] X. Pan, P. Cloutier, D. Hunting, and L. Sanche, Physical Review Letters **90** (20), 208102 (2003).

[10] M. M. Vilenchik and A. G. Knudson, Proceedings of the National Academy of Sciences of the United States of America **100** (22), 12871 (2003).

[11] R. Barrios, P. Skurski, and J. Simons, Journal of Physical Chemistry B **106** (33), 7991 (2002).

[12] J. Berdys, I. Anusiewicz, P. Skurski, and J. Simons, Journal of the American Chemical Society **126** (20), 6441 (2004).

[13] I. Bald, J. Kopyra, and E. Illenberger, Angewandte Chemie-International Edition **45** (29), 4851 (2006).

[14] B. Liu, P. Hvelplund, S. B. Nielsen, and S. Tomita, Journal of Chemical Physics **121** (9), 4175 (2004).

[15] H. Abdoul-Carime, J. Langer, M. A. Huels, and E. Illenberger, European Physical Journal D **35** (2), 399 (2005).

[16] S. Denifl, S. Ptasinska, M. Probst, J. Hrusak, P. Scheier, and T. D. Mark, Journal of Physical Chemistry A **108** (31), 6562 (2004).

[17] H. Abdoul-Carime, S. Gohlke, and E. Illenberger, Physical Review Letters **92** (16), 168103 (2004).

[18] X. F. Li, M. D. Sevilla, and L. Sanche, Journal of Physical Chemistry B **108** (49), 19013 (2004).

[19] X. F. Li, L. Sanche, and M. D. Sevilla, Radiation Research **165** (6), 721 (2006).

[20] S. Ptasinska, S. Denifl, P. Scheier, E. Illenberger, and T. D. Mark, Angewandte Chemie-International Edition **44** (42), 6941 (2005).

[21] I. S. Hong and M. M. Greenberg, Journal of the American Chemical Society **127** (11), 3692 (2005).

[22] I. S. Hong, H. Ding, and M. M. Greenberg, Journal of the American Chemical Society **128** (2), 485 (2006).

[23] X. G. Bao, J. Wang, J. D. Gu, and J. Leszczynski, Proceedings of the National Academy of Sciences of the United States of America **103** (15), 5658 (2006).

[24] J. D. Gu, J. Wang, and J. Leszczynski, Journal of the American Chemical Society **128** (29), 9322 (2006).

[25] A. F. Jalbout, J. Smets, and L. Adamowicz, Chemical Physics **273** (1), 51 (2001).

[26] S. S. Wesolowski, M. L. Leininger, P. N. Pentchev, and H. F. Schaefer, Journal of the American Chemical Society **123** (17), 4023 (2001).

[27] F. A. Evangelista, A. Paul, and H. F. Schaefer, Journal of Physical Chemistry A **108** (16), 3565 (2004).

[28] L. T. M. Profeta, J. D. Larkin, and H. F. Schaefer, Molecular Physics **101** (22), 3277 (2003).

[29] Q. Luo, J. Li, Q. S. Li, S. Kim, S. E. Wheeler, Y. M. Xie, and H. F. Schaefer, Physical Chemistry Chemical Physics **7** (5), 861 (2005).

[30] J. K. Wolken, E. A. Syrstad, S. Vivekananda, and F. Turecek, Journal of the American Chemical Society **123** (24), 5804 (2001).

[31] S. Ptasinska, S. Denifl, B. Mroz, M. Probst, V. Grill, E. Illenberger, P. Scheier, and T. D. Mark, Journal of Chemical Physics **123** (12), 124302 (2005).

[32] N. A. Richardson, S. S. Wesolowski, and H. F. Schaefer, Journal of the American Chemical Society **124** (34), 10163 (2002).

[33] N. A. Richardson, S. S. Wesolowski, and H. F. Schaefer, Journal of Physical Chemistry B **107** (3), 848 (2003).

[34] P. P. Bera and H. F. Schaefer, Proceedings of the National Academy of Sciences of the United States of America **102** (19), 6698 (2005).

[35] M. C. Lind, P. P. Bera, N. A. Richardson, S. E. Wheeler, and H. F. Schaefer, Proceedings of the National Academy of Sciences of the United States of America **103** (20), 7554 (2006).

[36] A. D. Becke, Journal of Chemical Physics **98** (7), 5648 (1993).

[37] C. T. Lee, W. T. Yang, and R. G. Parr, Physical Review B **37** (2), 785 (1988).

[38] S. Huzinaga, Journal of Chemical Physics **42** (4), 1293 (1965).

[39] T. H. Dunning, Journal of Chemical Physics **53** (7), 2823 (1970).

[40] T. J. Lee and H. F. Schaefer, Journal of Chemical Physics **83** (4), 1784 (1985).

[41] Y. Shao, L. F. Molnar, Y. Jung, J. Kussmann, C. Ochsenfeld, S. T. Brown, A. T. B. Gilbert, L. V. Slipchenko, S. V. Levchenko, D. P. O'Neill, R. A. DiStasio, R. C. Lochan, T. Wang, G. J. O. Beran, N. A. Besley, J. M. Herbert, C. Y. Lin, T. Van Voorhis, S. H. Chien, A. Sodt, R. P. Steele, V. A. Rassolov, P. E. Maslen, P. P. Korambath, R. D. Adamson, B. Austin, J. Baker, E. F. C. Byrd, H. Dachsel, R. J. Doerksen, A. Dreuw, B. D. Dunietz, A. D. Dutoi, T. R. Furlani, S. R. Gwaltney, A. Heyden, S. Hirata, C. P. Hsu, G. Kedziora, R. Z. Khalliulin, P. Klunzinger, A. M. Lee, M. S. Lee, W. Liang, I. Lotan, N. Nair, B. Peters, E. I. Proynov, P. A. Pieniazek, Y. M. Rhee, J. Ritchie, E. Rosta, C. D. Sherrill, A. C. Simmonett, J. E. Subotnik, H. L. Woodcock, W. Zhang, A. T. Bell, A. K. Chakraborty, D. M. Chipman, F. J. Keil, A. Warshel, W. J. Hehre, H. F. Schaefer, J. Kong, A. I. Krylov, P. M. W. Gill, and M. Head-Gordon, Physical Chemistry Chemical Physics **8** (27), 3172 (2006).

[42] S. D. Wetmore, R. J. Boyd, and L. A. Eriksson, Journal of Physical Chemistry B **102** (51), 10602 (1998).

[43] S. D. Wetmore, R. J. Boyd, and L. A. Eriksson, Journal of Physical Chemistry B **102** (27), 5369 (1998).

[44] E. Nir, K. Kleinermanns, and M. S. de Vries, Nature **408** (6815), 949 (2000).

[45] C. Chatgilialoglu, M. Guerra, and Q. G. Mulazzani, Journal of the American Chemical Society **125** (13), 3839 (2003).

[46] C. Plutzer, I. Hunig, K. Kleinermanns, E. Nir, and M. S. de Vries, Chemphyschem **4** (8), 838 (2003).

[47] X. Yang, X. B. Wang, E. R. Vorpagel, and L. S. Wang, Proceedings of the National Academy of Sciences of the United States of America **101** (51), 17588 (2004).

[48] C. E. Crespo-Hernandez, B. Cohen, P. M. Hare, and B. Kohler, Chemical Reviews **104** (4), 1977 (2004).

[49] C. Chatgilialoglu, M. Duca, C. Ferreri, M. Guerra, M. Ioele, Q. G. Mulazzani, H. Strittmatter, and B. Giese, Chemistry-a European Journal **10** (5), 1249 (2004).

[50] A. Abo-Riziq, L. Grace, E. Nir, M. Kabelac, P. Hobza, and M. S. de Vries, Proceedings of the National Academy of Sciences of the United States of America **102** (1), 20 (2005).

[51] S. Ptasinska, S. Denifl, V. Grill, T. D. Mark, P. Scheier, S. Gohlke, M. A. Huels, and E. Illenberger, Angewandte Chemie-International Edition **44** (11), 1647 (2005).

[52] H. W. Jochims, M. Schwell, H. Baumgartel, and S. Leach, Chemical Physics **314** (1-3), 263 (2005).

[53] A. Abo-Riziq, B. Crews, L. Grace, and M. S. de Vries, Journal of the American Chemical Society **127** (8), 2374 (2005).

[54] D. Radisic, K. H. Bowen, I. Dabkowska, P. Storoniak, J. Rak, and M. Gutowski, Journal of the American Chemical Society **127** (17), 6443 (2005).

[55] M. Schneider, R. Maksimenka, F. J. Buback, T. Kitsopoulos, L. R. Lago, and I. Fischer, Physical Chemistry Chemical Physics **8** (25), 3017 (2006).

[56] D. Huber, M. Beikircher, S. Denifl, F. Zappa, S. Matejcik, A. Bacher, V. Grill, T. D. Mark, and P. Scheier, Journal of Chemical Physics **125** (8), 084304 (2006).

[57] H. Satzger, D. Townsend, M. Z. Zgierski, S. Patchkovskii, S. Ullrich, and A. Stolow, Proceedings of the National Academy of Sciences of the United States of America **103** (27), 10196 (2006).

[58] S. Denifl, F. Zappa, I. Mahr, J. Lecointre, M. Probst, T. D. Mark, and P. Scheier, Physical Review Letters **97** (4), 043201 (2006).

[59] G. Pratviel and B. Meunier, Chemistry-a European Journal **12** (23), 6018 (2006).

[60] M. Russo, L. B. Jimenez, Q. G. Mulazzani, M. D'Angelantonio, M. Guerra, M. A. Miranda, and C. Chatgilialoglu, Chemistry-a European Journal **12** (29), 7684 (2006).

[61] S. Ptasinska, S. Denifl, S. Gohlke, P. Scheier, E. Illenberger, and T. D. Mork, Angewandte Chemie-International Edition **45** (12), 1893 (2006).

[62] A. O. Colson, B. Besler, D. M. Close, and M. D. Sevilla, Journal of Physical Chemistry **96** (2), 661 (1992).

[63] C. Chatgilialoglu, C. Caminal, A. Altieri, G. C. Vougioukalakis, Q. G. Mulazzani, T. Gimisis, and M. Guerra, Journal of the American Chemical Society **128** (42), 13796 (2006).

[64] S. E. Wheeler, HFSMOL (Univ. of Georgia, Athens, GA, 2005).

Table 3.1. Relative energies (ΔE), Relaxation Energies (RE), and Dissociation Energies (DE) of Hydrogen-Abstracted A-T radicals (ZPVE Corrected Energies in Parentheses)[a]

Radical	ΔE	RE	DE
A-T(C7)$^{\bullet}$	0.00 (0.00)	15.81	12.48
A-T(N1)$^{\bullet}$	8.66 (7.96)	5.52	12.04
A(N9)$^{\bullet}$-T	9.37 (9.12)	12.81	13.64
A(N6b)$^{\bullet}$-T	17.22 (16.63)	4.35	8.75
A(N6a)$^{\bullet}$-T	21.63 (20.57)	8.36	5.88
A(C2)$^{\bullet}$-T	21.79 (21.88)	2.32	10.71
A-T(C6)$^{\bullet}$	24.31 (23.97)	1.60	12.92
A(C8)$^{\bullet}$-T	27.71 (27.76)	1.29	12.46
A-T(N3)$^{\bullet}$	31.98 (31.55)	8.15	11.88

[a] Dissociation energies DE are for either the process A-(T–H)$^{\bullet}$ → A + (T–H)$^{\bullet}$ or (A–H)$^{\bullet}$-T → (A–H)$^{\bullet}$- + T. All energies are reported in kcal mol^{-1}.

Table 3.2. Selected Interatomic Distances (Å) for Hydrogen Abstracted A-T Radicals

radical	r[A(H6a)•••T(O4)]	r[A(N1)•••T(H3)]	r[A(H2)•••T(O2)]
A-T	1.891	1.797	2.835
A-T(C7)$^{\bullet}$	1.910	1.789	2.787
A-T(N1)$^{\bullet}$	1.941	1.789	2.808
A(N9)$^{\bullet}$-T	1.783	1.841	3.022
A(C2)$^{\bullet}$-T	1.829	1.920	-
A(N6b)$^{\bullet}$-T	2.131	1.847	2.707
A(N6a)$^{\bullet}$-T	-	2.058	2.262
A-T(C6)$^{\bullet}$	1.900	1.781	2.805
A(C8)$^{\bullet}$-T	1.882	1.808	2.847
A-T(N3)$^{\bullet}$	1.649	-	2.088

Table 3.3. X-H Bond Dissociation Energies (eV) for Adenine and Thymine, Compared with the Hydrogen-Bonded A-T Base Pair.

Radical	BDE		Radical	BDE
T(C7)$^{\bullet}$	3.68		A-T(C7)$^{\bullet}$	3.68
T(N1)$^{\bullet}$	4.00		A-T(N1)$^{\bullet}$	4.02
A(N9)$^{\bullet}$	4.12		A(N9)$^{\bullet}$-T	4.07
A(N6b)$^{\bullet}$	4.24		A(N6b)$^{\bullet}$-T	4.40
A(N6a)$^{\bullet}$	4.28		A(N6a)$^{\bullet}$-T	4.57
A(C2)$^{\bullet}$	4.55		A(C2)$^{\bullet}$-T	4.63
T(C6)$^{\bullet}$	4.74		A-T(C6)$^{\bullet}$	4.72
A(C8)$^{\bullet}$	4.88		A(C8)$^{\bullet}$-T	4.88
T(N3)$^{\bullet}$	5.02		A-T(N3)$^{\bullet}$	5.05

[a] These dissociation energies have been corrected for zero-point vibrational energies.

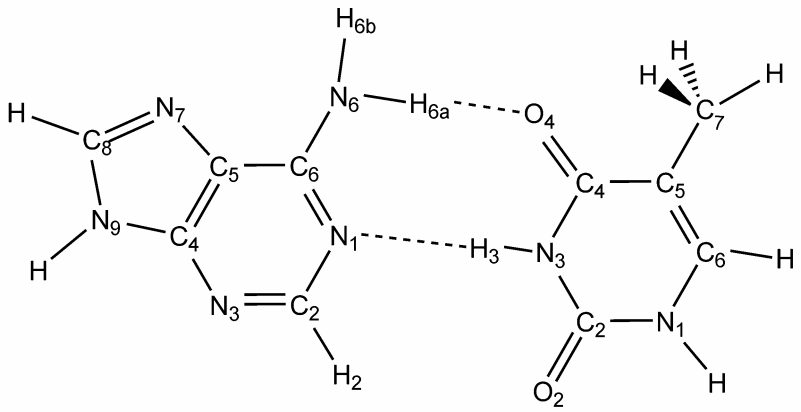

Figure 3.1. IUPAC numbering scheme for the A-T base pair.

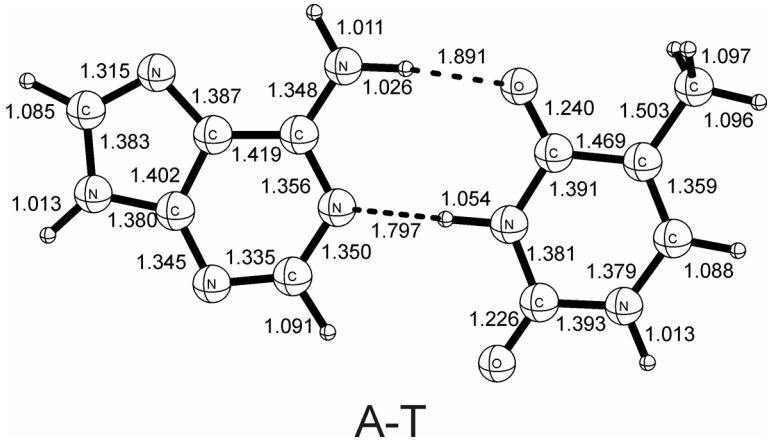

Figure 3.2. Optimized geometry of the closed-shell neutral ground state A-T base pair. All bond lengths are reported in Angstroms.

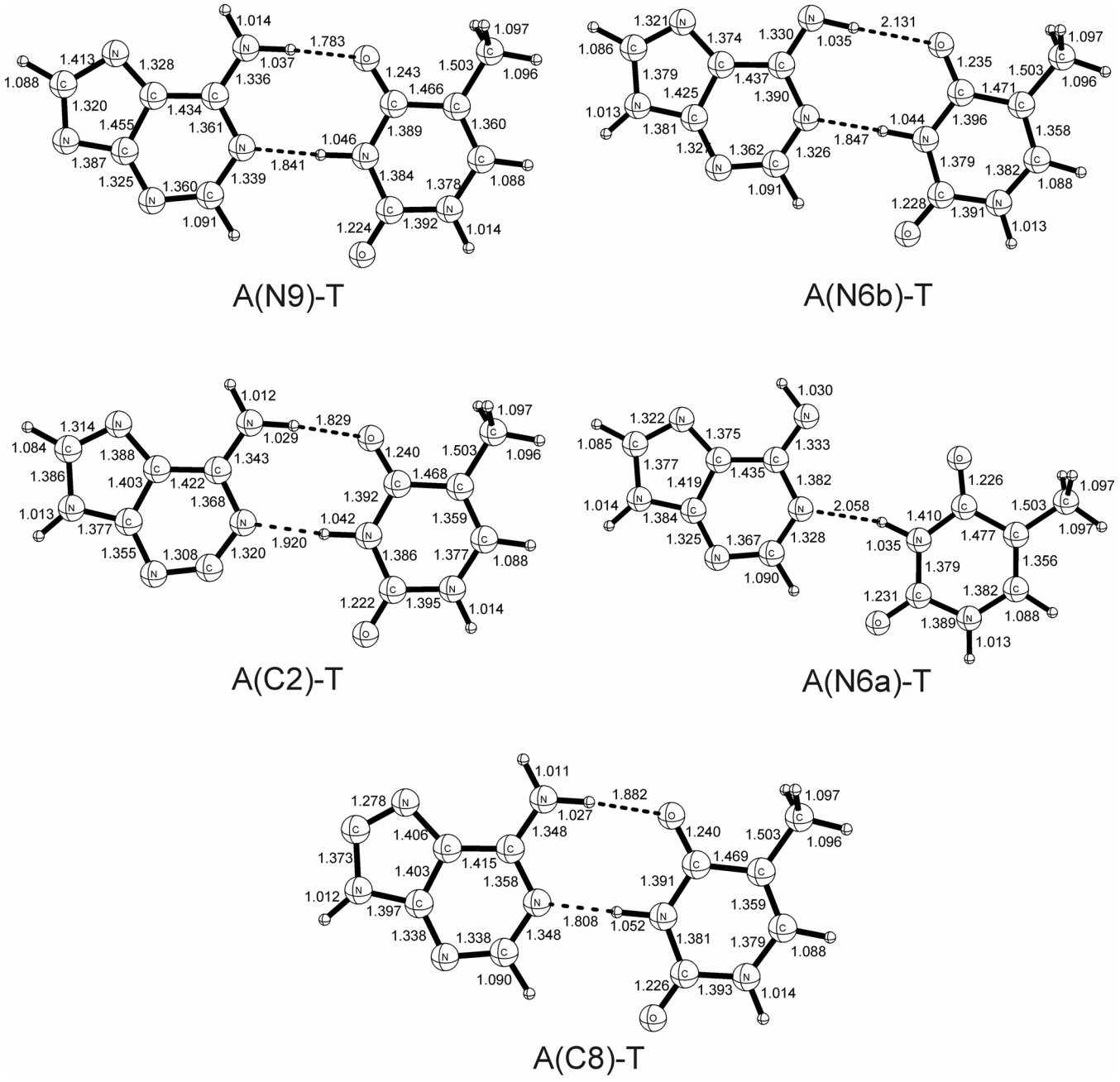

Figure 3.3. Optimized geometries of neutral doublet radicals derived from A-T by abstraction of one hydrogen atom from adenine. All bond lengths are reported in Angstroms.

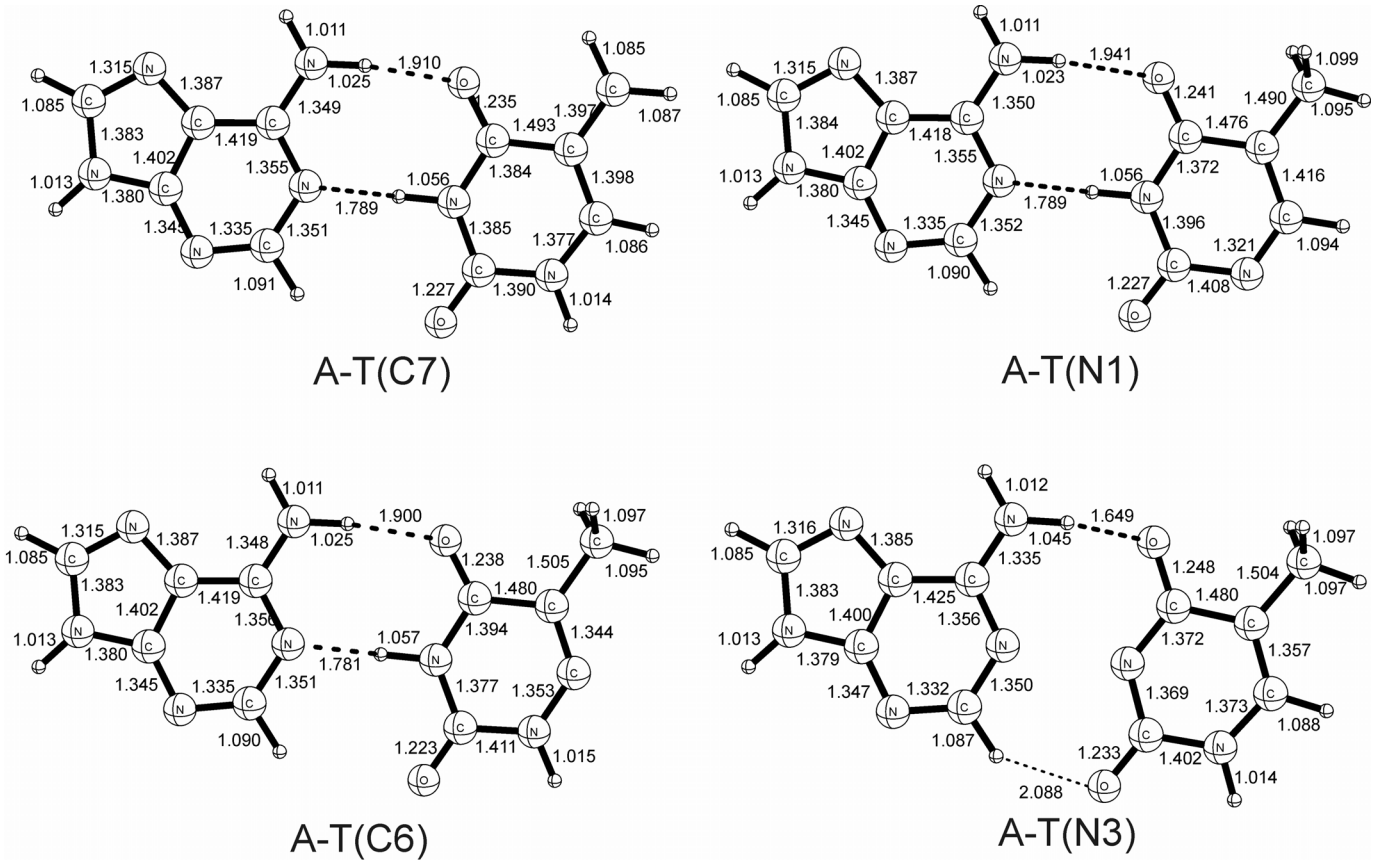

Figure 3.4. Optimized geometries of neutral doublet radicals derived from A-T by abstraction of one hydrogen atom from thymine. All bond lengths are reported in Angstroms.

CHAPTER 4

CHARACTERIZATION OF THE HSiN – HNSi SYSTEM IN ITS ELECTRONIC GROUND STATE[†]

[†] Maria C. Lind, Frank C. Pickard, Justin B. Ingels, Heather M. Jaeger, Ankan Paul, Yukio Yamaguchi, and Henry F. Schaefer III, *submitted, Journal of Chemical Physics*.

4.1 ABSTRACT

The electronic ground states ($\tilde{X}\ ^1\Sigma^+$) of HNSi, HSiN, and the transition state connecting the two isomers were systematically studied using single reference self-consistent-field (SCF), configuration interaction with single and double excitations (CISD), coupled cluster with single and double excitations (CCSD), CCSD with perturbative triple corrections [CCSD(T)], multireference complete active space self-consistent-field (CASSCF), and internally contracted multireference configuration interaction (ICMRCI) methods. The correlation-consistent polarized valence (cc-pVXZ), augmented correlation-consistent polarized valence (aug-cc-pVXZ) (X=T,Q,5), correlation-consistent polarized core-valence (cc-pCVYZ), and augmented correlation-consistent polarized core-valence (aug-cc-pCVYZ) (Y= T and Q) basis sets were used. The HNSi isomer has been confirmed to be the global minimum on the ground state HSiN-HNSi surface and is predicted to lie 68.8 kcal/mol (24100 cm^{-1}, 2.98 eV) [65.4 kcal/mol (22900 cm^{-1}, 2.84 eV) with the zero-point vibrational energy (ZPVE) corrections] below the HSiN isomer at the aug-cc-pCVQZ CCSD(T) level of theory. The dipole moments of the HNSi and HSiN isomers are determined to be 0.26 and 4.36 debye, respectively. The theoretical vibrational isotopic shifts for the HNSi/DNSi and HSiN/DSiN isotopomers are in reasonable agreement with the available experimental values. The barrier height for the isomerization reaction (HSiN→HNSi) is predicted to be 10.8 kcal/mol (10.1 kcal/mol with the ZPVE corrections), while the barrier height for the isomerization reaction (HNSi→ HSiN) is determined to be 79.6 kcal/mol (75.5 kcal/mol with the ZPVE corrections). The dissociation energy for HNSi [HNSi ($\tilde{X}\ ^1\Sigma^+$) → H(^{2}S)+NSi($X\ ^2\ \Sigma^+$)] is predicted to be D_e=132.0 kcal/mol (D_0=125.0 kcal/mol),

whereas the dissociation energy for HSiN [HSiN ($\tilde{X}\ ^1\Sigma^+$) → H(^{2}S)+SiN ($X\ ^2\ \Sigma^+$)] is predicted to be D_e= 63.2 kcal/mol (D_0=59.6 kcal/mol).

4.2 INTRODUCTION

The HSiN-HNSi system is isovalent to the exhaustively studied HCN-HNC system with ten valence electrons but interestingly, exhibits the opposite trend in relative stability of the isomers. The HNSi and HSiN isomers have been the subject of many astrophysical, experimental, and theoretical studies addressing their formation and existence in interstellar space, spectroscopic detection in laboratories, characterization of the silicon containing bonds, relative stability, and chemical reactivities.

In 1966 Ogilvie and Cradock investigated the infrared (IR) absorption spectra of the silyl and trideuterosilyl azides (SiH_3N_3 and SiD_3N_3) and their photodecomposition products in argon matrices near 4 K.[1] After irradiation of SiH_3N_3 and SiD_3N_3 separately in argon near 4 K by means of a high-pressure mercury lamp, the IR absorption spectra showed a decrease in intensity of bands assigned to silyl azides, and the appearance of several new bands. The most notable of those were 3583, 523, and 1198 cm^{-1} for the HNSi (iminosilicon) isomer and 2669, 395, and 1166 cm^{-1} for the DNSi (deuteroiminosilicon) isomer. After analyzing the force constants of the three vibrations, Ogilvie and Cradock concluded that iminosilicon represents the first detected discrete stable molecule with silicon multiply bonded to another atom.

In 1991 Elhanine, Farrenq, and Guelachvili reported the first spectroscopic observation of the HNSi molecule in the gas phase.[2] The emission spectrum of the fundamental vibration-rotation ν_1 band (NH stretch) of HNSi was observed near 2.7 μm

(3584 cm^{-1}) by high resolution Fourier transform spectroscopy from a mixture of N_2 + SiH_4 excited in a radio frequency discharge. Also in 1991, Bogey, Demuynck, Destombes, and Walters investigated the rotational spectrum of HNSi in the 150-460 GHz frequency range.[3] The HNSi molecule was produced by a discharge in a mixture of SiH_4 and N_2. The observation of nine lines led to the determination of the rotational constant B_0 and the centrifugal distortion constant D_0 values: B_0=19018.8 MHz and D_0=20.63 KHz. The identification of the HNSi molecule was confirmed by the observation of the ^{29}Si and ^{30}Si isotopomers.

From the vibration-rotation term energies calculated variationally and perturbatively using the CEPA-1 potential and the experimental rotational constants B_0 of $HN^{28}Si$, $HN^{29}Si$, and $HN^{30}Si$, Botschwina *et. al.* determined the equilibrium geometry of HNSi.[4] Their equilibrium bond lengths based on the variational ro-vibrational method are r_e(NH)=1.00047 and r_e(SiN)=1.54820 Å and those based on the ro-vibrational perturbation theory are r_e(NH)=0.99983 and r_e(SiN)=1.54803 Å.

In 1993 Goldberg, Iraqi, Hrušák, and Schwarz reported the generation and identification of neutral and cationic HNSi by neutralization-reionization mass spectrometry with Gaussian-1 *ab initio* molecular orbital (MO) calculations.[5] Mass spectrometric studies demonstrated that electron bombardment of a mixture of N_2/SiH_3I resulted in the formation of $HNSi^+$ which can be neutralized to the HNSi species. Both theory and experiment pointed to the formation of $HNSi^+(^2\Sigma^+)$/$HNSi(^1\Sigma^+)$ rather than the isomeric forms $NSiH^+(^2\Sigma^+)$/$NSiH(^1\Sigma^+)$. In the same year, Elhanine, Hanoune, and Guelachvili observed four hot bands of HNSi, $2\nu_1$-ν_1, ν_1+ν_3-ν_3, $2\nu_1$+ν_3-(ν_1+ν_3), and ν_1+ν_2-ν_2 in emission from a radio frequency excited plasma with a high resolution

Fourier transform interferometer.[6] Utilizing the four hot band frequencies, they determined the equilibrium rotational and vibrational parameters for the first time.

Maier and Glatthaar reported a matrix isolation study of silane nitrile (HSiN) and its adduct with hydrogen in 1994.[7] They were able to detect aminosilylene $HSiNH_2$, silane imine H_2SiNH, iminosilylene HNSi, and silane nitrile HSiN by irradiation of silyl azides (H_2SiN_3 and D_2SiN_3) in an argon matrix with different wavelengths of light source, using ultraviolet (UV) and IR spectroscopy. For the HNSi isomer, IR absorptions were observed at ν=3585, 3580 (NH stretching), 1202, 1200 (SiN stretching), and 522 (bending) cm^{-1}, whereas for the HSiN isomer IR absorptions were observed at 2151, 2149 (SiH stretching) and 1163, 1161 (SiN stretching) cm^{-1}. They stated that the HSiN molecule is the first compound with a formal Si≡N triple bond of the nitrile type to be identified spectroscopically. Additional structural evidence for HSiN was derived from the fact that it loses a hydrogen atom on prolonged irradiation at 193 nm, and is transformed into the well-known SiN radical.

In the earlier theoretical *ab initio* studies carried out by two independent groups[8,9] it was predicted that HNSi should be considerably more stable than HSiN, in contrast to the situation for the isovalent HCN-HNC system, where HCN is the more stable isomer.

In 1986 Luke *et. al.* reported a theoretical survey of unsaturated or multiply bonded and divalent silicon compounds using *ab initio* HF and MP4SDTQ methods.[10] At the MP4SDTQ/6-31G* level of theory they found HCN is 16.8 kcal/mol more stable than HNC, whereas HNSi with a lone pair on silicon is 55.0 kcal/mol more stable than HSiN with a lone pair on nitrogen. Their rationalization was based on the argument that silicon

prefers to have nonbonding electrons in atomic orbitals with a high percentage of s-character.[11-13]

In 1991 Apeloig and Albrecht theoretically studied the relative stabilities and energy barriers separating silanitiriles (RSiN) and silaisonitiriles (RNSi).[14] They found that in general, elements which are more electropositive than Si increase the RSiN vs. RNSi energy differences (relative to R=H), while the more electronegative elements decrease the energy gap. The activation energy for the RSiN → RNSi isomerization is relatively small for R=H (~11.4 kcal/mol). For R=F and OH the barrier heights (RNSi → RSiN) are larger, i.e. ~22.7 and 28.4 kcal/mol, respectively, suggesting that these rearrangements will be slow even at ambient temperatures.

In 1996 and 1997 Parisel, Hanus, and Ellinger published a series of theoretical papers on interstellar silicon-nitrogen chemistry.[15,16] In the first part of the series they reported the microwave and infrared signatures of the HSiN, HNSi, $HSiNH_2$, $HNSiH_2$, and $HSiNH^+$ species. A number of comparisons with the available rotational and vibrational experimental spectra led to the determination of accurate scaling factors used to calibrate original *ab initio* results. They pointed out that non-dynamic correlation effects are of particular importance in investigating the HSiN isomer.

In 2003 Hu, Wang, Wang, Chu, and Liu reported a theoretical study on gas-phase reactions between silane (SiH_4) and ammonia (NH_3) using *ab initio* methods at the CCSD(T)/6-311++G**//MP2/6-31+G* level of theory.[17] Within a 180 kcal/mol energy range, they located 34 equilibria and 23 transition states for various products of the two molecules. In their study, the HNSi isomer was found to be 67.5 kcal/mol [64.7 kcal/mol with the zero-point vibrational energy (ZPVE) corrections] lower in energy than the

HSiN isomer. The barrier height for the lower-barrier isomerization reaction (HSiN → HNSi) was predicted to be 11.1 kcal/mol (10.0 kcal/mol with ZPVE corrections).

In the present research, the electronic ground state potential energy surface of the HSiN-HNSi system has been systematically investigated employing *ab initio* single reference SCF, CISD, CCSD,[18,19] and CCSD(T),[20,21] multireference complete active space self-consistent-field (CASSCF),[22-24] and internally contracted multireference configuration interaction (ICMRCI)[25-27] methods with significantly larger basis sets than used in previous studies. The physical properties and energetics predicted in the current work are expected to be of most extensive and highest accuracy to date.

4.3 ELECTRONIC STRUCTURE CONSIDERATIONS

The electronic structure of the linear $\tilde{X}\ ^1\Sigma^+$ HNSi molecule may be described as:

$$[\text{core}](5\sigma)^2(6\sigma)^2(7\sigma)^2(2\pi)^4 \quad \tilde{X}\ ^1\Sigma^+, \tag{1}$$

where [core] denotes the six core orbitals (Si: 1s-, 2s-, 2p-like; N:1s-like). The 5σ and 6σ orbitals are associated with the NH and SiN σ bonds. The 7σ orbital is related to the lone pair (non-bonding) orbital on the Si atom. The 2π orbital has SiN π bonding character. The two highest occupied molecular orbitals (HOMOs, 7σ and 2π) of HNSi at the cc-pVTZ CASSCF level of theory are depicted in Figure 1. For reference, the 3π (LUMO) orbital is also included in Figure 1. The electronic structure of the linear $\tilde{X}\ ^1\Sigma^+$ HSiN isomer may likewise be expressed as:

$$[\text{core}](5\sigma)^2(6\sigma)^2(7\sigma)^2(2\pi)^4 \quad \tilde{X}\ ^1\Sigma^+. \tag{2}$$

Here the 5σ and 6σ orbitals describe the SiN and SiH σ bonds, respectively. The 7σ orbital is related to the lone pair (non-bonding) orbital on the N atom. The 2π orbital has

a SiN π bonding nature. The two HOMOs (7σ and 2π) and the 3π of HSiN at the cc-pVTZ CASSCF level of theory are depicted in Figure 2. The electronic structure at the isomerization reaction transition state may be written as:

$$[\text{core}](6a')^2(7a')^2(8a')^2(2a'')^2(9a')^2 \quad \tilde{X}\ ^1A'. \qquad (3)$$

For bent configurations, the in-plane π orbital (of the linear configuration) may interact with the σ orbitals and form C_s symmetry admixtures of the σ and π bonds.

4.4 THEORETICAL PROCEDURES

Correlation-consistent polarized valence (cc-pVXZ), augmented correlation-consistent polarized valence (aug-cc-pVXZ) [X=T,Q,5], correlation-consistent polarized core-valence (cc-pCVYZ), and augmented correlation-consistent core-valence (aug-cc-pCVYZ) [Y= T and Q] basis sets basis sets developed by Dunning and coworkers[28-31] were used to investigate electronic structures of the HSiN - HNSi system in its ground state. Zeroth-order descriptions of all stationary points were obtained using restricted Hartree-Fock (RHF) self-consisent field theory (SCF). Non-dynamic (static) correlation effects were included using complete active space SCF (CASSCF) method,[22-24] while dynamic correlation effects were included using configuration interaction with single and double excitations (CISD), coupled cluster with single and double excitations (CCSD),[18,19] CCSD with perturbative triple corrections [CCSD(T)],[20,21] and internally contracted multireference configuration interaction (ICMRCI) methods.[25-27] A full valence (10 e^-/9 MO) active space was chosen for the CASSCF wavefunctions. The CASSCF wavefunctions consist of 1436 configuration state functions (CSFs) for the linear HNSi and HSiN isomers (in C_{2v} point group symmetry) and 2744 CSFs for the

bent isomerization reaction transition state (in C_s point group symmetry). The correlated wavefunctions were constructed by doubly occupying the six core orbitals (Si: 1s, 2s, 2p-like; N: 1s-like) for the cc-pVXZ and aug-cc-pVXZ basis sets, and freezing only the one core orbital (Si: 1s-like) for the cc-pCVYZ and aug-cc-pCVYZ basis sets. The structures of the three stationary points were optimized using analytic derivative methods.[32-34] Harmonic vibrational frequencies at the SCF and CASSCF levels were evaluated analytically. The CISD, CCSD, CCSD(T), and ICMRCI geometries and harmonic vibrational frequencies were determined via numerical differentiation of the total energies. The dipole moments were evaluated by numerical differentiation of the total energies with finite external electric fields. Computations were carried out using the MOLPRO[35] and PSI2[36] quantum chemistry packages.

4.5 RESULTS AND DISCUSSION

The potential energy curves for the HSiN-HNSi system at the six different levels of theory with the cc-pVTZ basis set are shown in Figure 3. Optimized geometries for the ground states of the HNSi and HSiN isomers at the six different correlation levels with the six basis sets are depicted in Figures 4 and 5, respectively. The optimized structures for the isomerization reaction (HNSi ←→ HSiN) transition state on the ground state surface are shown in Figure 6. The total energies and physical properties of HNSi and HSiN are presented in Tables 1 and 2. The corresponding quantities for the isomerization reaction transition state are provided in Table 3. In Tables 4 and 5 the isotopic shifts for the vibrational frequencies of HNSi/DNSi and HSiN/DSiN isotopomers are presented, respectively. The relative energies for the HNSi-HSiN system are

presented in Table 6, while the dissociation energies for HNSi and HSiN are provided in Table 7.

A. Potential energy surface

In the different potential energy surfaces for the HSiN-HNSi system in Figure 3, each curve consists of 91 energy points. The two bond lengths were optimized at a *fixed* bond angle for each level of theory. In Figure 3, it is clearly seen that the linear HNSi isomer is the global minimum on the ground state potential energy surface at all levels of theory. The isomerization reaction transition state structure is energetically very close to the HSiN isomer with the SCF method. However, treatment of correlation effects shifts the transition state toward the HNSi isomer and decreases the barrier height for the isomerization reaction (HSiN→HNSi). The barrier height for the isomerization reaction (HSiN→HNSi) is small (~1 kcal/mol) with the SCF method, whereas it is noticeable (~10 kcal/mol) with the correlated methods. The CCSD, CCSD(T), and ICMRCI methods overall present qualitatively similar potential energy curves.

B. CASSCF wavefunctions

It is beneficial to analyze the CASSCF wavefunctions for the three stationary points at this point. The dominant CI coefficients of the CASSCF (with the cc-pVTZ basis set) wavefunction in terms of the CASSCF natural orbitals (NOs) for the linear HNSi isomer at the equilibrium geometry are:

$+0.964[\text{core}](5\sigma)^2(6\sigma)^2(7\sigma)^2(2\pi_x)^2(2\pi_y)^2$

$-0.104[\text{core}](5\sigma)^2(6\sigma)^2(7\sigma)^2(2\pi_y)^2(3\pi_x)^2$

$-0.104[\text{core}](5\sigma)^2(6\sigma)^2(7\sigma)^2(2\pi_x)^2(3\pi_y)^2$

$+0.069[core](5\sigma)^2(6\sigma)^2(7\sigma)^2(2\pi_x)^{\alpha}(2\pi_y)^{\beta}(3\pi_x)^{\beta}(3\pi_y)^{\alpha}$

$+0.069[core](5\sigma)^2(6\sigma)^2(7\sigma)^2(2\pi_x)^{\beta}(2\pi_y)^{\alpha}(3\pi_x)^{\alpha}(3\pi_y)^{\beta}$

$-0.052[core](5\sigma)^2(6\sigma)^2(9\sigma)^2(2\pi_x)^2(2\pi_y)^2$, (4)

where π_x and π_y are the π orbitals perpendicular to the molecular axis (z axis). The CASSCF wavefunction involves the contributions from $2\pi^2 \rightarrow 3\pi^2$ and $7\sigma^2 \rightarrow 9\sigma^2$ types of double excitations. The electron occupation numbers for the valence CASSCF NOs are n(5σ)=1.997, n(6σ)=1.981, n(7σ)=1.976, n(8σ)=0.023, and n(9σ)=0.022 for the σ orbitals, n(2π)=1.949 and n(3π)=0.052 for the π orbitals. The numbers of electrons shifted from the occupied MOs (in terms of RHF) to the virtual MOs are 0.045 for the σ space and 0.104 for the π space.

The dominant CI coefficients of the CASSCF wavefunction (with the cc-pVTZ basis set) for the linear HSiN isomer at its equilibrium geometry are:

$+0.937[core](5\sigma)^2(6\sigma)^2(7\sigma)^2(2\pi_x)^2(2\pi_y)^2$

$-0.134[core](5\sigma)^2(6\sigma)^2(7\sigma)^2(2\pi_y)^2(3\pi_x)^2$

$-0.134[core](5\sigma)^2(6\sigma)^2(7\sigma)^2(2\pi_x)^2(3\pi_y)^2$

$-0.087[core]\ (5\sigma)^2(6\sigma)^2(8\sigma)^2(2\pi_x)^2(2\pi_y)^2$

$+0.081[core](5\sigma)^2(6\sigma)^2(7\sigma)^2(2\pi_x)^{\alpha}(2\pi_y)^{\beta}(3\pi_x)^{\beta}(3\pi_y)^{\alpha}$

$+0.081[core](5\sigma)^2(6\sigma)^2(7\sigma)^2(2\pi_x)^{\beta}(2\pi_y)^{\alpha}(3\pi_x)^{\alpha}(3\pi_y)^{\beta}$. (5)

The CASSCF wavefunction involves the contributions from $2\pi^2 \rightarrow 3\pi^2$ and $7\sigma^2 \rightarrow 8\sigma^2$ types of double excitations. The electron occupation numbers for the valence CASSCF NOs are n(5σ)=1.997, n(6σ)=1.983, n(7σ)=1.936, n(8σ)=0.065, and n(9σ)=0.013 for the σ orbitals, n(2π)=1.911 and n(3π)=0.092 for the π orbitals. The numbers of electrons

excited from the occupied MOs (in terms of RHF) to the virtual MOs are 0.078 for the σ space and 0.184 for the π space. It is clear that correlation effects are more important for HSiN than for HNSi.

The CASSCF wavefunction (with the cc-PVTZ basis set) for the isomerization reaction transition state at the optimized geometry consists of the following dominant configurations:

$+0.926[\text{core}](6a')^2(7a')^2(8a')^2(9a')^2(2a'')^2$

$-0.181[\text{core}](6a')^2(7a')^2(8a')^2(10a')^2(2a'')^2$

$-0.135[\text{core}](6a')^2(7a')^2(8a')^2(9a')^2(3a'')^2$

$-0.094[\text{core}](6a')^2(7a')^2(8a')^2(9a')^{\alpha}(10a')^{\beta}(2a'')^{\beta}(3a'')^{\alpha}$

$-0.094[\text{core}](6a')^2(7a')^2(8a')^2(9a')^{\beta}(10a')^{\alpha}(2a'')^{\alpha}(3a'')^{\beta}$

$-0.061[\text{core}](6a')^2(7a')^2(9a')^2(10a')^2(2a'')^2$. (6)

The CASSCF wavefunction involves contributions from $2a''^2 \rightarrow 3a''^2$, $9a'^2 \rightarrow 10a'^2$, and $8a'^2 \rightarrow 10a'^2$ types of double excitations. The electron occupation numbers for the valence CASSCF NOs are n(6a′)=1.990, n(7a′)=1.977, n(8a′)=1.952, n(9a′)=1.866, n(10a′)=0.150, n(11a′)=0.036, n(12a′)= 0.025 for the a′ orbitals, and n(2a″)= 1.908 and n(3a″)= 0.095 for the a″ orbitals. The numbers of electrons shifted from the occupied MOs (in terms of RHF) to the virtual MOs are 0.211 for the a′ space and 0.095 for the a″ space.

C. Geometries

The optimized structures for the $\tilde{X}\ ^1\Sigma^+$ state of the HNSi isomer are depicted in Figure 4. For a given basis set, an advanced treatment of correlation effects

increases both the NH and SiN bond lengths. The increase in the NH bond length between the SCF and CCSD(T) levels of theory is 0.016 Å and that of the SiN bond length is 0.034 Å using the aug-cc-pV5Z basis set. With a given level of sophistication, augmented basis sets (aug-cc-pVXZ and aug-cc-pCVYZ) provide slightly longer NH and SiN bond lengths compared to the standard basis sets (cc-pVXZ and cc-pCVYZ). On the other hand, the core-valence basis sets (cc-pCVYZ and aug-cc-pCVYZ) present somewhat shorter NH and SiN bond distances relative to the polarized-valence basis sets (cc-pVXZ and aug-cc-pVXZ). It is evident that the SCF wavefunctions overestimate the multiple bonding character of the SiN bond, while the CASSCF wavefunctions overestimate the NH bond length. The ICMRCI method provides geometries similar to the CCSD(T) method. The larger elongation of the SiN bond distance due to correlation effects may be attributed to the double excitations from the bonding 2π orbital (in Figure 1-b) to the antibonding 3π orbital (see Figure 1-c) as demonstrated in Eq. (4). At the CCSD(T) level of theory the predicted geometry of the HNSi isomer is r_e(NH)=1.0001 and r_e(SiN)=1.5547 Å with the aug-cc-pV5Z basis set, and r_e(NH)=0.9994 and r_e(SiN)=1.5508 Å with the aug-cc-pCVQZ basis set. These structures are in good agreement with the equilibrium geometry deduced from a combination of CEPA potential and experimental B_0 values by Botschwina *et al.*;[4] r_e(NH)=1.00047 and r_e(SiN)=1.54820 □ (based on variational methods), and r_e(NH)=0.99983 and r_e(SiN)=1.54803 □ (based on perturbation methods).

The selected optimized geometries of the $\tilde{X}\ ^1\Sigma^+$ state of the HSiN isomer are shown in Figure 5. Increasingly sophisticated treatment of correlation effects lengthens both the SiH and SiN bond distances. Elongations of the SiH and SiN bond distances

between the SCF and CCSD(T) methods are 0.025 and 0.059 Å using the aug-cc-pV5Z basis set, respectively. The core-valence basis sets (cc-pCVYZ and aug-cc-pCVYZ) provide shorter SiH and SiN bond distances (by 0.004 and 0.014 □, respectively) compared to the corresponding polarized-valence basis sets (cc-pVXZ and aug-cc-pVXZ). It is observed that the SiN bond in the HSiN isomer is more sensitive to correlation effects than the SiN bond in the HNSi isomer. This feature may be associated with the fact that the coefficient (0.937) of the reference configuration for the HSiN isomer is smaller than the corresponding coefficient (0.964) for the HNSi isomer. Similarly, the CI coefficients (0.134) of the 2π (in Figure 2-b) $\rightarrow$ 3π (in Figure 2-c) double excitations for the HSiN isomer in Eq. (5) are larger than those (0.104) for the $2\pi^2$ (in Figure 1-b) $\rightarrow$ $3\pi^2$ (in Figure 1-c) double excitations for the HNSi isomer in Eq. (4). As mentioned in Subsection IV-C, the numbers of electrons shifted from the occupied MOs to the virtual MOs are significantly larger for the HSiN isomer ($0.262e^-$) than the HNSi isomer ($0.149e^-$). At the CCSD(T) level of theory the predicted structure of the HSiN isomer is r_e(SiH)=1.4842 and r_e(SiN)=1.5792 Å with the aug-cc-pV5Z basis set, and r_e(SiH)=1.4810 and r_e(SiN)=1.5749 Å with the aug-cc-pCVQZ basis set. The bond distance of the diatomic X $^2\Sigma^+$ SiN molecule is predicted to be 1.5789□ with the aug-cc-pV5Z basis set and 1.5747□ with the aug-cc-pCVQZ basis set at the same level of theory (in this study). Therefore, the SiN bond length of the HNSi isomer is about 0.024 Å shorter than the diatomic SiN, whereas the SiN bond length of the HSiN isomer is similar to the diatomic SiN. These observations are in accord with Kuzelnigg's argument[12] that second row atoms do not favor the formation of multiple bonds compared to the analogous first row atoms. According to the bond order analysis based on the vibrational

force constants by Maier and Glathaar,[7] the SiN bond order is 2.3 for HNSi and 2.0 for HSiN. Our theoretical SiN bond distances for the two isomers appear to be consistent with their analysis.

The optimized geometries of the transition state for the isomerization reaction (HNSi ←→HSiN) are shown in Figure 6. With the SCF method the HSiN bond angle is determined to be about 140˚. However, this HSiN bond angle drastically decreases to 92-84˚ with the correlated wavefunctions and the transition state is shifted toward the HNSi isomer. The SiN bond distance increases with more sophisticated treatment of correlation effects, and it is longer than the SiN distances of the HNSi and HSiN isomers at all levels of theory. This phenomenon may be explained as the double excitations in Eq. (6) have a strong tendency to weaken the SiN multiple bond. As a matter of fact, the numbers of electrons shifted from the occupied MOs to the virtual MOs for the transition state (0.306 e^-) is the largest among the three stationary points. The transition state structures predicted from the ICMRCI method are similar to those from the CCSD(T) method.

D. Dipole moments

The dipole moment of the HNSi isomer in Table 1 generally decreases with improved treatments of correlation effects (except at the CASSCF level). At a given level of theory, the dipole moment is predicted to be slightly larger with the augmented (aug-cc-pVXZ and aug-cc-pCVYZ) basis sets relative to the standard (cc-pVXZ and cc-pCVYZ) basis sets. The magnitude of the dipole moment for the HNSi isomer is quite small, since the electropositive H and Si atoms reside in both ends. With our highest level of theory, CCSD(T), the dipole moment of the HNSi isomer is predicted to be 0.254

debye with the aug-cc-pV5Z basis set and 0.263 debye with the aug-cc-pCVQZ basis set with the direction of $^{-}$HNSi^{+}. At the CCSD(T) level of theory the dipole moment of the diatomic X $^{2}\Sigma^{+}$ SiN is computed to be 2.627 debye with the aug-cc-pV5Z basis set and 2.621 debye with the aug-cc-pCVQZ basis set, the direction being $^{+}$SiN^{-} (in this study). An addition of the H atom to the N end of diatomic SiN indeed greatly decreases the magnitude of the dipole moment for the HNSi isomer.

The dipole moment for the HSiN isomer in Table 2 decreases with advanced treatments of correlation effects. At a given level of theory the dipole moment is predicted to be slightly larger with the augmented (aug-cc-pVXZ and aug-cc-pCVYZ) basis sets compared to the standard (cc-pVXZ and cc-pCVYZ) basis sets. At the CCSD(T) level of theory the dipole moment for the HSiN isomer is predicted to be 4.373 debye with the aug-cc-pV5Z basis set and 4.359 debye with the aug-cc-pCVQZ basis set, with the direction being $^{+}$HSiN^{-}. Note that the direction of the dipole moment (in terms of the H atom) for the HSiN isomer is opposite to that for the HNSi structure. An attachment of the H atom to the Si end of diatomic SiN significantly increases the magnitude of the dipole moment. Due to its relatively large dipole moment, the HSiN isomer may be observable via microwave (MW) spectroscopy.

The dipole moment for the isomerization reaction transition state presented in Table 3 is quite sensitive to the correlation level and basis sets. It is seen that the transition state is significantly more polarized than the HNSi isomer, but it is less polarized than the HSiN isomer.

E. Harmonic vibrational frequencies

The three harmonic vibrational frequencies for the HNSi isomer in Table 1 decrease with increasingly sophisticated treatments of correlation effects, reflecting the elongated HN and SiN bond distances. This feature follows Badger's rule[37,38] that the shorter (longer) bond distance is associated with the larger (smaller) force constant and resultant higher (lower) stretching frequency. At the CCSD(T) level of theory the three harmonic vibrational frequencies are computed to be ω_1=3747, ω_2=531, and ω_3=1217 cm^{-1} with the aug-cc-pV5Z basis set, and ω_1=3753, ω_2=533, and ω_3=1219 cm^{-1} with the aug-cc-pCVQZ basis set. They are in reasonable agreement with experimentally observed fundamental frequencies of ν_1=3583, ν_2=523, and ν_3=1198 cm^{-1} by Ogilvie and Cradock[1] and ν_1=3585, ν_2=522, and ν_3=1202 cm^{-1} by Maier and Glatthaar.[7] The differences between theoretical and experimental frequencies may be largely attributed to anharmonicity.

The three harmonic vibrational frequencies for the HSiN isomer in Table 2 generally decrease with the inclusion of correlation effects, mainly due to the elongation of the SiH and SiN bond lengths. At the highest correlated level of theory in this study, CCSD(T), the three harmonic vibrational frequencies are computed to be ω_1=2205, ω_2=154, and ω_3=1167 cm^{-1} with the aug-cc-pV5Z basis set, and ω_1=2205, ω_2=141, and ω_3=1171 cm^{-1} with the aug-cc-pCVQZ basis set. They are in reasonable agreement with experimental fundamental frequencies of ν_1=2152.2 and ν_3=1162.2 cm^{-1} by Maier and Glatthaar.[7] The harmonic vibrational frequency of the diatomic X $^2\Sigma^+$ SiN is predicted to be 1145 cm^{-1} at the aug-cc-pV5Z CCSD(T) level of theory (in this study). The SiN stretching frequencies (ω_3) of the HNSi and HSiN isomers are 72 cm^{-1} and 22 cm^{-1} higher

than the diatomic SiN, respectively. A significantly lower bending frequency (ω_2) for the HSiN isomer relative to that for the HNSi isomer is consistent with the smaller activation energy for the isomerization reaction (HSiN → HNSi).

The two stretching vibrational frequencies (ω_1 and ω_3) for the isomerization reaction transition state (shown in Table 3) decrease with increasingly sophisticated treatments of correlation effects. The ω_1 frequency of the transition state is lower than the NH stretching frequency of HNSi (ω_1 in Table 1) and the SiH stretching frequency of HSiN (ω_1 in Table 2) at all levels of theory. Similarly, the ω_3 frequency of the transition state is lower than the SiN stretching frequencies of the HNSi (ω_3 in Table 1) isomer and the HSiN (ω_3 in table 2) isomer. The reaction coordinate (ω_2) mainly consists of an out-of-phase motion of HN and SiH stretchings (or HNSi-HSiN bendings). The magnitude of the ω_2 imaginary frequency significantly increases with an increase of correlation effects, reflecting the structural decrease of the HSiN bond angle. A smaller HSiN bond angle and a steeper curvature at the transition state with the correlated wavefunctions indicate a higher energy barrier for the isomerization reaction (HSiN → HNSi) relative to the SCF wavefunction.

F. Vibrational isotopic shifts

The isotopic shifts for the vibrational frequencies of the HNSi and DNSi species are presented in Table 4. The theoretical harmonic frequencies are determined via the GF matrix method,[39] at the CCSD, CCSD(T) , and ICMRCI levels of theory, while the experimental fundamental frequencies are from Ogilvie and Cradock.[1] Theoretically evaluated isotopic shifts for the two stretching frequencies (ω_1 and ω_3) are in satisfactory agreement with the experimental observations. The CCSD(T) frequency shifts are closer

to the experimental values than the CCSD frequency shifts by about 10 cm^{-1} for $\Delta\omega_1$ and 2 cm^{-1} for $\Delta\omega_3$. The predicted isotopic shift for the bending frequency ($\Delta\omega_2$) is in good accordance with the experimental value. For the bending mode the CCSD frequency shift is closer to the experimental value than the CCSD(T) frequency shift.

The isotopic shifts for the vibrational frequencies of the HSiN and DSiN isotopomers at the CCSD, CCSD(T), and ICMRCI levels of theory are provided in Table 5. The experimental fundamental frequencies are from Maier and Glathaar.[7] Theoretical isotopic shifts for the two stretching frequencies (ω_1 and ω_3) are in satisfactory agreement with the experimental measurements. The CCSD(T) frequency shifts are closer to the experimental values than the CCSD frequency shifts by about 12 cm^{-1} for $\Delta\omega_1$ and 3 cm^{-1} for $\Delta\omega_3$. Relatively large deviations for $\Delta\omega_1$ for the XH (X=N or Si) stretching frequencies may be due to large differences in anharmonicity between the XH and XD stretching modes.

G. Relative energies

The HNSi isomer has been confirmed to be the global minimum on the HSiN→HNSi ground state surface as previous *ab initio*[8,9,14,16,17,40-43] and DFT[40,44] studies indicated. The classical energy separation between the HNSi and HSiN isomers is computed to be 89.05(SCF), 67.44(CASSCF), 77.87(CISD), 73.49(CCSD), 68.01 [CCSD(T)], and 66.37 kcal/mol (ICMRCI) using the aug-cc-pV5Z basis set. The HSiN isomer is preferentially stabilized relative to the HNSi isomer by as much as about 21 kcal/mol with advanced treatments of correlation effects. This feature may be due to the higher multireference character of the HSiN isomer in Eq. (5) compared to the HNSi isomer in Eq. (4). Furthermore, as mentioned in Section IV-D, the diatomic X $^2\Sigma^+$ SiN

molecule has a large dipole moment (2.627 debye) with the diretion of $^{+}SiN^{-}$. The attachment of the electropositive H atom to the N end (to form the HNSi isomer) is much preferable to the attachment to the Si end (to form the HSiN isomer). The quantum mechanical energy separation (i.e., with the ZPVE corrections) is predicted to be 64.66 kcal/mol (22620 cm^{-1}, 2.804 eV) with the aug-cc-pV5Z CCSD(T) method and 65.41 kcal/mol (22880 cm^{-1}, 2.836 eV) with the aug-cc-pCVQZ CCSD(T) method, and 62.98 kcal/mol (22030 cm^{-1}, 2.731 eV) with the aug-cc-pV5Z ICMRCI method.

The classical barrier height for the isomerization reaction (HNSi→ HSiN) is determined to be 90.08(SCF), 84.24(CASSCF), 89.81(CISD), 82.75(CCSD), 79.27 [CCSD(T)], and 78.91 kcal/mol (ICMRCI) with the aug-cc-pV5Z basis set. Correlation effects stabilize the transition state structure relative to the linear HNSi isomer by as much as about 11 kcal/mol. The barrier height for the isomerization reaction (HNSi → HSiN) is predicted to be 75.17 kcal/mol (26290 cm^{-1}, 3.260 eV) with the ZPVE corrections using the aug-cc-pV5Z CCSD(T) method, 75.54 kcal/mol (26420 cm^{-1}, 3.276 eV) with the aug-cc-pCVQZ CCSD(T) method, and 74.48 kcal/mol (26050 cm^{-1}, 3.230 eV) with the aug-cc-pV5Z ICMRCI method. Therefore, once the global minimum HNSi isomer is formed, the isomerization reaction to the HSiN isomer is unlikely to occur at low temperatures. With the SCF method, the classical barrier height for the isomerization reaction (HSiN→ HNSi) is computed to be only about 1 kcal/mol. However, inclusion of correlation effects increases this barrier height by as much as about 10 kcal/mol. The transition state in Eq. (6) has stronger mixing with excited configurations than the HNSi isomer in Eq. (4). The classical and quantum mechanical barrier heights for the isomerization reaction (HSiN → HNSi) are 11.26 kcal/mol (3940

cm^{-1}, 0.488 eV) and 10.51 kcal/mol (3680 cm^{-1}, 0.456 eV) with the aug-cc-pV5Z CCSD(T) method, and 10.83 kcal/mol (3790 cm^{-1}, 0.470 eV) and 10.13 kcal/mol (3540 cm^{-1}, 0.439 eV) with the aug-cc-pCVQZ CCSD(T) method, and 12.54 kcal/mol (4390 cm^{-1}, 0.544 eV) and 11.90 kcal/mol (4160 cm^{-1}, 0.516 eV) with the aug-cc-pV5Z ICMRCI method, respectively.

The schematic potential energy surface for the HSiN-HNSi system is presented in Figure 7. The relative energies in Figure 7 are at the aug-cc-pV5Z ICMRCI (in roman), aug-cc-pV5Z CCSD(T) (in italic), and aug-cc-pCVQZ CCSD(T) (in bold) levels of theory. The isomerization reaction (HNSi→HSiN) is an endothermic process and the transition state structure is close to the HSiN (product) isomer. This feature appears to follow Hammond's postulate,[45] which states that the transition state structure resembles the reactant for an exothermic reaction and the transition state geometry is close to that of the product for an endothermic reaction.

H. Dissociation Energies

The dissociation energies for

$$HNSi\ (\tilde{X}\ ^1\Sigma^+) \rightarrow H\ (^2S) + SiN\ (X\ ^2\Sigma^+) \qquad (7)$$

and

$$HSiN\ (\tilde{X}\ ^1\Sigma^+) \rightarrow H\ (^2S) + SiN\ (X\ ^2\Sigma^+) \qquad (8)$$

at the four size consistent levels of theory are presented in Table 7. The dissociation energy of the HNSi isomer increases with correlation effects as much as 15 kcal/mol. With our most reliable method, CCSD(T), the dissociation energies for the Eq. (7) are predicted to be D_e= 131.84 kcal/mol and D_0= 124.87 kcal/mol with the aug-cc-pV5Z basis set and D_e= 131.96 kcal/mol and D_0= 124.97 kcal/mol with the aug-cc-pCVQZ

basis set. The dissociation energy of the HSiN isomer is more sensitive than that for the HNSi isomer and increases with correlation effects as much as 36 kcal/mol. The H-SiN dissociation energies for Eq. (8) are predicted to be D_e= 63.83 kcal/mol and D_0= 60.21 kcal/mol with the aug-cc-pV5Z basis set, and D_e = 63.15 kcal/mol and D_0 = 59.56 kcal/mol with the aug-cc-pCVQZ basis set. It is seen that both the HNSi and HSiN isomers are favorably stabilized with correlation effects compared to the diatomic SiN molecule. The difference in the dissociation energies for Eqs. (7) and (8) is, of course, equivalent to the relative energy of the HNSi and HSiN isomers. The three stationary points (HNSi, HSiN, and isomerization reaction transition state) studied in this research are found to be energetically well below the dissociation channel H + SiN.

4.6 CONCLUDING REMARKS

The electronic ground state potential energy surface of the HNSi-HSiN system has been characterized employing highly correlated *ab initio* quantum mechanical coupled cluster and multireference configuration interaction wave functions in conjunction with large correlation consistent type basis sets. The HNSi isomer is confirmed to be the global minimum on the ground state surface and is determined to be 68.8 kcal/mol (24100 cm^{-1}, 2.98 eV)[65.4 kcal/mol (22900 cm^{-1}, 2.84 eV) with the ZPVE corrections] lower in energy than the HSiN isomer at the aug-cc-pCVQZ CCSD(T) level of theory. The barrier height for the isomerization reaction (HSiN→HNSi) is predicted to be 10.8 kcal/mol (10.1 kcal/mol with the ZPVE corrections), whereas the barrier height for the isomerization reaction (HNSi→HSiN) is predicted to be 79.6 kcal/mol (75.5 kcal/mol with the ZPVE corrections). The dipole moment of the HNSi isomer is

predicted to be very small, 0.26 debye with direction $^{-}$HNSi^{+}, while that of the HSiN isomer is determined to be 4.36 debye with the direction $^{+}$HSiN^{-}. The dissociation energy for the HNSi isomer is predicted to be D_e=132.0 kcal/mol (D_0=125.0 kcal/mol), while that for the HSiN isomer to be D_e=63.2 kcal/mol (D_0=59.6 kcal/mol). We hope that the reliable physical properties and energetics for the HNSi and HSiN isomers presented in the present study will assist in further spectroscopic characterization of the HNSi-HSiN system.

4.7 ACKNOWLEDGEMENTS

This work was supported by National Science Foundation Grant CHE-0451445.

4.8 REFERENCES

1 J. F. Ogilvie and S. Cradock, Chemical Communications (12), 364 (1966).

2 M. Elhanine, R. Farrenq, and G. Guelachvili, Journal of Chemical Physics **94** (4), 2529 (1991).

3 M. Bogey, C. Demuynck, J. L. Destombes, and A. Walters, Astronomy and Astrophysics **244** (2), L47 (1991).

4 P. Botschwina, M. Tommek, P. Sebald, M. Bogey, C. Demuynck, J. L. Destombes, and A. Walters, Journal of Chemical Physics **95** (10), 7769 (1991).

5 N. Goldberg, M. Iraqi, J. Hrusak, and H. Schwarz, International Journal of Mass Spectrometry and Ion Processes **125** (2-3), 267 (1993).

6 M. Elhanine, B. Hanoune, and G. Guelachvili, Journal of Chemical Physics **99** (7), 4970 (1993).

[7] G. Maier and J. Glatthaar, Angewandte Chemie-International Edition in English **33** (4), 473 (1994).

[8] J. N. Murrell, H. W. Kroto, and M. F. Guest, Journal of the Chemical Society-Chemical Communications (17), 619 (1977).

[9] R. Preuss, R. J. Buenker, and S. D. Peyerimhoff, Journal of Molecular Structure **49** (1), 171 (1978).

[10] B. T. Luke, J. A. Pople, M. B. Kroghjespersen, Y. Apeloig, J. Chandrasekhar, and P. R. Schleyer, Journal of the American Chemical Society **108** (2), 260 (1986).

[11] R. Walsh, Accounts of Chemical Research **14** (8), 246 (1981).

[12] W. Kutzelnigg, Angewandte Chemie-International Edition in English **23** (4), 272 (1984).

[13] G. Olbrich, P. Potzinger, B. Reimann, and R. Walsh, Organometallics **3** (8), 1267 (1984).

[14] Y. Apeloig and K. Albrecht, Journal of the American Chemical Society **117** (27), 7263 (1995).

[15] O. Parisel, M. Hanus, and Y. Ellinger, Chemical Physics **212** (2-3), 331 (1996).

[16] O. Parisel, M. Hanus, and Y. Ellinger, Journal of Physical Chemistry A **101** (3), 299 (1997).

[17] S. W. Hu, Y. Wang, X. Y. Wang, T. W. Chu, and X. Q. Liu, Journal of Physical Chemistry A **107** (43), 9189 (2003).

[18] G. D. Purvis and R. J. Bartlett, Journal of Chemical Physics **76** (4), 1910 (1982).

[19] M. Rittby and R. J. Bartlett, Journal of Physical Chemistry **92** (11), 3033 (1988).

[20] K. Raghavachari, G. W. Trucks, J. A. Pople, and M. Headgordon, Chemical Physics Letters **157** (6), 479 (1989).

[21] G. E. Scuseria, Chemical Physics Letters **176** (1), 27 (1991).

[22] P. Siegbahn, A. Heiberg, B. Roos, and B. Levy, Physica Scripta **21** (3-4), 323 (1980).

[23] B. O. Roos and P. R. Taylor, Chemical Physics **48** (2), 157 (1980).

[24] B. O. Roos, International Journal of Quantum Chemistry **17**, 175 (1980).

[25] H. J. Werner and E. A. Reinsch, Journal of Chemical Physics **76** (6), 3144 (1982).

[26] P. J. Knowles and H. J. Werner, Chemical Physics Letters **145** (6), 514 (1988).

[27] H. J. Werner and P. J. Knowles, Journal of Chemical Physics **89** (9), 5803 (1988).

[28] T. H. Dunning, Journal of Chemical Physics **90** (2), 1007 (1989).

[29] D. E. Woon and T. H. Dunning, Journal of Chemical Physics **98** (2), 1358 (1993).

[30] D. E. Woon and T. H. Dunning, Journal of Chemical Physics **103** (11), 4572 (1995).

[31] K. A. Peterson and T. H. Dunning, Journal of Chemical Physics **117** (23), 10548 (2002).

[32] P. Pulay, Molecular Physics **17** (2), 197 (1969).

[33] *Modern Theoretical Chemistry*, edited by P. Pulay (Plenum, New York, 1977), Vol. 4.

[34] Y. Yamaguchi, Y. Osamura, J. D. Goddard, and H. F. Schaefer, *A New Dimension to Quantum Chemistry: Analytic Derivative Methods in Ab Initio Molecular Electronic Structure Theory*. (Oxford University Press, New York, 1994).

[35] H. J. Werner, P. J. Knowles, R. Lindh, F. Manby, M. Schutz, P. Celani, T. Korona, G. Rauhut, R. D. Amos, A. Bernhardsson, A. Berning, D. L. Cooper, M. J. O. Deegan, A. J. Dobbyn, F. Eckert, C. Hampel, G. Hetzer, A. W. Lloyd, S. J. McNicholas, W. Meyer, M. E. Mura, A. Nicklass, P. Palmieri, R. Pitzer, U. Schumann, H. Stoll, A. J. Stone, R. Tarroni, and T. Thorsteinsson.

[36] PSI 2.0 (PSITECH, Inc., 1991).

[37] R. M. Badger, Journal of Chemical Physics **2**, 128 (1934).

[38] R. M. Badger, Journal of Chemical Physics **3**, 710 (1934).

[39] E. B. Wilson, J. C. Decius, and P. C. Cross, *Molecular Vibrations*. (McGraw-Hill, New York, 1955).

[40] O. Kwon and Y. Kwon, Journal of Molecular Structure-Theochem **460** (1-3), 213 (1999).

[41] D. Danovich, F. Ogliaro, M. Karni, Y. Apeloig, D. L. Cooper, and S. Shaik, Angewandte Chemie-International Edition **40** (21), 4023 (2001).

[42] D. Sengupta and M. T. Nguyen, Chemical Physics Letters **265** (1-2), 35 (1997).

[43] R. Becerra, J. P. Cannady, and R. Walsh, Journal of Physical Chemistry A **107** (45), 9588 (2003).

[44] B. S. Jursic, Journal of Molecular Structure-Theochem **455** (1), 77 (1998).

[45] G. S. Hammond, Journal of the American Chemical Society **77** (2), 334 (1955).

TABLE 4.1. Theoretical predictions of the total energy (in hartree), dipole moment (in debye), harmonic vibrational frequencies (in cm^{-1}), and zero point vibrational energies (ZPVE in kcal mol^{-1}) for the linear ground state ($\tilde{X}\ ^1\Sigma^+$) of HNSi.

Level of Theory	*Total Energy*	μ_e	ω_1 (σ^+)	ω_2 (π)	ω_3 (σ^+)	*ZPVE*
cc-pVQZ SCF	-343.981 134	0.572	3994	608	1364	9.40
aug-cc-pVQZ SCF	-343.981 675	0.650	3992	608	1361	9.39
cc-pV5Z SCF	-343.984 424	0.616	3994	613	1363	9.41
aug-cc-pV5Z SCF	-343.984 579	0.640	3994	611	1362	9.40
cc-pCVTZ SCF	-343.975 228	0.452	3992	618	1366	9.43
aug-cc-pCVTZ SCF	343.977 212	0.651	3990	600	1358	9.36
cc-pCVQZ SCF	343.983 376	0.559	3995	612	1366	9.41
aug-cc-pCVQZ SCF	343.983 918	0.640	3994	612	1362	9.41
cc-pVQZ CISD	-344.287 659	0.367	3861	567	1296	8.99
aug-cc-pVQZ CISD	-344.290 184	0.464	3858	564	1291	8.97
cc-pV5Z CISD	-344.296 399	0.426	3861	571	1298	9.01
aug-cc-pV5Z CISD	-344.297 516	0.458	3859	569	1296	9.00
cc-pCVTZ CISD	-344.571 657	0.311	3905	592	1316	9.16
aug-cc-pCVTZ CISD	-344.577 497	0.547	3899	564	1307	9.05
cc-pCVQZ CISD	-344.626 294	0.444	3914	587	1325	9.17
aug-cc-pCVQZ CISD	-344.628 767	0.536	3911	584	1321	9.15
cc-pVQZ CCSD	-344.315 144	0.289	3795	547	1262	8.79
aug-cc-pVQZ CCSD	-344.317 848	0.396	3791	543	1258	8.77
cc-pV5Z CCSD	-344.324 156	0.355	3795	551	1265	8.81
aug-cc-pV5Z CCSD	-344.325 331	0.392	3792	549	1263	8.80
cc-pCVTZ CCSD	-344.632 365	0.142	3797	560	1261	8.83
aug-cc-pCVTZ CCSD	-344.639 018	0.408	3798	531	1252	8.74
cc-pCVQZ CCSD	-344.691 293	0.292	3803	555	1270	8.84
aug-cc-pCVQZ CCSD	-344.694 017	0.400	3799	552	1266	8.82
cc-pVQZ CCSD(T)	-344.334 274	0.136	3751	529	1216	8.61
aug-cc-pVQZ CCSD(T)	-344.337 283	0.256	3746	525	1212	8.59
cc-pV5Z CCSD(T)	-344.343 743	0.212	3750	533	1219	8.63
aug-cc-pV5Z CCSD(T)	-344.345 055	0.254	3747	531	1217	8.61
cc-pCVTZ CCSD(T)	-344.653 479	0.021	3753	541	1213	8.65
aug-cc-pCVTZ CCSD(T)	-344.660 915	0.269	3743	512	1204	8.54
cc-pCVQZ CCSD(T)	-344.714 547	0.143	3758	536	1224	8.65
aug-cc-pCVQZ CCSD(T)	-344.717 573	0.263	3753	533	1219	8.63
cc-pVQZ CASSCF	-344.114 272	0.045	3679	552	1221	8.58
aug-cc-pVQZ CASSCF	-344.114 862	0.048	3678	551	1218	8.57
cc-pV5Z CASSCF	-344.117 276	0.019	3680	556	1221	8.60
aug-cc-pV5Z CASSCF	-344.117 443	0.048	3680	555	1220	8.59
cc-pVQZ ICMRCI	-344.317 020	0.012	3740	530	1216	8.60
aug-cc-pVQZ ICMRCI	-344.319 616	0.117	3737	526	1212	8.58
cc-pV5Z ICMRCI	-344.325 643	0.077	3739	533	1219	8.61
aug-cc-pV5Z ICMRCI	-344.326 780	0.113	3737	532	1217	8.60
Expt. ν_1 [Ref. 1]			3583	523	1198	
Expt. ν_1 [Ref. 2]			3588			
Expt ω_1 [Ref. 6]			3748			
Expt. ν_1 [Ref. 7]			3585	522	1202	

TABLE 4.2. Theoretical predictions of the total energy (in hartree), dipole moment (in debye), harmonic vibrational frequencies (in cm^{-1}), and zero point vibrational energies (ZPVE in kcal mol^{-1}) for the linear ground state ($\tilde{X}\ ^1\Sigma^+$) of HSiN.

Level of Theory	*Total Energy*	μ_e	ω_1 (σ^+)	ω_2 (π)	ω_3 (σ^+)	*ZPVE*
cc-pVQZ SCF	-343.839 488	5.867	2409	248	1397	6.15
aug-cc-pVQZ SCF	-343.839 862	5.928	2408	247	1395	6.14
cc-pV5Z SCF	-343.842 570	5.910	2409	251	1397	6.16
aug-cc-pV5Z SCF	-343.842 676	5.934	2409	251	1397	6.16
cc-pCVTZ SCF	-343.834 057	5.722	2406	259	1398	6.18
aug-cc-pCVTZ SCF	-343.835 668	5.928	2407	265	1394	6.19
cc-pCVQZ SCF	-343.841 715	5.869	2408	249	1398	6.15
aug-cc-pCVQZ SCF	-343.842 046	5.935	2408	250	1397	6.15
cc-pVQZ CISD	-344.164 048	5.035	2325	192	1285	5.71
aug-cc-pVQZ CISD	-344.166 379	5.115	2324	202	1283	5.73
cc-pV5Z CISD	-344.172 326	5.107	2328	205	1289	5.76
aug-cc-pV5Z CISD	-344.173 419	5.138	2327	207	1289	5.76
cc-pCVTZ CISD	-344.442 761	5.067	2355	239	1312	5.93
aug-cc-pCVTZ CISD	-344.448 280	5.293	2358	255	1308	5.97
cc-pCVQZ CISD	-344.495 990	5.278	2367	243	1324	5.97
aug-cc-pCVQZ CISD	-344.498 289	5.355	2367	251	1323	5.99
cc-pVQZ CCSD	-344.198 612	4.664	2260	77	1226	5.20
aug-cc-pVQZ CCSD	-344.201 110	4.748	2258	98	1224	5.26
cc-pV5Z CCSD	-344.207 064	4.741	2262	106	1231	5.30
aug-cc-pV5Z CCSD	-344.208 211	4.775	2262	107	1230	5.30
cc-pCVTZ CCSD	-344.515 292	4.472	2254	89	1225	5.23
aug-cc-pCVTZ CCSD	-344.521 535	4.711	2256	121	1221	5.32
cc-pCVQZ CCSD	-344.572 873	4.690	2266	89	1237	5.26
aug-cc-pCVQZ CCSD	-344.575 363	4.775	2265	107	1236	5.31
cc-pVQZ CCSD(T)	-344.226 529	4.261	2204	139	1162	5.21
aug-cc-pVQZ CCSD(T)	-344.229 284	4.348	2202	151	1161	5.24
cc-pV5Z CCSD(T)	-344.235 411	4.339	2206	152	1167	5.26
aug-cc-pV5Z CCSD(T)	-344.236 675	4.373	2205	154	1167	5.26
cc-pCVTZ CCSD(T)	-344.545 547	4.055	2195	140	1160	5.20
aug-cc-pCVTZ CCSD(T)	-344.552 424	4.299	2196	157	1156	5.24
cc-pCVQZ CCSD(T)	-344.605 175	4.271	2206	129	1172	5.20
aug-cc-pCVQZ CCSD(T)	-344.607 916	4.359	2205	141	1171	5.23
cc-pVQZ CASSCF	-344.007 322	4.454	2306	146	1154	5.36
aug-cc-pVQZ CASSCF	-344.007 723	4.519	2306	145	1154	5.36
cc-pV5Z CASSCF	-344.009 865	4.509	2308	144	1156	5.36
aug-cc-pV5Z CASSCF	-344.009 968	4.533	2308	142	1155	5.36
cc-pVQZ ICMRCI	-344.211 798	4.203	2232	107	1155	5.15
aug-cc-pVQZ ICMRCI	-344.214 178	4.284	2232	120	1155	5.19
cc-pV5Z ICMRCI	-344.219 921	4.277	2236	121	1162	5.20
aug-cc-pV5Z ICMRCI	-344.221 016	4.309	2235	123	1161	5.21
Expt. [Ref. 7]			2152		1162	

TABLE 4.3. Theoretical predictions of the total energy (in hartree), dipole moment (in debye), harmonic vibrational frequencies (in cm^{-1}), and zero point vibrational energy (ZPVE in kcal mol^{-1}) for the transition state ($\tilde{X}\ ^1A'$) of the HSiN ←→ HNSi isomerization reaction.

Level of Theory	*Total Energy*	μ_e	ω_1 (a′)	ω_2 (a′)	ω_3 (a′)	*ZPVE*
cc-pVQZ SCF	-343.837 966	4.980	2364	287*i*	1267	5.19
aug-cc-pVQZ SCF	-343.838 314	5.014	2364	288*i*	1263	5.19
cc-pV5Z SCF	-343.840 920	4.970	2362	288*i*	1260	5.18
aug-cc-pV5Z SCF	-343.841 034	4.984	2362	287*i*	1260	5.18
cc-pCVTZ SCF	-343.832 313	4.815	2356	296*i*	1259	5.17
aug-cc-pCVTZ SCF	-343.833 827	4.956	2355	299*i*	1252	5.16
cc-pCVQZ SCF	-343.840 089	4.941	2362	286*i*	1262	5.18
aug-cc-pCVQZ SCF	-343.840 407	4.981	2362	286*i*	1259	5.18
cc-pVQZ CISD	-344.145 145	3.201	2186	666*i*	1118	4.72
aug-cc-pVQZ CISD	-344.147 394	3.273	2185	660*i*	1116	4.72
cc-pV5Z CISD	-344.153 376	3.275	2189	664*i*	1123	4.73
aug-cc-pV5Z CISD	-344154 391	3.301	2189	660*i*	1122	4.73
cc-pCVTZ CISD	-344.423 353	3.133	2225	631*i*	1108	4.76
aug-cc-pCVTZ CISD	-344.428 867	3.331	2224	626*i*	1106	4.76
cc-pCVQZ CISD	-344.476 782	3.291	2237	638*i*	1119	4.80
aug-cc-pCVQZ CISD	-344.478 996	3.359	2237	635*i*	1118	4.80
cc-pVQZ CCSD	-344.183 715	2.994	2112	696*i*	1099	4.59
aug-cc-pVQZ CCSD	-344.186 302	3.068	2109	691*i*	1097	4.58
cc-pV5Z CCSD	-344.192 308	3.067	2114	693*i*	1103	4.60
aug-cc-pV5Z CCSD	-344.193 453	3.094	2113	691*i*	1103	4.60
cc-pCVTZ CCSD	-344.500 468	2.856	2112	689*i*	1097	4.59
aug-cc-pCVTZ CCSD	-344.507 182	3.066	2108	676*i*	1094	4.58
cc-pCVQZ CCSD	-344.558 562	3.031	2124	688*i*	1110	4.62
aug-cc-pCVQZ CCSD	-344.561 176	3.106	2122	682*i*	1108	4.62
cc-pVQZ CCSD(T)	-344.208 240	2.950	2055	797*i*	1096	4.50
aug-cc-pVQZ CCSD(T)	-344.211 208	3.032	2050	793*i*	1094	4.49
cc-pV5Z CCSD(T)	-344.217 409	3.026	2056	792*i*	1101	4.51
aug-cc-pV5Z CCSD(T)	-344.218 728	3.055	2055	791*i*	1101	4.51
cc-pCVTZ CCSD(T)	-344.527 203	2.795	2054	792*i*	1093	4.50
aug-cc-pCVTZ CCSD(T)	-344.534 862	3.019	2046	780*i*	1089	4.48
cc-pCVQZ CCSD(T)	-344.587 665	2.975	2065	786*i*	1105	4.53
aug-cc-pCVQZ CCSD(T)	-344.590 655	3.056	2062	781*i*	1104	4.53
cc-pVQZ CASSCF	-343.977 433	2.715	1946	844*i*	1065	4.30
aug-cc-pVQZ CASSCF	-343.980 809	3.021	2150	942*i*	1083	4.62
cc-pV5Z CASSCF	-343.979 972	2.758	1949	845*i*	1066	4.31
aug-cc-pV5Z CASSCF	-343.983 203	3.037	2153	944*i*	1085	4.63
cc-pVQZ ICMRCI	-344.192 717	2.864	2053	774*i*	1079	4.48
aug-cc-pVQZ ICMRCI	-344.194 039	2.982	2106	791*i*	1081	4.56
cc-pV5Z ICMRCI	-344.201 060	2.931	2055	771*i*	1084	4.49
aug-cc-pV5Z ICMRCI	-344.201 025	3.005	2111	791*i*	1087	4.57

TABLE 4.4. Theoretical predictions of harmonic vibrational frequencies (in cm^{-1}) for the linear ($\tilde{X}\ ^1\Sigma^+$) states of the HNSi and DNSi molecules at the CCSD, CCSD(T), and ICMRCI levels of theory.

	HNSi			DNSi			*Isotopic Shifts*		
Level of Theory	$\omega_1(\sigma^+)$	$\omega_2(\pi)$	$\omega_3(\sigma^+)$	$\omega_1(\sigma^+)$	$\omega_2(\pi)$	$\omega_3(\sigma^+)$	$\Delta(\omega_1)$	$\Delta(\omega_2)$	$\Delta(\omega_3)$
cc-pVQZ CCSD	3794.8	546.3	1263.3	2800.7	418.5	1225.0	994.1	127.8	38.3
aug-cc-pVQZ CCSD	3791.5	542.9	1259.0	2798.1	415.9	1220.8	993.4	127.0	38.2
cc-pV5Z CCSD	3794.7	550.3	1265.6	2800.6	421.6	1227.1	994.1	128.7	38.5
aug-cc-pV5Z CCSD	3792.5	548.6	1264.0	2799.0	420.3	1225.6	993.5	128.3	38.4
cc-pCVQZ CCSD	3803.2	554.2	1271.2	2807.1	424.7	1232.5	996.1	129.5	38.7
aug-cc-pCVQZ CCSD	3799.5	551.3	1267.0	2804.3	422.5	1228.5	995.2	128.8	38.5
cc-pVQZ CCSD(T)	3750.9	528.3	1216.7	2767.2	404.6	1180.2	983.7	123.7	36.5
aug-cc-pVQZ CCSD(T)	3746.5	524.8	1212.4	2763.9	402.0	1176.1	982.6	122.8	36.3
cc-pV5Z CCSD(T)	3749.8	532.4	1219.6	2766.6	407.9	1182.9	983.2	124.5	36.7
aug-cc-pV5Z CCSD(T)	3747.1	530.9	1218.0	2764.5	406.7	1181.4	982.6	124.2	36.6
cc-pCVQZ CCSD(T)	3757.7	535.6	1224.4	2772.5	410.3	1187.6	985.2	125.3	36.8
aug-cc-pCVQZ CCSD(T)	3752.8	532.7	1220.3	2768.8	408.1	1183.6	984.0	124.6	36.7
cc-pVQZ ICMRCI	3739.7	529.6	1215.8	2758.2	405.6	1179.6	981.5	124.0	36.2
aug-cc-pVQZ ICMRCI	3736.6	526.1	1212.1	2755.9	403.0	1176.1	980.7	123.1	36.0
cc-pV5Z ICMRCI	3739.3	533.2	1218.7	2758.0	408.5	1182.5	981.3	124.7	36.2
aug-cc-pV5Z ICMRCI	3737.2	531.6	1217.4	2756.4	407.2	1181.2	980.8	124.4	36.2
Expt. [Ref. 1]	3583	523	1198	2669	395	1166	914	128	32.0

TABLE 4.5. Theoretical predictions of harmonic vibrational frequencies (in cm^{-1}) for the linear ($\tilde{X}\ ^1\Sigma^+$) states of the HSiN and DSiN molecules at the CCSD, CCSD(T), and ICMRCI levels of theory.

	HSiN			DSiN			*Isotopic Shifts*		
Level of Theory	$\omega_1(\sigma^+)$	$\omega_2(\pi)$	$\omega_3(\sigma^+)$	$\omega_1(\sigma^+)$	$\omega_2(\pi)$	$\omega_3(\sigma^+)$	$\Delta(\omega_1)$	$\Delta(\omega_2)$	$\Delta(\omega_3)$
cc-pVQZ CCSD	2260.3	76.3	1226.7	1646.7	58.3	1205.0	613.6	18.0	21.7
aug-cc-pVQZ CCSD	2258.8	97.3	1225.2	1645.6	74.3	1203.5	613.2	23.0	21.7
cc-pV5Z CCSD	2262.6	103.9	1231.7	1648.4	79.4	1209.8	614.2	24.5	21.9
aug-cc-pV5Z CCSD	2261.9	107.0	1231.0	1647.9	81.7	1209.2	614.0	25.3	21.8
cc-pCVQZ CCSD	2266.2	88.4	1238.1	1651.4	67.6	1215.9	614.8	20.8	22.2
aug-cc-pCVQZ CCSD	2265.6	106.2	1236.7	1650.9	81.2	1214.5	614.7	25.0	22.2
cc-pVQZ CCSD(T)	2203.9	138.9	1163.0	1603.2	106.1	1144.2	600.7	32.8	18.8
aug-cc-pVQZ CCSD(T)	2202.2	151.0	1161.4	1602.0	115.3	1142.5	600.2	35.7	18.9
cc-pV5Z CCSD(T)	2206.4	152.0	1168.1	1605.1	116.1	1149.1	601.3	35.9	19.0
aug-cc-pV5Z CCSD(T)	2205.6	153.6	1167.4	1604.5	117.4	1148.4	601.1	36.2	19.0
cc-pCVQZ CCSD(T)	2205.9	128.7	1173.1	1605.0	98.3	1153.9	600.9	30.4	19.2
aug-cc-pCVQZ CCSD(T)	2205.1	140.9	1171.6	1604.4	107.6	1152.4	600.7	33.3	19.2
cc-pVQZ ICMRCI	2232.1	107.1	1156.2	1622.6	81.7	1138.2	609.5	25.4	18.0
aug-cc-pVQZ ICMRCI	2231.5	120.3	1155.2	1622.2	91.8	1137.2	609.3	28.5	18.0
cc-pV5Z ICMRCI	2235.9	121.1	1161.6	1625.3	92.5	1143.5	610.6	28.6	18.1
aug-cc-pV5Z ICMRCI	2235.5	122.7	1161.2	1625.0	93.7	1143.2	610.5	29.0	18.0
Expt. [Ref. 7]	2152.2		1162.2	1580.5		1145.4	571.7		16.8

TABLE 4.6. Relative energies in kcal mol^{-1} (zero-point vibrational energy corrected values in parentheses) for the HSiN - HNSi system with respect to the global minimum $\tilde{X}\ ^1\Sigma^+$ state of HNSi.

Level of Theory	*HNSi*	*HSiN*		*Barrier Height HNSi → HSiN*		*Barrier Height HSiN → HNSi*	
cc-pVQZ SCF	0.00	88.88	(85.63)	89.84	(85.63)	0.96	(0.00)
aug-cc-pVQZ SCF	0.00	88.99	(85.74)	89.96	(85.76)	0.97	(0.02)
cc-pV5Z SCF	0.00	89.01	(85.76)	90.05	(85.82)	1.04	(0.06)
aug-cc-pV5Z SCF	0.00	89.05	(85.81)	90.08	(85.86)	1.03	(0.05)
cc-pCVTZ SCF	0.00	88.59	(85.34)	89.68	(85.42)	1.09	(0.08)
aug-cc-pCVTZ SCF	0.00	88.82	(85.65)	89.98	(85.78)	1.16	(0.13)
cc-pCVQZ SCF	0.00	88.89	(85.63)	89.91	(85.68)	1.02	(0.05)
aug-cc-pCVQZ SCF	0.00	89.03	(85.77)	90.05	(85.82)	1.03	(0.06)
cc-pVQZ CISD	0.00	77.57	(74.29)	89.43	(85.16)	11.86	(10.87)
aug-cc-pVQZ CISD	0.00	77.69	(74.45)	89.60	(85.35)	11.91	(10.90)
cc-pV5Z CISD	0.00	77.86	(74.67)	89.75	(85.47)	11.89	(10.86)
aug-cc-pV5Z CISD	0.00	77.87	(74.63)	89.81	(85.54)	11.94	(10.91)
cc-pCVTZ CISD	0.00	80.88	(77.65)	93.06	(88.66)	12.18	(11.01)
aug-cc-pCVTZ CISD	0.00	81.08	(78.00)	93.27	(88.98)	12.18	(10.97)
cc-pCVQZ CISD	0.00	81.77	(78.57)	93.82	(89.45)	12.05	(10.88)
aug-cc-pCVQZ CISD	0.00	81.88	(78.72)	93.98	(89.63)	12.11	(10.92)
cc-pVQZ CCSD	0.00	73.12	(69.53)	82.47	(78.27)	9.35	(8.74)
aug-cc-pVQZ CCSD	0.00	73.25	(69.74)	82.55	(78.36)	9.29	(8.61)
cc-pV5Z CCSD	0.00	73.48	(69.97)	82.74	(78.53)	9.26	(8.56)
aug-cc-pV5Z CCSD	0.00	73.49	(69.99)	82.75	(78.55)	9.26	(8.56)
cc-pCVTZ CCSD	0.00	73.46	(69.86)	82.77	(78.53)	9.30	(8.66)
aug-cc-pCVTZ CCSD	0.00	73.72	(70.30)	82.73	(78.57)	9.01	(8.27)
cc-pCVQZ CCSD	0.00	74.31	(70.73)	83.29	(79.07)	8.98	(8.34)
aug-cc-pCVQZ CCSD	0.00	74.46	(70.95)	83.36	(79.16)	8.90	(8.21)
cc-pVQZ CCSD(T)	0.00	67.61	(64.21)	79.09	(74.98)	11.48	(10.77)
aug-cc-pVQZ CCSD(T)	0.00	67.77	(64.42)	79.11	(75.01)	11.34	(10.59)
cc-pV5Z CCSD(T)	0.00	67.98	(64.61)	79.28	(75.16)	11.30	(10.55)
aug-cc-pV5Z CCSD(T)	0.00	68.01	(64.66)	79.27	(75.17)	11.26	(10.51)
cc-pCVTZ CCSD(T)	0.00	67.73	(64.28)	79.24	(75.09)	11.51	(10.81)
aug-cc-pCVTZ CCSD(T)	0.00	68.08	(64.78)	79.10	(75.04)	11.02	(10.26)
cc-pCVQZ CCSD(T)	0.00	68.63	(65.18)	79.62	(75.50)	10.99	(10.32)
aug-cc-pCVQZ CCSD(T)	0.00	68.81	(65.41)	79.64	(75.54)	10.83	(10.13)
cc-pVQZ CASSCF	0.00	67.11	(63.89)	85.87	(81.59)	18.76	(17.70)
aug-cc-pVQZ CASSCF	0.00	67.23	(64.02)	84.12	(80.17)	16.89	(16.15)
cc-pV5Z CASSCF	0.00	67.40	(64.16)	86.16	(81.87)	18.76	(17.71)
aug-cc-pV5Z CASSCF	0.00	67.44	(64.21)	84.24	(80.28)	16.80	(16.07)
cc-pVQZ ICMRCI	0.00	66.03	(62.58)	78.00	(73.88)	11.97	(11.30)
aug-cc-pVQZ ICMRCI	0.00	66.16	(62.77)	78.80	(74.78)	12.64	(12.01)
cc-pV5Z ICMRCI	0.00	66.34	(62.93)	78.18	(74.06)	11.84	(11.13)
aug-cc-pV5Z ICMRCI	0.00	66.37	(62.98)	78.91	(74.88)	12.54	(11.90)

TABLE 4.7. Total SCF, CASSCF, CCSD, and CCSD(T) energies in hartrees for the ground states of H(^{2}S) and SiN ($X\ ^1\Sigma^+$), and the dissociation energies of HNSi and HSiN to H + SiN in kcal mol^{-1}.

	H	SiN	HNSi $D_e(D_0)$	HSiN $D_e(D_0)$
cc-pVQZ SCF	-0.499 946	-343.295 268	116.67(109.15)	27.78(23.51)
aug-cc-pVQZ SCF	-0.499 948	-343.295 559	116.82(109.30)	27.83(23.56)
cc-pV5Z SCF	-0.499 995	-343.298 172	116.88(109.35)	27.86(23.58)
aug-cc-pV5Z SCF	-0.499 995	-343.298 268	116.92(109.40)	27.87(23.59)
cc-pCVTZ SCF	-0.499 810	-343.289 774	116.49(108.94)	27.91(23.61)
aug-cc-pCVTZ SCF	-0.499 821	-343.291 084	116.91(109.42)	28.09(23.77)
cc-pCVQZ SCF	-0.499 946	-343.297 353	116.77(109.24)	27.87(23.60)
aug-cc-pCVQZ SCF	-0.499 948	-343.297 650	116.92(109.39)	27.89(23.62)
cc-pVQZ CASSCF	-0.499 946	-343.416 207	124.32(117.35)	57.21(53.46)
aug-cc-pVQZ CASSCF	-0.499 948	-343.416 467	124.53(117.57)	57.30(53.55)
cc-pV5Z CASSCF	-0.499 995	-343.418 529	124.72(177.73)	57.32(53.57)
aug-cc-pV5Z CASSCF	-0.499 995	-343.418 612	124.77(117.79)	57.33(53.58)
cc-pVQZ CCSD	-0.499 946	-343.604 371	132.30(125.22)	59.17(55.68)
aug-cc-pVQZ CCSD	-0.499 948	-343.606 612	132.59(125.53)	59.33(55.78)
cc-pV5Z CCSD	-0.499 995	-343.612 298	132.95(125.86)	59.47(55.89)
aug-cc-pV5Z CCSD	-0.499 995	-343.613 327	132.04(125.96)	59.54(55.96)
cc-pCVTZ CCSD	-0.499 810	-343.923 413	131.24(124.12)	57.77(54.25)
aug-cc-pCVTZ CCSD	-0.499 821	-343.928 961	131.93(124.89)	58.20(54.58)
cc-pCVQZ CCSD	-0.499 946	-343.979 420	132.99(125.88)	58.68(55.15)
aug-cc-pCVQZ CCSD	-0.499 948	-343.981 694	133.27(126.17)	58.81(55.22)
cc-pVQZ CCSD(T)	-0.499 946	-343.625 470	131.06(124.08)	63.45(59.87)
aug-cc-pVQZ CCSD(T)	-0.499 948	-343.627 961	131.38(124.42)	63.61(60.00)
cc-pV5Z CCSD(T)	-0.499 995	-343.633 813	131.74(124.75)	63.76(60.14)
aug-cc-pV5Z CCSD(T)	-0.499 995	-343.634 959	131.84(124.87)	63.83(60.21)
cc-pCVTZ CCSD(T)	-0.499 810	-343.946 760	129.84(122.82)	62.11(58.54)
aug-cc-pCVTZ CCSD(T)	-0.499 821	-343.952 936	130.62(123.70)	62.54(58.92)
cc-pCVQZ CCSD(T)	-0.499 946	-344.004 811	131.65(124.64)	63.01(59.45)
aug-cc-pCVQZ CCSD(T)	-0.499 948	-344.007 329	131.96(124.97)	63.15(59.56)

FIGURE 4.1a**.**

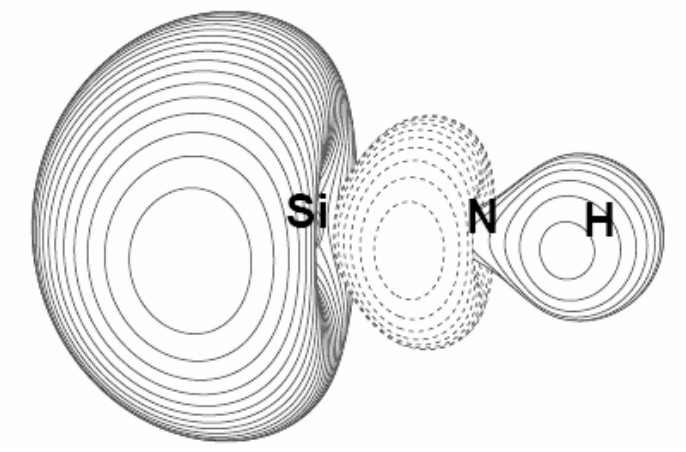

FIGURE 4.1b.

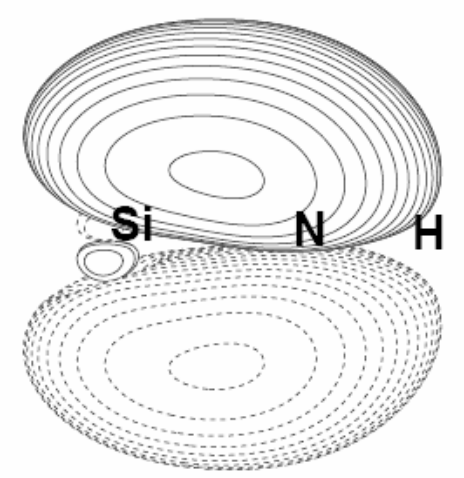

FIGURE 4.1c.

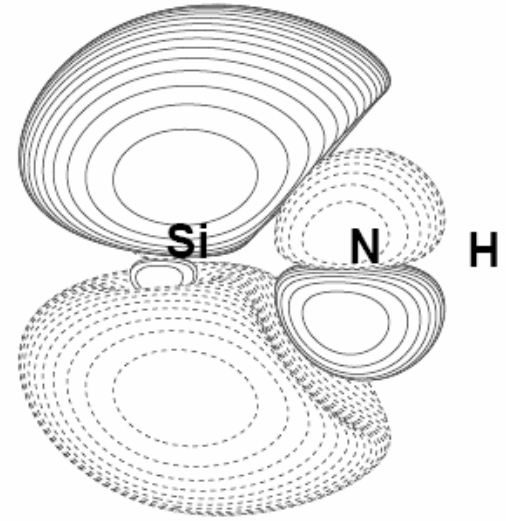

FIGURE 4.2a.

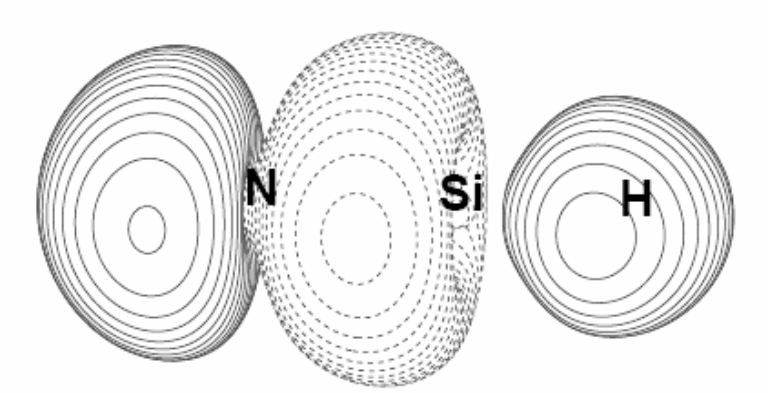

FIGURE 4.2b.

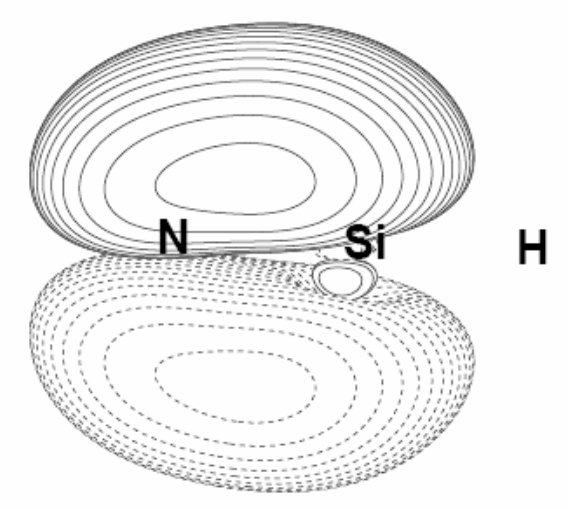

FIGURE 4.2c.

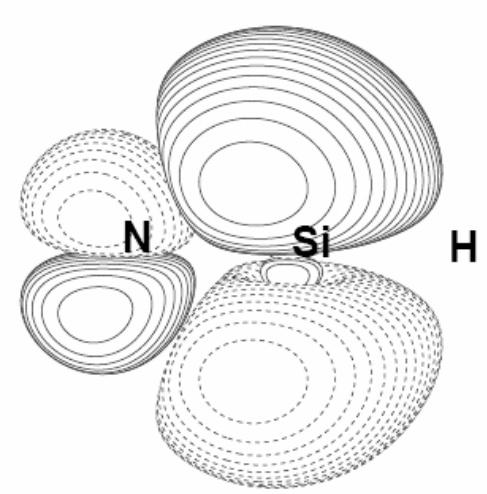

FIGURE 4.3.

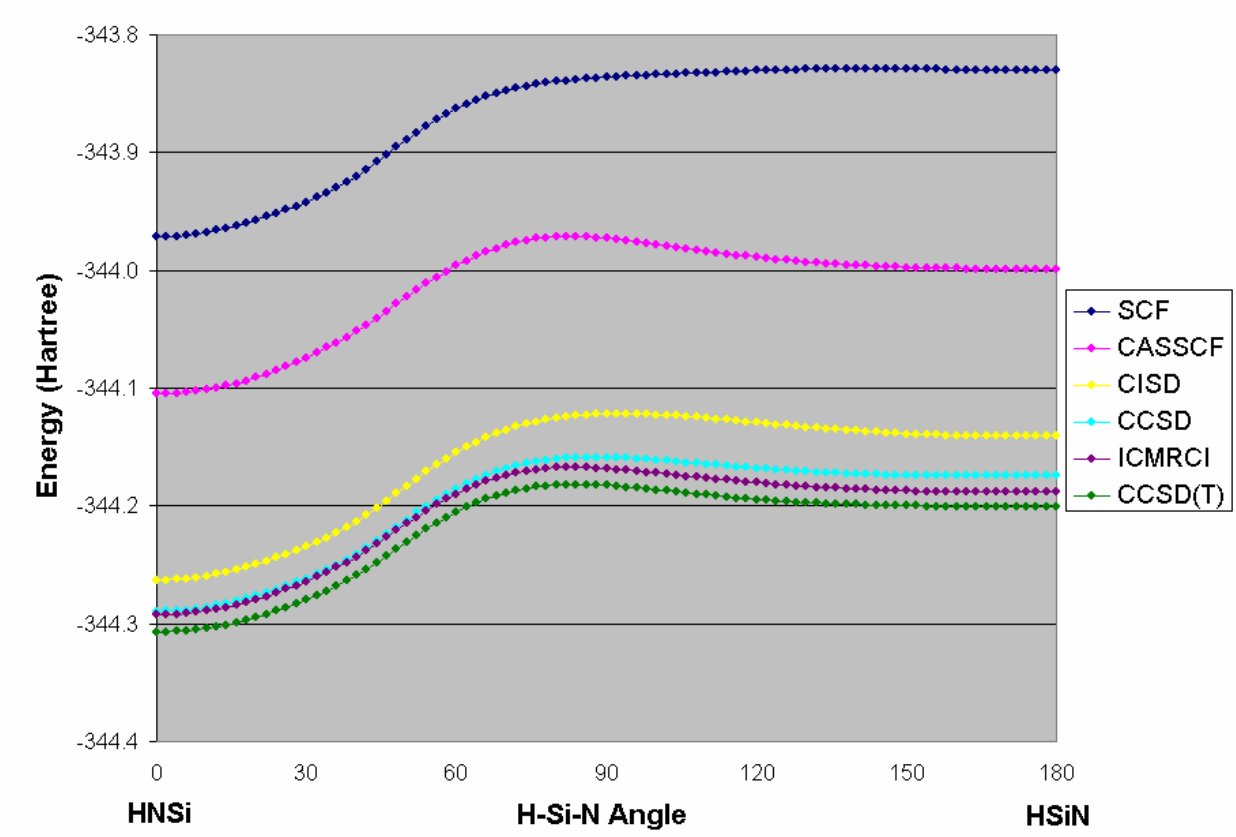
-343.8
-343.9
-344.0
-344.1
-344.2
-344.3
-344.4
Energy (Hartree)
0
30
60
90
120
150
180
HNSi
H-Si-N Angle
HSiN
SCF
CASSCF
CISD
CCSD
ICMRCI
CCSD(T)

FIGURE 4.4.

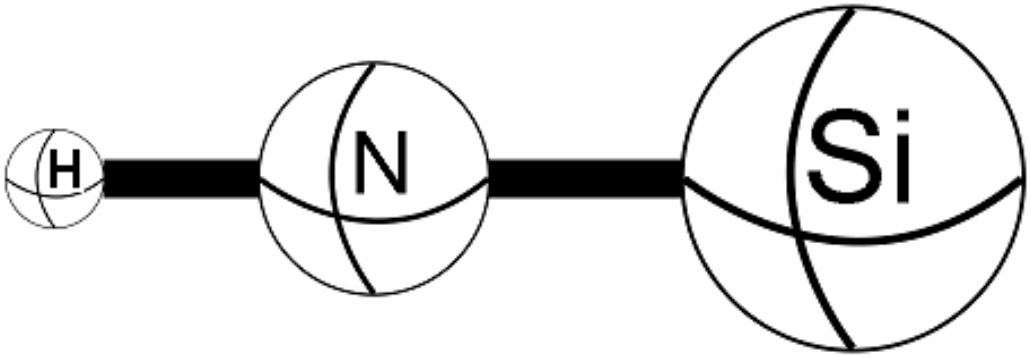

cc-pVQZ SCF	0.9841	1.5229
aug-cc-pVQZ SCF	0.9842	1.5235
cc-pV5Z SCF	0.9840	1.5205
aug-cc-pV5Z SCF	0.9841	1.5207
cc-pCVQZ SCF	0.9840	1.5197
aug-cc-pCVQZ SCF	0.9842	1.5204
cc-pVQZ CISD	0.9923	1.5393
aug-cc-pVQZ CISD	0.9927	1.5403
cc-pV5Z CISD	0.9922	1.5362
aug-cc-pV5Z CISD	0.9923	1.5365
cc-pCVQZ CISD	0.9882	1.5261
aug-cc-pCVQZ CISD	0.9885	1.5272
cc-pVQZ CCSD	0.9968	1.5473
aug-cc-pVQZ CCSD	0.9972	1.5484
cc-pV5Z CCSD	0.9967	1.5442
aug-cc-pV5Z CCSD	0.9969	1.5445
cc-pCVQZ CCSD	0.9957	1.5394
aug-cc-pCVQZ CCSD	0.9961	1.5405
cc-pVQZ CCSD(T)	0.9999	1.5575
aug-cc-pVQZ CCSD(T)	1.0004	1.5587
cc-pV5Z CCSD(T)	0.9999	1.5543
aug-cc-pV5Z CCSD(T)	1.0001	1.5547
cc-pCVQZ CCSD(T)	0.9989	1.5495
aug-cc-pCVQZ CCSD(T)	0.9994	1.5508
cc-pVQZ CASSCF	1.0068	1.5587
aug-cc-pVQZ CASSCF	1.0069	1.5593
cc-pV5Z CASSCF	1.0066	1.5563
aug-cc-pV5Z CASSCF	1.0067	1.5565
cc-pVQZ ICMRCI	1.0003	1.5595
aug-cc-pVQZ ICMRCI	1.0007	1.5605
cc-pV5Z ICMRCI	1.0002	1.5563
aug-cc-pV5Z ICMRCI	1.0003	1.5566

FIGURE 4.5.

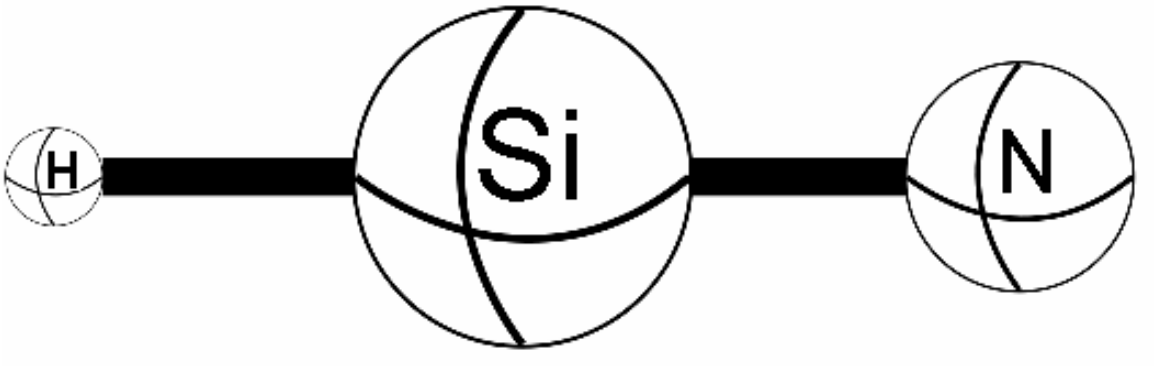

cc-pVQZ SCF	1.4601	1.5224
aug-cc-pVQZ SCF	1.4600	1.5225
cc-pV5Z SCF	1.4597	1.5199
aug-cc-pV5Z SCF	1.4597	1.5199
cc-pCVQZ SCF	1.4598	1.5194
aug-cc-pCVQZ SCF	1.4598	1.5197
cc-pVQZ CISD	1.4688	1.5507
aug-cc-pVQZ CISD	1.4688	1.5510
cc-pV5Z CISD	1.4681	1.5473
aug-cc-pV5Z CISD	1.4682	1.5474
cc-pCVQZ CISD	1.4599	1.5343
aug-cc-pCVQZ CISD	1.4599	1.5346
cc-pVQZ CCSD	1.4773	1.5658
aug-cc-pVQZ CCSD	1.4774	1.5661
cc-pV5Z CCSD	1.4766	1.5621
aug-cc-pV5Z CCSD	1.4767	1.5623
cc-pCVQZ CCSD	1.4731	1.5573
aug-cc-pCVQZ CCSD	1.4731	1.5577
cc-pVQZ CCSD(T)	1.4849	1.5826
aug-cc-pVQZ CCSD(T)	1.4849	1.5831
cc-pV5Z CCSD(T)	1.4841	1.5790
aug-cc-pV5Z CCSD(T)	1.4842	1.5792
cc-pCVQZ CCSD(T)	1.4810	1.5744
aug-cc-pCVQZ CCSD(T)	1.4810	1.5749
cc-pVQZ CASSCF	1.4737	1.5828
aug-cc-pVQZ CASSCF	1.4736	1.5829
cc-pV5Z CASSCF	1.4731	1.5804
aug-cc-pV5Z CASSCF	1.4730	1.5804
cc-pVQZ ICMRCI	1.4806	1.5832
aug-cc-pVQZ ICMRCI	1.4805	1.5835
cc-pV5Z ICMRCI	1.4796	1.5795
aug-cc-pV5Z ICMRCI	1.4797	1.5796

FIGURE 4.6.

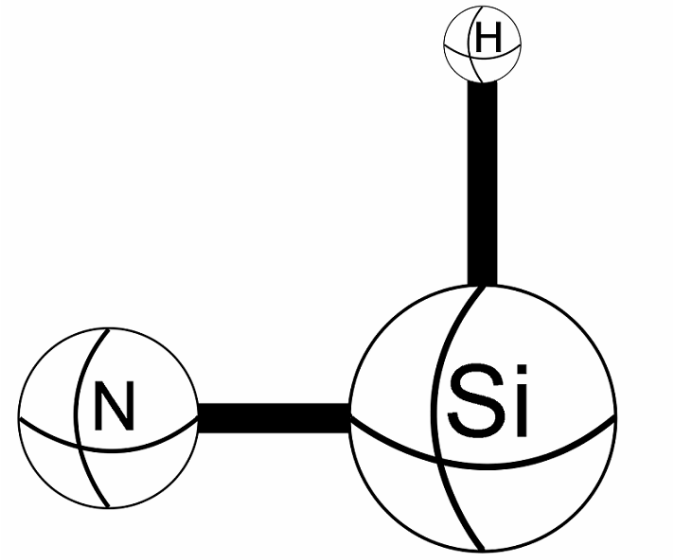

	r_e(SiH)	r_e(SiN)	∠HSiN
cc-pVQZ SCF	1.4674	1.5467	141.59
aug-cc-pVQZ SCF	1.4675	1.5473	141.28
cc-pV5Z SCF	1.4670	1.5456	140.39
aug-cc-pV5Z SCF	1.4670	1.5456	140.37
cc-pCVQZ SCF	1.4670	1.5450	140.45
aug-cc-pCVQZ SCF	1.4670	1.5455	140.28
cc-pVQZ CISD	1.4953	1.5971	92.53
aug-cc-pVQZ CISD	1.4956	1.5972	92.64
cc-pV5Z CISD	1.4938	1.5928	92.65
aug-cc-pV5Z CISD	1.4940	1.5928	92.68
cc-pCVQZ CISD	1.4836	1.5845	94.77
aug-cc-pCVQZ CISD	1.4838	1.5847	94.87
cc-pVQZ CCSD	1.5065	1.6130	87.71
aug-cc-pVQZ CCSD	1.5071	1.6134	87.76
cc-pV5Z CCSD	1.5051	1.6087	87.90
aug-cc-pV5Z CCSD	1.5053	1.6089	87.92
cc-pCVQZ CCSD	1.5001	1.6034	88.48
aug-cc-pCVQZ CCSD	1.5006	1.6039	88.54
cc-pVQZ CCSD(T)	1.5151	1.6198	84.04
aug-cc-pVQZ CCSD(T)	1.5161	1.6204	84.03
cc-pV5Z CCSD(T)	1.5138	1.6156	84.21
aug-cc-pV5Z CCSD(T)	1.5142	1.6159	84.21
cc-pCVQZ CCSD(T)	1.5088	1.6109	84.64
aug-cc-pCVQZ CCSD(T)	1.5096	1.6116	84.63
cc-pVQZ CASSCF	1.5350	1.6305	82.40
aug-cc-pVQZ CASSCF	1.5061	1.6226	82.46
cc-pV5Z CASSCF	1.5334	1.6276	82.48
aug-cc-pV5Z CASSCF	1.5046	1.6197	82.51
cc-pVQZ ICMRCI	1.5147	1.6220	83.88
aug-cc-pVQZ ICMRCI	1.5082	1.6208	83.40
cc-pV5Z ICMRCI	1.5132	1.6178	84.02
aug-cc-pV5Z ICMRCI	1.5063	1.6164	83.52

FIGURE 4. 7.

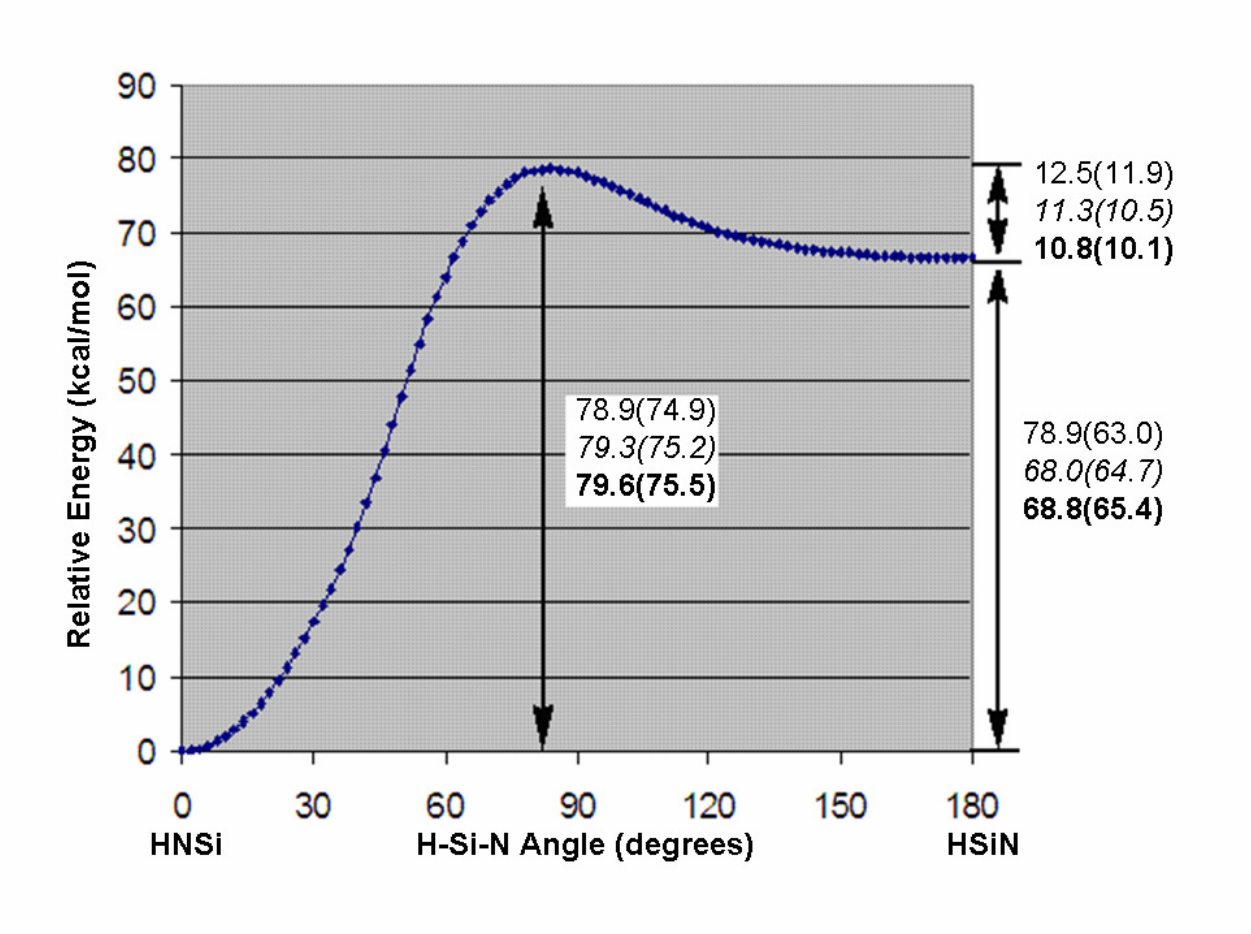
Relative Energy (kcal/mol)
90
80
70
60
50
40
30
20
10
0
0
30
60
90
120
150
180
HNSi
H-Si-N Angle (degrees)
HSiN
12.5(11.9)
11.3(10.5)
10.8(10.1)
78.9(74.9)
79.3(75.2)
79.6(75.5)
78.9(63.0)
68.0(64.7)
68.8(65.4)

CHAPTER 5

CONCLUDING REMARKS

The application of Density Functional Theory in the study of the electronic properties of molecules yields reliable results. The various deprotonated Guanine-Cytosine and hydrogen-abstracted Adenine-Thymine base pairs and were studied at the B3LYP/DZP++ level of theory. Deprotonation and H-abstraction are two possible ways that radiation causes damage to DNA, and by using computational methods, we can tell more about which sites might be most susceptible as targets for such damage.

The ten neutral doublet H-abstracted G-C base pairs were found to have electron affinities between 1.93 and 3.65 eV as predicted by DFT. The energetically most favored anion structure results from deprotonation at the N1 site on cytosine. Several of the resulting closed-shell anions displayed significant distortion in the dihedral angle between the two bases (*i.e.* the two bases twisted apart) as well as changes in bond lengths of up to 0.5 Å, suggestive of potential sites susceptible irradiative damage to double-stranded DNA.

In the case of the A-T base pair, DFT predicts that removal of a hydrogen from the methyl group results in a more stable structure than does H-abstraction from the glycosidic bond sites. Surprisingly, the A-T structures do not exhibit much distortion upon deprotonation compared to G-C, based on the dihedral angle between the bases. However, removal of either of the two hydrogens involved from the N6 site on adenine results in a significant lowering of the dissociation energy of the base pair.

In general, we can see that DFT is a useful tool to obtain reliable predictions for energetics, structures and electronic properties of molecules inaccessible by *ab initio* methods.